ADVANCES IN INORGANIC CHEMISTRY, VOL. 45

STRUCTURE AND PROPERTIES OF COPPER–ZINC SUPEROXIDE DISMUTASES

IVANO BERTINI,* STEFANO MANGANI,† AND MARIA SILVIA VIEZZOLI*

*Department of Chemistry, University of Florence, 50121 Florence, Italy
†Department of Chemistry, University of Siena, 53400 Siena, Italy

I. The Need for Superoxide Dismutase
II. The Crystal Structures of Dimeric Copper–Zinc Superoxide Dismutases
  A. Bovine Cu_2Zn_2SOD
  B. Human Cu_2Zn_2SOD
  C. *Xenopus laevis* Cu_2Zn_2SOD
  D. Spinach Cu_2Zn_2SOD
  E. Yeast Cu_2Zn_2SOD
  F. Bovine Cu_2Co_2SOD
  G. Peroxynitrite-Modified Cu_2Zn_2SOD
  H. Mutants of Cu_2Zn_2SOD
  I. Reduced Cu_2Zn_2SODs
  J. Inorganic Anion Complexes of Cu_2Zn_2SOD
III. Activity
  A. Activity Measurements
  B. pH Dependence of Activity
  C. Ionic Strength Dependence of Activity
  D. Computational Studies on Copper–Zinc SOD
IV. Molecular Biology and Chemical Modifications
  A. Expression Methods
  B. Chemical Modifications
  C. The Mutants
V. Metal Substitutions
VI. Water in the Active Site Cavity
VII. Redox Properties
  A. Reduction Potentials
  B. Electron Transfer between $[Fe(CN)_6]^{4-}$ and Cu_2Zn_2SOD
VIII. The Spectroscopic Properties of Metal Ions
  A. Copper(II) in Native Protein
  B. Copper(II) in the Cu_2E_2 Enzyme
  C. Copper(II) with Other Metal Ions in the Zinc Site
  D. Nickel(II) in the Copper Site
  E. Cobalt(II) in the Copper Site
  F. Anion Derivatives
  G. Other Metals at the Zinc Site

0898-8838/98 $25.00

H. Cadmium at Both Copper and Zinc Sites
I. ^1H NMR Spectra of Cu_2Co_2 and Cu_2Ni_2SOD
J. ^1H NMR Spectra of the Reduced Enzyme
IX. Mechanistic Aspects of Cu_2Zn_2SOD
A. Noncatalyzed Disproportionation of O_2^-
B. Some Pertinent Facts about Cu_2Zn_2SOD Catalysis
C. Mechanism of Action of Cu_2Zn_2SOD
D. Comparison with MnSOD and FeSOD Mechanisms
X. Concluding Remarks
Note Added in Proof
References

I. The Need for Superoxide Dismutase

Following discovery of the superoxide dismutase[1] (SOD) enzymes by Keilin and Mann (*1*), and their ability to catalyze the dismutation of the superoxide radical anion (O_2^-) in laboratory experiments (*2*), discussion has taken place over the intervening years as to whether such enzymes do catalyze O_2^- dismutation *in vivo*, and whether there is a need for a complex enzyme to accelerate a reaction that is already very fast. This is not the place to address these points, but the current feeling is that the answer to both questions is in the affirmative.

The superoxide radical anion is physiologically produced in controlled amounts in animals and plants from the one-electron reduction of dioxygen occurring in several metabolic pathways (*3–5*). Under pathological conditions, large amounts of superoxide and related active oxygen species are released (*6*, *7*). Thus, a twofold aspect of superoxide effects on living organisms emerges from the available experimental data. First, excess of O_2^- should be eliminated to avoid the formation of radicals and toxic species such as OH and singlet oxygen, which are characterized by very high reactivity; second, O_2^- appears also to be involved in useful processes for the organism, for example, the cell killing effect of tumor necrosis factor and the antibacterial effect of myeloperoxidases (*7*, *8*). The actual role of superoxide dismutase enzymes in living organisms needs to be reconsidered in view of this wider framework. The overall disproportionation reaction, which is catalyzed by SODs, is shown in Eq. (1):

$$2O_2^- + 2H^+ \rightarrow O_2 + H_2O_2. \quad (1)$$

[1] The enzyme residue sequence numbering used throughout the text is that of human Cu_2Zn_2 superoxide dismutase, unless otherwise stated explicitly at the beginning of the section.

Although the stoichiometry of the reaction is correct, it must be taken with the caveat that the reactions that are actually occurring are those of Eqs. (2) and (3):

$$HO_2 + O_2^- \rightarrow O_2 + HO_2^- \tag{2}$$

and/or

$$2HO_2 \rightarrow O_2 + H_2O_2. \tag{3}$$

The direct reaction of superoxide with itself does not play, in practice, a role in the dismutation (see Section IX,A). It is recalled here that the pK_a of HO_2 is 4.8. Hydrogen peroxide is then subject to a further disproportionation by catalases to yield water and dioxygen or it is used as a substrate in reactions of peroxidases. In fact, O_2^- is often produced when a living organism needs H_2O_2 as an oxidant. Reactions such as Eq. (4),

$$NAD(P)H + 2O_2 \rightarrow 2O_2^- + NAD(P)^+ + H^+, \tag{4}$$

are known to be catalyzed by the respiratory burst oxidase in order to produce H_2O_2. Hydrogen peroxide is needed, for example, by horseradish peroxidase to oxidize phenols, by ligninase to attack lignin, by myeloperoxidases to form ClO^-, etc.

In photosynthesis, secondary pathways for electron transfer actually lead to superoxide production (*9–12*), the thylakoid-bound Cu_2Zn_2SOD catalyzing the O_2^- dismutation. Because the chloroplasts lack catalase, the excess H_2O_2 is a substrate for ascorbate peroxidases to produce dehydroascorbate, which is further re-reduced by NADPH via the glutathione–glutathione reductase pathway (*12*).

If we now believe that SOD catalyzes reaction (1), we should be aware that any metal having two oxidation states with a reduction potential between that of the O_2/O_2^- (−0.33 V vs. NHE, pH 7, P_{O_2} = 0.101 MPa)[2] and O_2^-/H_2O_2 (+0.89 V vs. NHE, pH 7) redox couples can catalyze the dismutation according to Eqs. (5) and (6):

$$M^{n+} + O_2^- \rightarrow M^{(n-1)+} + O_2 \tag{5}$$

$$M^{(n-1)+} + O_2^- + 2H^+ \rightarrow M^{n+} + H_2O_2. \tag{6}$$

[2] If unit activity is used for the standard state of O_2, instead of unit pressure, the reduction potential must be adjusted by +0.17 V.

However, the concentration of free transition-metal ions in living organisms is very low because such ions are complexed or precipitated at physiological pH.

From all the above considerations it would appear that, in order to protect species from toxic effects of superoxide release in tissues, living organisms need an efficient catalyst for superoxide dismutation, and that SOD accomplishes this task with maximum efficiency. In this respect, recent experiments have demonstrated that SOD-deficient bacteria and yeast mutants are highly sensitive to dioxygen (*13*, *14*), suggesting that SOD activity is important for aerobial cell growth. Furthermore, evidence has been provided that, in *Drosophila melanogaster,* Cu_2Zn_2SOD may protect against ionizing radiation and may even give increased longevity in combination with catalase (*15*, *16*). In humans, motor neuron degenerative diseases are in some cases associated with genetic mutations leading to cytosolic SOD of reduced activity (*17*, *18*), or of altered peroxidase-like activity (*19*, *20*).

Besides the O_2^- production by stimulated immune system cells (such as macrophages and neutrophils exposed to oxidative burst during the inflammatory process) (*21–25a*), the steady release of O_2^- over time intervals has been observed in human fibroblasts in response to cytokines such as interleukin-1α and tumor necrosis factor-α (*25*). This suggests that continuous O_2^- production may have a role in the regulation of inflammatory processes (*7*). Consequently, the role of superoxide dismutases in such compartments may be that of ensuring O_2^- homeostasis rather than its scavenging.

The physiological processing of O_2^- is performed by three different metalloenzymes: Fe, Mn, and Cu–Zn SOD. Recently, a protein having superoxide activity, containing nickel, has been isolated from *Streptomices grisens* (*25b*). The Cu–Zn SOD enzyme, which we are dealing with here, is found in eukaryotes and in bacteria (*25a*). The enzyme maintains an intracellular level of O_2^- at 10^{-12}–10^{-11} *M* (*26*). A common isoenzyme is isolated from red blood cells and is a dimer of 32,000 MW, like cytoplasmic and most of the periplasmic Cu_2Zn_2 SODs. On the other hand, chloroplastic and extracellular enzymes are tetrameric. A natural monomeric species has been isolated from the periplasmic space of an *Escherichia coli* strain. This CuZnSOD displays a catalytic activity comparable to that of bovine SOD, but is highly sensitive to proteases (*27*).

A comparison of sequences of different Cu_2Zn_2SODs (Fig. 1) shows that 23 amino acids are invariant, and that most of them are residues close to or part of the active site. Some are at the dimer interface and some are a part of the conserved "Greek key" β-barrel supersecondary

structure (*28*). At the active site, besides those amino acids coordinating the copper and zinc ions, there are other invariant residues, such as Arg-143, involved in substrate guidance and recognition, and Asp-124, which helps to orientate correctly copper and zinc ligands by hydrogen bonding to His-46 (Cu ligand) and His-71 (Zn ligand). There are also five glycines that, because of their small size, contribute to maintaining the structure of the active site (see Section II). Pro-66 is another conserved residue close to the active site; due to its rigid stereochemical constraints, it contributes to stabilizing the conformation of the zinc loop (see Section II).

At the dimer interface Gly-51 and Gly-114 are invariant residues that form hydrogen bonds with the nonconserved residue at position 151; Cys-57 and Cys-146 form a disulfide bridge stabilizing a region of the protein structure involved in monomer/monomer contact (see Section II). Four invariant residues, two Gly (16 and 147), one Phe (45), and one Leu (106) seem to contribute to maintaining the stable Greek key β-barrel fold (see Section II).

Even if sequence invariance occurs for residues connected with the active site or with the dimeric nature of the protein, it has been demonstrated through site-directed mutagenesis that invariance does not necessarily prove that a residue is essential for activity (*28*).

The dimeric enzyme is very stable (*29*, *30*). Copper and zinc play a relevant role in stabilizing the structure (*31*). To unfold human SOD requires 6 *M* guanidinium chloride, whereas 3.5 *M* concentration unfolds the metal-depleted form. Unfolding measurements on SOD using variable concentrations of the denaturing agents guanidinium chloride and urea indicate the presence of a concentration-dependent monomer $\rightleftharpoons$ dimer equilibrium (*32*, *33*); 8 *M* urea causes dissociation of bovine SOD into active subunits (*34*, *35*). The possible monomer $\rightleftharpoons$ dimer equilibrium *in vivo* is an intriguing issue (*33*). It is noteworthy that an isoenzyme of rice SOD and an isoenzyme from *E. coli* were isolated as an active monomer (*27*, *36*).

FIG. 1. Multiple alignment of amino acid sequences of 38 Cu–Zn SODs: The amino acid numbering scheme of bovine SOD, used as a reference, is at the top of the figure. Alignment positions in β-strand conformation in the bovine structure are included in shaded boxes. Residues involved in subunit contacts in the dimeric form of bovine SOD are indicated by black boxes placed above the bovine sequence. The amino acids forming the upper rim of the electrostatic channel are denoted by empty boxes. Reprinted with permission from Ref. *347*.

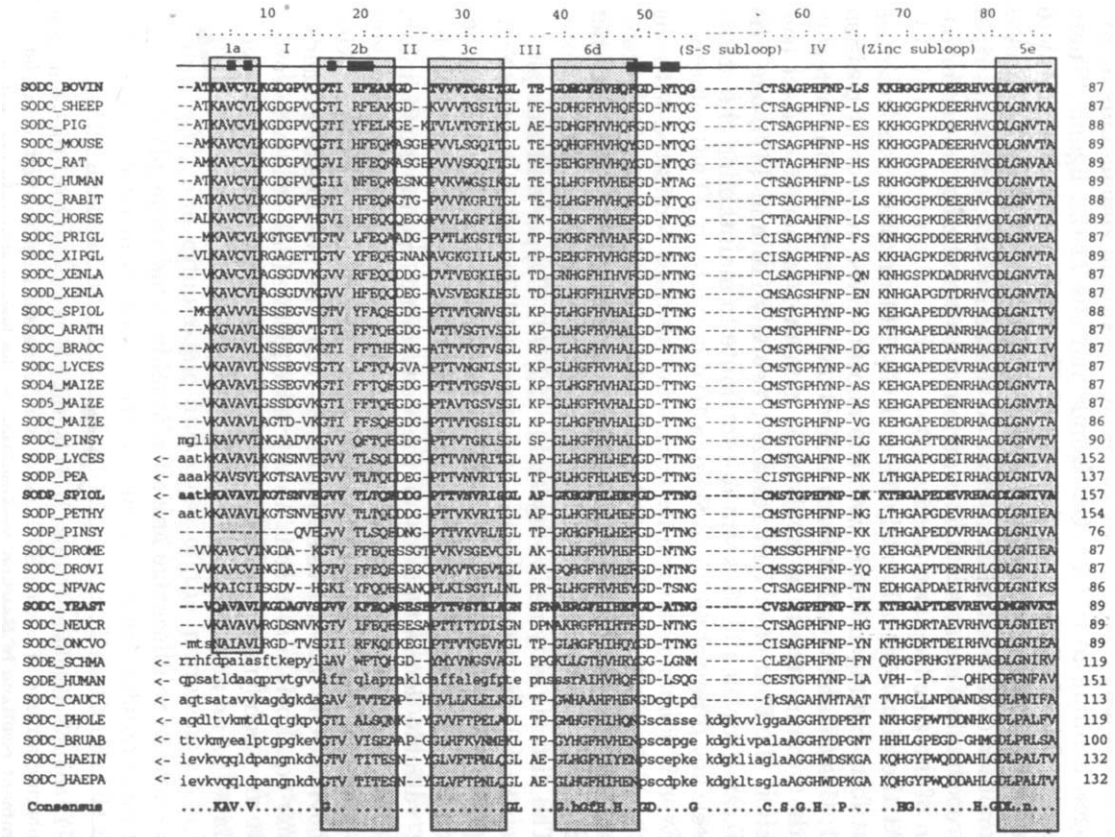
10
20
30
40
50
60
70
80
1a
I
2b
II
3c
III
6d
(S-S subloop)
IV
(Zinc subloop)
5e
SODC_BOVIN
SODC_SHEEP
SODC_PIG
SODC_MOUSE
SODC_RAT
SODC_HUMAN
SODC_RABIT
SODC_HORSE
SODC_PRIGL
SODC_XIPGL
SODC_XENLA
SODD_XENLA
SODC_SPIOL
SODC_ARATH
SODC_BRAOC
SODC_LYCES
SOD4_MAIZE
SOD5_MAIZE
SODC_MAIZE
SODC_PINSY
SODP_LYCES
SODP_PEA
SODP_SPIOL
SODP_PETHY
SODP_PINSY
SODC_DROME
SODC_DROVI
SODC_NPVAC
SODC_YEAST
SODC_NEUCR
SODC_ONCVO
SODE_SCHMA
SODE_HUMAN
SODC_CAUCR
SODC_PHOLE
SODC_BRUAB
SODC_HAEIN
SODC_HAEPA
Consensus

FIG. 1.

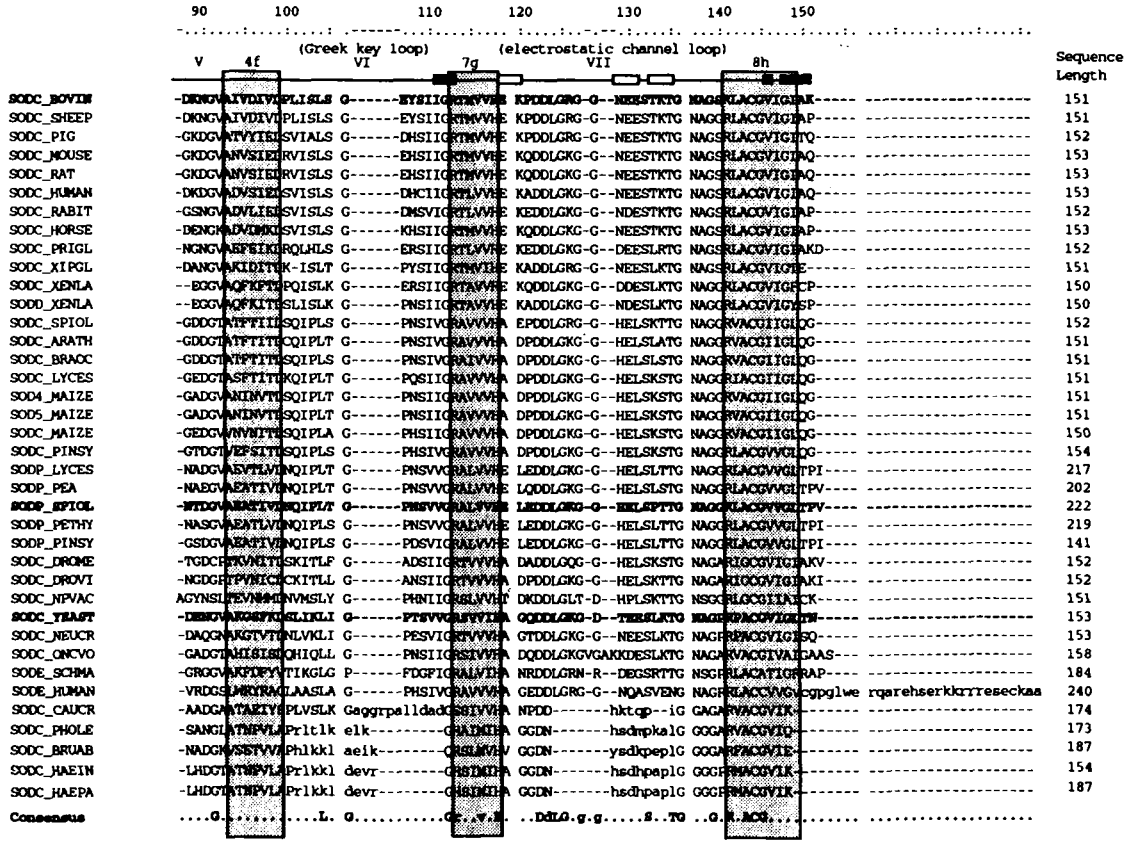

FIG. 1. Continued.

II. The Crystal Structures of Dimeric Copper–Zinc Superoxide Dismutases

Accurate three-dimensional structures of proteins by single-crystal X-ray diffraction experiments provide a powerful aid in the interpretation of information from other techniques, leading to a deeper understanding of the chemistry and the biological function of the molecules. The X-ray crystal structure determination of Cu_2Zn_2SOD[3] represents a fundamental step toward a thorough knowledge of the enzyme.

It must be recognized that precise information about the local structure of metal centers in different phases (solution, glassy or frozen solutions, amorphous) has also been provided by spectroscopic techniques such as nuclear magnetic resonance, X-ray absorption spectroscopy, and electron–nuclear double resonance on native, reduced, or metal-substituted SOD derivatives.

A. Bovine Cu_2Zn_2SOD

1. The Overall Structure

The first X-ray studies on a Cu_2Zn_2SOD were performed by the Richardson group over the decade 1972–1982 on the enzyme from bovine erythrocytes (*37–40*) and resulted in a structure refined at 2.0 Å resolution (*41a*). The Cu_2Zn_2SOD dimers from bovine erythrocytes are made of two subunits of identical amino acid composition, each containing 151 residues. The crystal structure has revealed that the two monomers are related by an almost exact, noncrystallographic twofold axis. The monomers show extensive contact mediated by hydrophobic and hydrophilic interactions that involve about 9% of the total monomer surface (*41a*) (see Section II,A,5).

The main features of the SOD monomer fold are a characteristic eight-stranded β-barrel and three long loops of nonorganized secondary structure. The β-barrel is made of eight antiparallel β-strands connected by seven turns and loops in the Greek key β-barrel motif (*41a*). Figure 2 shows a side view (a) and a top view (b) of the enzyme ribbon diagram with the traditional numbering used for bovine Cu_2Zn_2SOD (*41a*). The turn and loop numbering follows that introduced by Getzoff *et al.* (*28*). The strands are numbered consecutively starting from the N terminus and proceeding clockwise around the barrel. The turns and loops connecting the eight β-strands are indicated by ro-

[3] Within this section the enzyme residue numbering will follow that of the sequence of each structurally determined SOD; hence, residues having the same role in the enzyme may differ in their numbering.

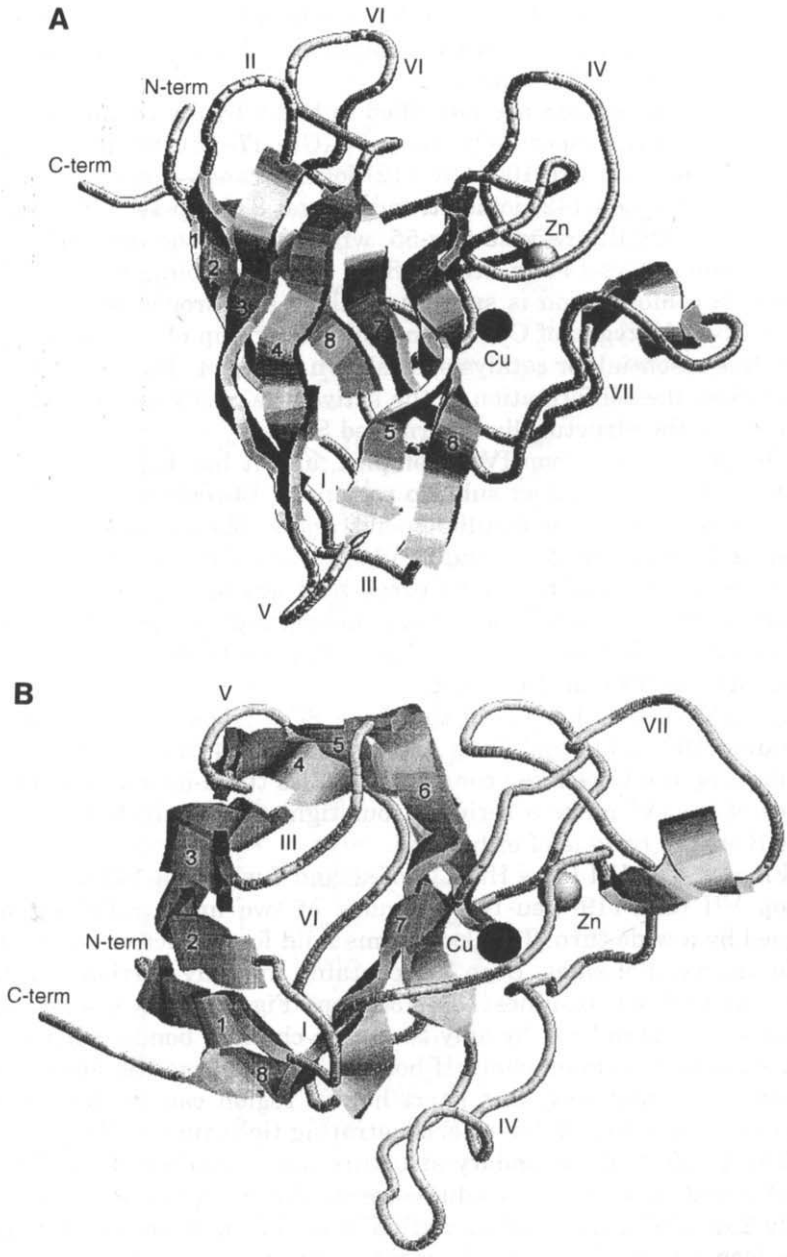

FIG. 2. Ribbon diagram of the Cu_2Zn_2SOD monomer showing the secondary structures of the enzyme and the arrangement of the eight strands in the Greek-key barrel fold. (the β strands and loops are numbered following the conventions established in Refs. *28* and *41*). The metal ions are represented as spheres of arbitrary radius. (A) Side view; (B) top view highlighting the β-barrel and the active site location.

man numerals that follow the order in which they occur in the amino acid sequence. Figure 3 shows the amino acid sequence and topology of a bovine Cu_2Zn_2SOD subunit.

The three long loops are identified in Fig. 2 by the roman numerals IV, VI, and VII, respectively. Loop IV (Gln-47–Leu-82) joins strands 6 and 5, loop VI (Pro-100–Gly-112) joins strands 4 and 7, and loop VII (Glu-119–Leu-142) joins strands 7 and 8. Loop IV is the longest loop and hosts the residue Cys-55, which makes the disulfide bridge with residue Cys-144 in strand 8. It must be pointed out that the disulfide conformation is such as to allow a hydrogen bond between the carbonyl oxygen of Cys-55 and the NH_2 group of residue Arg-141, which is essential for catalysis, as shown in Fig. 4. The disulfide bond influences the conformation of the active site cavity and is conserved among all the structurally determined SODs.

The structure of loop IV is complex, and it has been described as composed of two distinct subloop regions: a 14-residue loop (Gln-47–Pro-60) containing the disulfide bond, and a 22-residue loop (His-61–Leu-82) bearing the Zn-ligand residues (*41a*). The first subloop region contains a series of five tight turns that are linked by three main-chain hydrogen bonds. The second subloop region starts from His-61 and contains four more turns. This region hosts the Zn binding site and includes all four Zn ligands.

Loop VI is the shortest of the three SOD loops and it is made by residues 100 to 112 and links Asp-99 of strand 4 to Arg-113 of strand 7, forming the Greek key connection across the β-barrel. The 13 residues of loop VI make a series of four tight turns, which also involve one β-strand residue of either end.

Finally, loop VII links His-118 of strand 7 with Ala-143 of strand 8. Loop VII (Glu-119–Leu-142) is made of two antiparallel stretches joined by a wide turn. This loop forms a lid for the active site with its two antiparallel sides. Loop VII contains the only portion of α-helix present in SOD (residues 131–136) (see Fig. 2). It is a six-residue-long α-helix stabilized by only two main-chain H bonds, whereas the six side-chain to main-chain H bonds distort it from the ideal conformation. Alternatively, this short helical region can be described as formed by a series of five interpenetrating tight turns (*41a*).

The Cu_2Zn_2SOD secondary structure has a marked β-character in that about 62% of the residues are in the β conformation whereas only 26% are in the α conformation. Most of the latter are located in the loop regions and only six residues build the α-helix in loop VII. About 70 residues are involved in the eight-stranded β-barrel.

The eight β-strands forming the walls of the β-barrel display an overall right-handed twist. Strands 1,2 and 5,4 are joined by five-

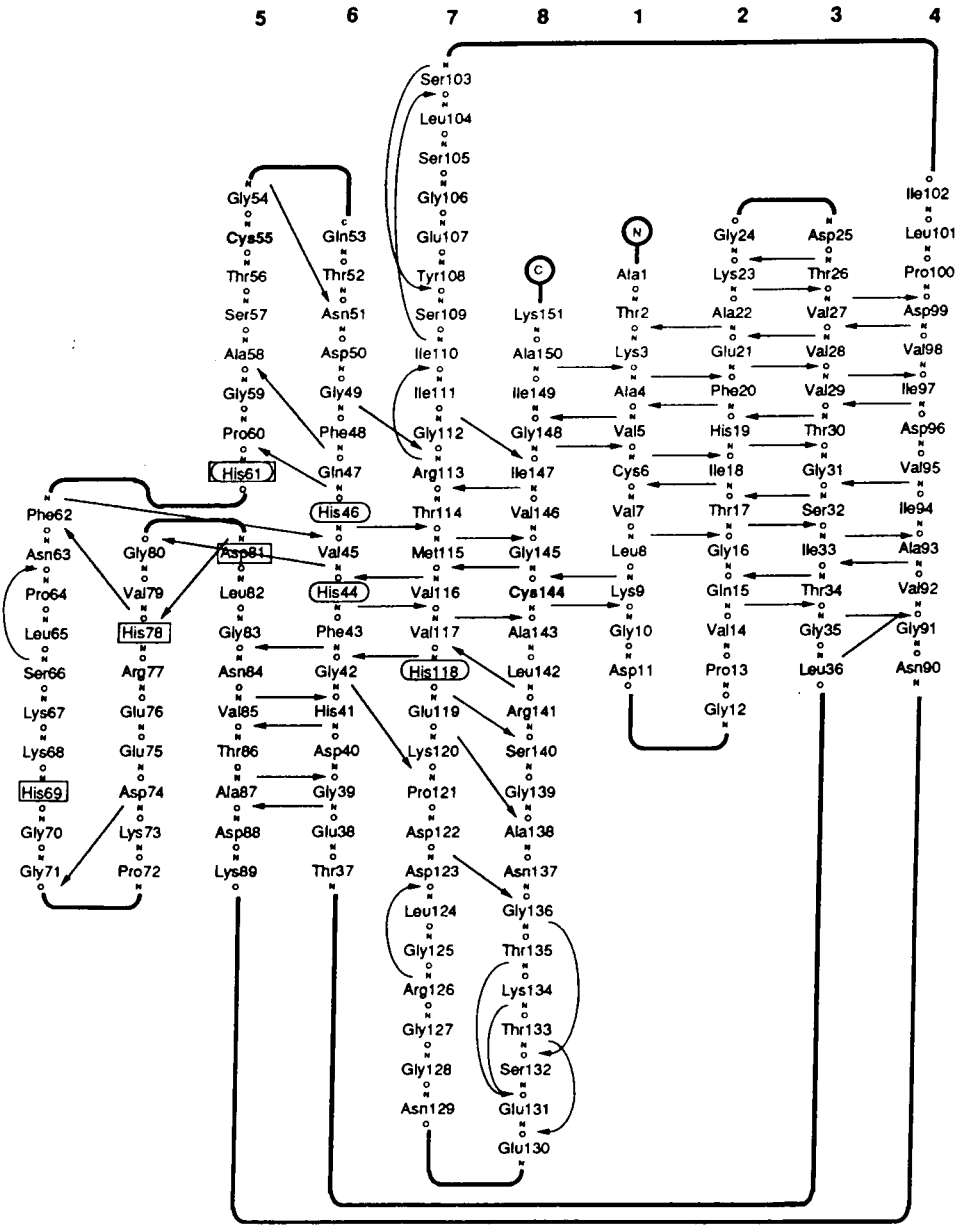

FIG. 3. Amino acid sequence of bovine SOD and its topology. Main-chain to main-chain hydrogen bonds are represented by arrows. Residues coordinating the copper ion are marked with oval boxes; residues coordinating the zinc ion are marked with rectangular boxes. Cys-55 and Cys-144, which form the disulfide bridge, are in bold type. The conventional β-strand numbering is shown at the top of the figure. Reprinted with permission from Ref. *48*.

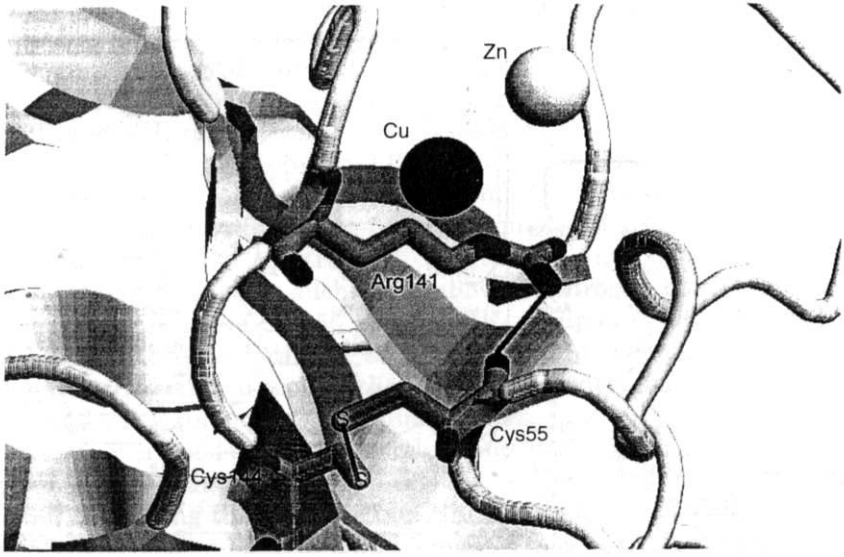

FIG. 4. View of the disulfide bridge between Cys-55 and Cys-144. The H bond linking the Cys-55 carbonyl oxygen with the guanidinium group of Arg-141 is also shown.

residue turns, whereas strands 2,3 are joined by a type II'[4] tight turn in a hairpin connection. Strand 3 links the nonadjacent strand 6 across the barrel in a Greek key topology and, as already mentioned, the other β-strand links are made by the three main loops.

Apart from the β-strands, the second major element of secondary structure in SOD is constituted by the tight turns that are made by four amino acid residues and that may contain a hydrogen bond between the carbonyl oxygen of the nth residue and the amide proton of the nth + 3 residue. The 56 residues are involved in such tight turns, and only one of them joins two adjacent β-strands while the remaining 17 occur in loop regions. Out of the 18 four-residue tight turns, 12 are of type I, two of type I', two of type II', and one of type II, and one of type IV. The category of five-residue turns is present in SOD with the two turns Gly-10–Val-14 and Asp-88–Val-92.

2. *Refinement Technique*

This crystal structure has been refined using the Hendrickson–Konnert restrained refinement technique (*42*, *43*), which minimizes the sum of weighted squares of the differences between the observed

[4] The nomenclature of the secondary structure follows the categories defined by Lewis *et al.* (*41b*).

and calculated structure factors and stereochemical parameters. The weights used were the inverse of the parameter variance. Noncrystallographic symmetry restraints were used between selected atoms of the four different subunits, which were selected as clearly equivalent atoms. In the active site the only imidazole ring of His-61 was refined unrestrained whereas the remaining metal-to-ligand bond lengths and angles were refined restrained. The structure has been refined to an R factor of 0.255 for the 4392 atoms of the model against the 16,245 reflections between 7.0- and 2.0-Å spacings. The model has been completed by adding the active site water molecules and further refined to an R factor of 0.193 against a selected subset of data containing 15,253 reflections between 4.0- and 2.0-Å spacings (*28*, *44*). The second model also contained hydrogen atoms added to one monomer in calculated positions.

3. The Active Site Cavity

The active site cavity is built outside the β-barrel, between loops IV and VII, and consists of a crevice about 15 Å deep and 12 Å long that narrows to about 3 Å in the proximity of the copper, making it perfectly suited to host the small cylindrical superoxide substrate. The copper has a solvent-exposed surface of only 5.2 Å^2, and the zinc is completely buried in the protein (*44*). The rim of the cavity is a highly conserved region in different Cu_2Zn_2SODs. It hosts charged residues that give rise to an electric field (*45*, *46*). The electrostatic gradient generated by the positive and negative charges present in the cavity is thought to be responsible for the steering of the superoxide anion toward the active site (*vide infra*). The side chains of Glu-130, Glu-131, Lys-134, and Thr-135 are on one side of the cavity, and on the opposite side the catalytically important Arg-141 side chain lies at about 6 Å from the copper. The side chains of Glu-119 and Lys-120 complete the edge of the opening. The cavity crevice extends from Thr-135 toward the zinc binding site. Figure 5 shows the cavity with the residues that are important in determining the shape and the strength of the electrostatic field (*45*).

The cavity hosts a chain of water molecules that are found in almost invariant positions in every crystal structure. This network extends from the water molecule coordinated to copper in two opposite directions and links that water molecule with the bulk solvent. The coordinate set deposited within the Protein Data Bank (*47*) (PDB code 2SOD) contains only the copper-bound water molecule; Fig. 6 shows, as an example, the water molecule chain observed in the reduced form of the bovine erythrocyte Cu_2Zn_2SOD structure (PDB code 1SXA) (*48*).

Usually these waters are well ordered and may indicate the path-

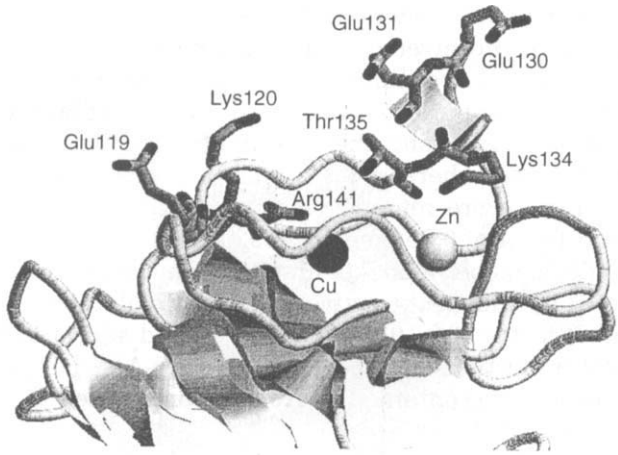

FIG. 5. Ribbon diagram of the enzyme showing the active site cavity. The residues considered important for activity are represented in full as sticks. The zinc and copper ions are represented as spheres of arbitrary radius.

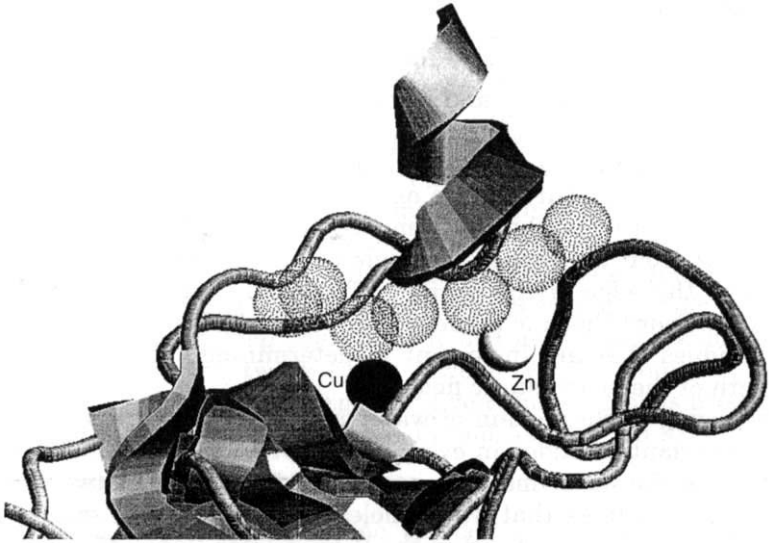

FIG. 6. The water structure in the active site of bovine SOD as obtained from the crystal structure of the reduced enzyme at pH 7.5 (1SXA). The water molecules are represented as spheres of radius corresponding to the van der Waals radius of the oxygen atom, superimposed on the ribbon diagram of the enzyme.

way of substrate diffusion into the active site. Furthermore, the water chain may provide an efficient relay system to deliver into the active site the protons needed by the reacting substrate. They may thus play an essential role in the catalytic mechanism (*48*, *49*). The function of water molecules in enzyme active sites has been reviewed (*50*, *51*) and it is a very attractive and active subject of investigation that can take advantage of the enormous amount of information contained in the crystal structure data collected in the PDB database.

4. The Active Site

Each monomer hosts an active site where one Cu(II) ion and one Zn(II) ion are bound. The active site is located between loops IV and VII on the external surface of the β-barrel, in front of β-strands 5, 6, and 7 (Fig. 2). The copper ligand residues are all located on the β-barrel except for His-61, which belongs to loop IV like the other zinc ligand residues.

The catalytic center is the copper ion, which is coordinated by four histidines (His-44, His-46, His-61, and His-118) and by a weakly bound water molecule in a geometry sometimes described as a distorted square pyramid (square planar) and sometimes as a distorted flattened tetrahedron (Fig. 7).

In any case, the Cu(II) site deviates markedly from an ideal coordination geometry. The water molecule occupies the apical position toward the opening of the cavity. The zinc ion is bound to three histidines (His-61, His-69, and His-78) and to an aspartate residue (Asp-81) in an al-

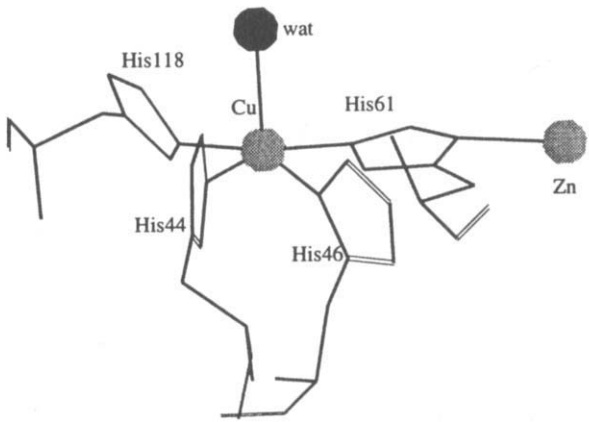

FIG. 7. Sketch of the copper coordination polyhedron obtained from the 2SOD crystal structure. The copper and zinc atoms and the water molecule are represented by spheres of arbitrary radius.

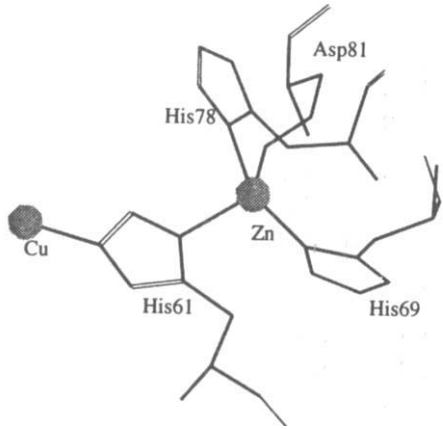

FIG. 8. Sketch of the zinc coordination polyhedron obtained from the 2SOD crystal structure. Copper and zinc are represented by spheres of arbitrary radius.

most regular tetrahedral geometry (Fig. 8). For a long time the zinc ion was believed to play merely a structural role in the enzyme; indeed it may be replaced by several other metals [Co(II), Cu(II), Cd(II), Hg(II)] with only a minor loss in activity with respect to native enzyme.

In this monoclinic form (space group $C2$) of the bovine Cu_2Zn_2SOD there are four independent subunits: no significant differences have been found in the metal site geometries of the four subunits. Figure

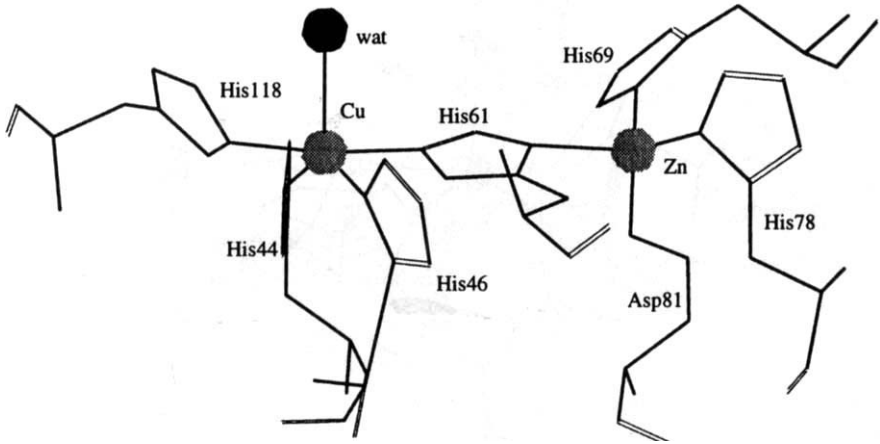

FIG. 9. Overall view of the metal coordination in the active site obtained from the 2SOD crystal structure. The metals and the water interacting with copper are represented by spheres of arbitrary radius.

9 shows an overall view of the metal coordination as determined in the 1982 crystal structure.

The unique feature of this metal site is that one of the histidines, His-61 in the bovine enzyme sequence, provides an imidazolate ligand to the two metals, bridging zinc and copper by binding them through the Nδ1 and Nε2 atoms of its pentaatomic ring, respectively. Such coordination brings the two cations to a distance of about 6.5 Å. Spectroscopic data have suggested that the imidazolate bridge is stable over the whole pH range where SOD activity is invariant (pH 5.0–9.5) (*52*). Indeed, the bridge has been observed unbroken in crystals of Cu_2Zn_2SOD obtained in the pH range 5.0–7.5 (*vide infra*). Imidazolate bridges between two metal ions are common in small molecule complexes, but this is the only case so far that such a ligand has been found in a protein. Studies on model compounds have shown that the binding of a metal ion to a histidine imidazole nitrogen can lower the pK_a of the other NH group by several pH units (*53*). The metal ion binding to histidine thus promotes the substitution of the free NH proton by a second metal ion so to cause an apparent reduction of the pK_{a2} of the histidine imidazole ring from 14.4 to below 5.0, a step of about 10 pH units.

It is important to point out that the shape of the active site cavity and the disposition of the copper ligands are such that the only access to the copper coordination is from the opening of the cavity, where a fifth coordination position is available for the substrate or the inhibitors. Indeed, in the crystal structures, every exogenous ligand is found bound to such position, which is usually associated with weaker bonding to the square planar cupric ion. Only the strongest ligands, such as azide and cyanide, are able to make a close approach to Cu(II) by causing the loosening of the Cu(II)–His-46 bond (see Section II,J). These structural aspects of the active site have obvious mechanistic implications that will be discussed in Section IX.

The orientation of the metal ligands is determined by a series of hydrogen bonds forming a complex network. All the potential H-bonding atoms of the seven groups acting as metal ligands are involved in hydrogen bonding with other protein atoms. Exceptions are provided by two of them, and these are exposed to the solvent: the His-61 peptide NH group, which is H-bonded to a water molecule in the active site channel, and the His-69 carbonyl oxygen, which is H-bonded to a water molecule external to that channel.

The zinc coordination bonds involve only the zinc-binding region of loop IV, and the residues that are H-bonded to Zn ligands are also located mainly in that region of the monomer (Asn-63, Lys-67, Lys-68, Arg-77, His-78, and Asp-81) or in loop VII (Asp-122 and Thr-133).

The Cu ligands instead join strands 6 and 7 with loop IV. The residues that are H-bonded to the Cu ligands involve β-strands 6 (His-41, Gly-42) and 7 (Thr-114, Val-116) as well as loop VII (Asp-122, Gly-139) and both regions of loop IV (Gly-59 in the disulfide region, Asn-63 in the zinc binding region).

Tainer *et al.* (*41a*) argue that the larger number of different structural elements brought together by the Cu binding network with respect to the Zn network may account for the larger effect of Cu site occupancy on the thermal stability of the enzyme. Indeed it has been shown that removal of the copper ion causes a greater lowering of the thermal denaturation temperature of the enzyme than does removal of the zinc ion (*54*). For a long time it has been noted that the involvement of residues from multiple structural elements and the wide separation in the amino acid sequence of metal ligands are characteristic of catalytic sites as opposed to structural or storage sites (*55*).

In all four independent monomers present in the asymmetric unit of the Cu_2Zn_2SOD monoclinic structure, there is a second bridge between Cu and Zn. This is made by the H bonds that link the Zn ligand His-69 with the Cu ligand His-44 through the fully deprotonated carboxyl group of Asp-122. This group is completely buried and inaccessible to the solvent and forms short, strong, charged H bonds with the above histidine residues, whose electron density is very well defined in all subunits. Residue Asp-122 is invariant in SOD sequences, and helps to properly orientate the Cu and Zn ligands. Tainer *et al.* (*41a*) have suggested that the H bonds between Asp-122, His-44, and His-69 may have a role in determining the reduction potential of the Cu(II) ion.

Table I reports the crystal structures of Cu_2Zn_2SOD enzymes so far determined and deposited with the Brookhaven Protein Data Bank (*47*). It should be noticed that Cu_2Zn_2SOD has the ability to crystallize in different space groups depending on the crystallization conditions. This suggests that the protein has the ability to make different intermolecular contacts with different groups depending on the pH and the medium used for crystallization. The variability of Cu_2Zn_2SOD crystal forms provides a unique opportunity to analyze and rationalize the factors influencing its crystal packing, and this has not yet been exploited.

The SOD dimer has been described as generated by the action of a dyad axis on one of the monomers. The two monomers are very similar, but an analysis of the coordinates deposited with the PDB shows that there are significant deviations from the binary symmetry involving the main polypeptide chain and also the active sites (obvi-

TABLE I

PUBLISHED CRYSTAL STRUCTURES OF Cu_2Zn_2SODs (EC 1.15.1.1)[a]

Source: Bovine erythrocytes (*41*)
PBD code, 2SOD; space group, $C2$; $Z = 4$
Cell: $a = 93.65$, $b = 90.33$, $c = 71.65$, $\beta = 95.1$
Asymmetric unit content: two dimers
Max. resolution, 2.0 Å; completeness, NR; R_m, NR; R, 0.255

Source: Human erythrocyte, recombinant, expressed in yeast (*S. cerevisiae*) (*63*)
PDB code; 1SOS; space group, $C222_1$; $Z = 8$
Cell: $a = 205.2$, $b = 167.0$, $c = 145.5$
Asymmetric unit content: five dimers
Max, resolution, 2.5 Å; completeness, 81.5%; R_m, NR; R, 0.210

Source: Human erythrocyte, recombinant, expressed in yeast (*S. cerevisiae*) (*18*)
PDB code, 1SPD; space group, $P6_3$; $Z = 6$
Cell: $a = b = 113.5$, $c = 71.5$
Asymmetric unit content: one dimer
Max. resolution, 2.4 Å; completeness, 89.8%; R_m, NR; R, 0.224

Source: *Xenopus laevis,* expressed in *E. coli* (*49*)
PDB code, 1XSO; space group, $P2_12_12_1$; $Z = 4$
Cell: $a = 73.33$, $b = 68.86$, $c = 59.73$
Asymmetric unit content: one dimer
Max. resolution, 1.5 Å; completeness, 98.8%; R_m, 0.078; R, 0.104

Source: Yeast (*S. cerevisiae*), 277 K (*74*, *75*)
PDB code, 1SDY; space group, $P2_12_12$; $Z = 4$
Cell: $a = 105.3$, $b = 143.0$, $c = 62.1$
Asymmetric unit content: two dimers
Max. resolution, 2.5 Å; completeness, 98.2%; R_m, 0.06; R, 0.158

Source: Spinach leaves (*72*)
PDB code, 1SRD; space group, $C2$; $Z = 4$
Cell: $a = 166.27$, $b = 45.97$, $c = 85.68$, $\beta = 99.38$
Asymmetric unit content: two dimers
Max. resolution, 2.0 Å; completeness, NR; R_m, 0.048; R, 0.249

Source: Yeast (*S. cerevisiae*) reduced, 93 K (*56*)
PDB code, 1JCV; space group, $R32$; $Z = 12$
Cell: $a = 118.39$, $b = 118.39$, $c = 73.50$
Asymmetric unit content: one monomer
Max. resolution, 1.55 Å; completeness, 86.7%; R_m, 0.092; R, 0.190

Source: Yeast (*S. cerevisiae*), reduced (*56*)
PDB code, 1JCW; space group, $R32$; $Z = 12$
Cell: $a = 119.28$, $b = 119.28$, $c = 75.05$
Asymmetric unit content: one monomer
Max. resolution, 1.7 Å; completeness, 82.3%; R_m, 0.099; R, 0.186

Source: Yeast (*Candida albicans*), reduced (*56*)
PDB code, 1YSO; space group, $R32$; $Z = 12$
Cell: $a = 119.33$, $b = 119.33$, $c = 75.19$
Asymmetric unit content: one monomer
Max. resolution; 1.73 Å; completeness, 92.4%; R_m, 0.063; R, 0.182

Source: Bovine erythrocytes, reduced, 277 K (*48*, *82*)
PDB code, 1SXA; space group, $P2_12_12_1$; $Z = 4$
Cell: $a = 47.89$, $b = 51.14$, $c = 148.15$
Asymmetric unit content: one dimer
Max. resolution, 1.9 Å; completeness, 90.5%; R_m, 0.073; R, 0.166

Source: Bovine erythrocytes, reduced, 277 K (*48*, *82*)
PDB code, 1SXB; space group, $P2_12_12_1$; $Z = 4$
Cell: $a = 47.71$, $b = 50.98$, $c = 147.82$
Asymmetric unit content: one dimer
Max. resolution, 2.0 Å; completeness, 98.0%; R_m, 0.076; R, 0.152

Source: Bovine erythrocytes, reduced, 277 K (*48*)
PDB code, 1SXC; space group, $P2_12_12_1$; $Z = 4$
Cell: $a = 47.89$, $b = 51.14$, $c = 148.15$
Asymmetric unit content: one dimer
Max. resolution, 1.9 Å; completeness, 97.0%; R_m, 0.100; R, 0.156

Source: Bovine erythrocyte mutant Cys-6Ala, 277 K (*80*)
PDB code, 3SOD; space group, $C2$; $Z = 4$
Cell: $a = 92.5$, $b = 89.4$, $c = 70.5$, $\beta = 95.7$
Asymmetric unit content: two dimers
Max. resolution, 2.1 Å; completeness, 82.0%; R_m, 0.099; R, 0.190

Source: Bovine erythrocytes, zinc substituted by cobalt, 277 K (*76*)
PDB code, 1COB; space group, $P2_12_12_1$; $Z = 4$
Cell: $a = 51.0$, $b = 147.6$, $c = 47.5$
Asymmetric unit content: one dimer
Max. resolution, 2.0 Å; completeness, 75.2%; R_m, 0.068; R, 0.176

Source: Bovine erythrocytes nitrated at Tyr-108 (*79*)
PDB code, 1SDA; space group, $C2$; $Z = 4$
Cell: $a = 93.65$, $b = 90.33$, $c = 71.65$, $\beta = 95.1$
Asymmetric unit content: two dimers
Max. resolution, 2.5 Å; completeness, 89.0%; R_m, 0.033; R, 0.187

Source: *Xenopus laevis,* native, complex with cyanide, 98 K (*87*)
PDB code, 1XSO; space group, $P2_12_12_1$; $Z = 4$
Cell: $a = 72.15$, $b = 68.10$, $c = 57.57$
Asymmetric unit content: one dimer
Max. resolution, 1.7 Å; completeness, 85.9%; R_m, 0.051; R, 0.172

(*Continues*)

TABLE I (*Continued*)

Source: Bovine erythrocytes, reduced, complex with azide, 277 K[b] PDB code, 1SXZ; space group, $C222_1$; $Z = 8$ Cell: $a = 104.6$, $b = 197.5$, $c = 50.8$ Asymmetric unit content: one dimer Max. resolution, 2.0 Å; completeness, 87.8%; R_m, 0.074; R, 0.165	Source: Bovine erythrocytes, native, complex with azide, 277 K (*90*) PDB code, not in PDB; space group, $P2_12_12_1$; $Z = 4$ Cell: $a = 50.99$, $b = 147.63$, $c = 47.53$ Asymmetric unit content: one dimer Max. resolution, 2.1 Å; completeness, 96.6%; R_m, 0.083; R, 0.166
Source: Bovine erythrocytes, reduced, complex with thiocyanide, 277 K[b] PDB code, 1SXS; space group, $C222_1$; $Z = 8$ Cell: $a = 104.6$, $b = 197.5$, $c = 50.8$ Asymmetric unit content: one dimer Max. resolution, 2.0 Å; completeness, 96.9%; R_m, 0.076; R, 0.175	

[a] Cell dimensions are in angstroms, cell angles are in degrees. The crystal structures have been determined at room temperature if not stated explicitly. NR, Not reported. $R_m = \Sigma|I_i - \langle I\rangle|/\Sigma\langle I\rangle$, where I_i is an individual intensity measurement, and $\langle I\rangle$ is the average intensity for this reflections; the sum is over all reflections. R is a conventional crystallographic agreement factor. PDB, Protein Data Bank.

[b] From Ref. *83b*.

ously the amino acid side chains respect less the dyadic symmetry). Table II lists the intradimer root-mean-square (RMS) deviations, relative to the Cα atoms of the Cu_2Zn_2SOD main chain. It can be seen that the average RMS deviation of Cα ranges between 0.25 and 1.13 Å with maximum deviations up to 5.1 Å. By considering that the reported error on the atomic positions from the crystallographic analysis is at most 0.20–0.25 Å, it may be concluded that the structure of Cu_2Zn_2SOD is far from being related by a dyad axis, and any discussion about the symmetry is in most cases only a rough approximation.

In only one case the Cu_2Zn_2SOD dimer has been observed to lie on a crystallographic twofold axis. This occurs in the three structures of Cu_2Zn_2SOD from yeast and fungii, which have been crystallized in the trigonal space group $R32$ (*56*) (see Section II,I,3). The single crystals were obtained from ammonium sulfate and sodium chloride at pH 7.5. Three different structure determinations were carried out both at room temperature and at 93 K. The crystal asymmetric unit consists of only one monomer because the dimer lies on the special positions of point symmetry two.

The differences observed in Cu_2Zn_2SOD crystal structures are indicative of flexibility (i.e., the ability to adopt slightly different conformations depending on the crystallization conditions), which is mainly due to extensive loop structure.

The main features of Cu_2Zn_2SOD so far described, namely the β-barrel, the disulfide bridge, and the metal ligands, are conserved among the different structurally determined dimers. Inspection of the

TABLE II

ROOT-MEAN-SQUARE DEVIATIONS AND MINIMUM AND MAXIMUM DISPLACEMENT[a]

Structure	RMSD (Å)	Min	Max
1COB	0.335	0.251	1.687
1SDA	0.398(OY)	0.299	2.425
	0.360(BG)	0.286	1.614
1SDY	0.672	0.348	5.113
2SOD	0.833(OY)	0.597	3.963
	0.737(BG)	0.522	2.458
1SOS	0.346(AF)	0.296	1.041
	0.325(BG)	0.290	0.758
	0.254(CH)	0.231	0.948
	0.425(DI)	0.348	2.051
	0.376(EJ)	0.324	1.667
1SPD	1.130	0.939	4.337
1SRD	0.299(AB)	0.264	0.885
	0.316(CD)	0.291	0.677
1SXA	0.294	0.251	1.340
1SXB	0.293	0.217	1.289
1XSO	0.359	0.216	2.911

[a] From the best fit of backbone Cα atoms of the SOD chain within the dimeric structures. The letters in parentheses are the monomer chain identification used in the Brookhaven Protein Data Bank (PDB) files. Coordinates are from the crystal structures released in the PDB (*47*). In cases in which the crystal structure consists of more than one dimer in the asymmetric unit, the corresponding values are reported and the naming of the monomers constituting the dimer couple follows the naming reported in the PDB. The calculations have been performed with the CCP4 suite of programs for protein crystallography (*341*).

structures reveals that the main differences in folding are located in the loops and turns connecting the eight β-barrel strands.

5. *The Cu_2Zn_2SOD Quaternary Structure: The Monomer / Monomer Interface*

The contact surface between the monomers (Fig. 10) comprises the N terminus and β-strand 1 (residues 1–7), the C terminus and β-strand 8 (residues 146–151), and the two loop regions between residues 47–52 in loop IV and 100–112 in loop IV (the Greek key loop).

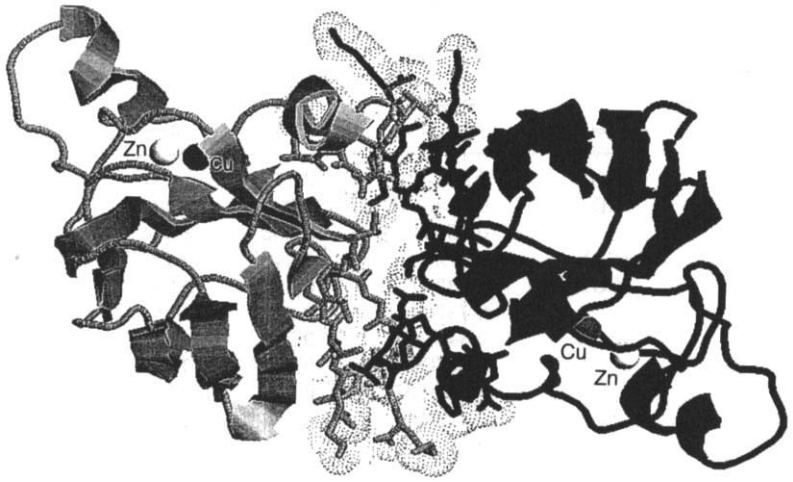

FIG. 10. The monomer/monomer interface in the 2SOD dimer represented as the dotted Connolly surface (*348*, *349*) of the residues facing the two monomers, which are represented in full as sticks superimposed on the ribbon diagram of the enzyme.

The extension of the contact region explains the high stability of the dimer to thermal and chemical denaturation. The enzyme is stable up to 353 K and remains active in 4% sodium dodecyl sulfate and in 8 *M* urea (*31*, *57–59*).

Highly optimized hydrophobic interactions can be observed across the monomer–monomer interface between residues related by the noncrystallographic twofold axis, e.g., the conserved residues Ile-111 and Val-146. Hydrophobic packing also involves Ala-4 with Leu-106 from the other monomeric unit. Mutations of residues in the interface region can lead to disruption of the quaternary structure, resulting in the formation of stable SOD monomers. Replacement of the human enzyme's two interface residues Phe-50 and Gly-51 with Glu has resulted in a stable, soluble SOD monomer that is almost devoid of catalytic activity (*60*).

Formation of natural mutants of the corresponding interface residues of human Cu_2Zn_2SOD in familial amyotrophic lateral sclerosis (FALS) has been demonstrated (*18*).

B. HUMAN Cu_2Zn_2SOD

Human Cu_2Zn_2SOD has been expressed in yeast (*61*, *62*) and its crystal structure determined at 2.5 Å resolution (*63*). The crystals belong to the $C222_1$ space group and contain five SOD dimers in the

asymmetric unit. The five dimers form honeycomb-like layers in the *ab* crystal plane. The layers are stacked so as to leave in the crystal lattice open channels that contain solvent (>68% by weight). The human enzyme contains 153 residues. The insertion of two residues in the bovine enzyme has little effect on the structure except for the loop where the insertion takes place, at position 25. The overall tertiary structure and the active site are conserved. The authors note a feature that was overlooked in the bovine enzyme analysis, namely, that the short six-residue helix present in SOD is oriented so as to stabilize, and be stabilized by, the Zn^{2+} cation in a favorable dipole–charge interaction. The zinc binding seems to contribute to the appropriate conformation of the electrostatically important residues Glu-132, Glu-133, and Lys-136, which are conserved throughout the sequences and are thought to be involved in substrate recognition (*45*, *64*).

The crystal structure of wild-type human SOD has also been determined, (space group $P6_3$) and refined to 2.4 Å resolution (see Table I) (*18*).

C. *Xenopus laevis* Cu_2Zn_2SOD

The South African frog *Xenopus laevis* has the peculiarity of having duplicated genes in its genome. Consequently, two isoenzymes of Cu_2Zn_2SOD with different amino acid sequences have been identified (*65*). The two isoenzymes X-SODa and X-SODb, are characterized by different thermal stabilities (*66*). The existence of two different *a* and *b* monomers gives rise, on association in the dimer, to three different isoenzymes of *aa*, *ab*, and *bb* composition, having different stabilities. The most stable X-SODb homodimer has been expressed in *E. coli* (*67*) and subjected to crystallographic analysis (*68*). It crystallyzes in the orthorhombic space group $P2_12_12_1$ (see Table I) with one dimer in the asymmetric unit. The monomer contains 150 amino acid residues, and shares a high degree of homology (>50%) with other known SODs. The crystals provided a complete data set (98.8%) to 1.49 Å resolution when X-rays from a synchrotron source were used. The structure has been refined to a very low final crystallographic *R* factor of 0.104 for all 49,209 reflections by using simulated-annealing and energy minimization techniques, followed by restrained least-squares refinement and finally by anisotropic refinement of all nonhydrogen atoms. The nonpolar H atoms have been introduced at calculated positions after the restrained refinement, converging to an *R* factor of 0.145. During the following anisotropic refinement of the nonhydrogen atoms in which the restraints on the metal–ligand distances were released, the *R* factor dropped to the final value of 0.104. The re-

sulting model has a very good geometry with small deviations from ideality. The anisotropic refinement satisfies the Hamilton test (*69*), which ensures that the data have not been overfitted, but the authors do not comment about improvement of the model obtained after anisotropic refinement, with respect to the model obtained from the more conventional restrained least-squares refinement at $R = 0.145$.

The X-SODb has the same overall tertiary and quaternary structure of all Cu_2Zn_2SODs reviewed so far, resulting in quite low values of 0.726 and 1.170 Å for the RMS deviations of the Cα atoms in the bovine and yeast enzymes, respectively. The SOD fold shows once again its robustness. Indeed, the several amino acid substitutions and the insertion in the bovine enzyme are absorbed well by the structure, the only substantially different part of it being the turn between residues 89 and 92, where a one-residue deletion occurs with respect to the bovine enzyme. It is of particular interest that the 10 substitutions of Pro and Gly residues in X-SODb and bovine SOD do not result in any evident changes in backbone conformations.

Site 149 of the X-SODb sequence is occupied by a Tyr residue, which is rather uncommon in SODs. The structure reveals that this tyrosine is involved in two intermolecular contacts related by the noncrystallographic twofold axis between the two monomers. The residues interacting with Tyr-149 are Phe-62 of the same subunit and Arg-113 of the other subunit. It is proposed that the increased thermostability of the XSODb homodimer with respect to the other possible dimers built with the *a* isoenzyme is due to these two interactions.

The active site structure is similar to the other metal sites in Cu_2Zn_2SODs, the only noticeable difference being the accurate observation of a shorter Cu(II)–water distance of 2.26 and 2.48 Å in the A and B subunits, respectively. In this site the noncovalent interactions responsible for the orientations of the ligands forming the metal binding site are conserved.

Once again a well-defined network of hydrogen-bonded water molecules is observed extending from the active site in two opposite directions spanning the cavity openings, reinforcing the proposal of an active role of the water in the enzyme mechanism (see Section IX).

D. Spinach Cu_2Zn_2SOD

SODS are present in plants, and Cu_2Zn_2SOD has been obtained from spinach leaves (*70*). Its amino acid sequence shares 55% homology with the bovine enzyme (*71*). The monomer contains 154 amino acids, three more than the bovine enzyme.

The structure has been determined at 2.0 Å resolution using a data

set obtained by merging data collected on a four-circle diffractometer from 25 different crystals (*72*). The crystals belong to the space group *C*2, the same as bovine SOD, but have a different unit cell (see Table I). The overall structure of this plant SOD is very similar to that of bovine erythrocyte SOD. However, the RMS deviation obtained from the best fit of the spinach and bovine SOD Cα and metal atoms (except for the three N-terminal residues) is 1.10 Å. Nevertheless, the topology of the two structures is identical. The metal ligands and functionally important residues Asp-124, Thr-137, Gly-141, and Arg-143 are conserved. A relevant difference between the bovine and spinach enzymes is that the copper-bound water molecule has not been detected in the latter structure. The authors do not report the completeness of the data, nor the figures relative to the quality of the data set used for refinement. This makes it difficult to compare and discuss confidently the observed small differences with the bovine enzyme active site model.

A major structural difference with respect to the bovine enzyme is found in the N-terminal region, where the spinach SOD has the insertion of an Asp residue in a turn at position 26. The turn is then enlarged and has a different conformation. Furthermore, the peptide NH group of Asp-25 is hydrogen bonded to the carbonyl oxygen of Ala-1; this H-bond is not present in bovine SOD and is responsible for a different extended conformation of the N-terminal region in the spinach enzyme. The H bond from Ala-1 to Asp-25 connects the Glu-24–Asp-26 turn region with the N terminus, causing a rigid, stable conformation of this part of the molecule. A second difference is found in the region near Val-33 and Ala-97 in the β-barrel. Val-33 is located in strand 3 and Ala-97 in strand 6, but they are adjacent in the tertiary structure, though they are far apart in the sequence. The corresponding residues in bovine SOD are Gly-31 and Val-95. The side chain of Val-33 in spinach SOD occupies the same spatial position of the Val-95 side chain in bovine SOD. The double exchange of a bulky residue with a small residue, and of a small residue with a bulky one, has no effect on the β-barrel, and maintains its structure unchanged. This finding brings forward the interesting observation that the same stabilization effect on the β-barrel structure, by side-chain interactions, has been achieved in different ways in the spinach and bovine enzymes, through concerted mutations allowing for the exchange of the complementary side chain of residues that may be far apart in the sequence.

E. Yeast Cu_2Zn_2SOD

Yeast SOD has been obtained and crystallized from the yeast *S. cerevisiae* (*73*). It has the same dimeric structure as the bovine and

spinach enzymes. Each subunit has 153 amino acids and shares a 55% homology with the bovine enzyme. Yeast SOD crystallizes in the space group $P2_12_12$ with a cell containing two dimers per asymmetric unit (see Table I). The structure has been solved by the molecular replacement technique using a bovine SOD monomer as a starting model. The refinement has been carried out in two stages. In the first one consecutive molecular dynamics and conventional restrained least-squares refinement led to a crystallographic R factor of 0.22 for the data between 6.0 and 2.5 Å (*74*). Subsequently, the structure was further refined to $R = 0.158$ by completing the model with the introduction of 516 water molecules (*75*).

The overall β-barrel and loop structure of Cu_2Zn_2SOD is maintained, despite an overall RMS deviation of 0.977 Å between the α-carbons of yeast and bovine SOD. The largest differences between the two structures occur at two insertion sites (residues 23–25 and 35–38) in loops II (2, 3) and III (3, 6), and at the interface between the two dimers (residues 127 and 128). The structure of the active site appears to be conserved in the bovine enzyme, with only minor differences in the overall geometry.

F. Bovine Cu_2Co_2SOD

Cobalt(II) has been used as a chromophoric probe to replace the spectroscopically and magnetically silent zinc(II), hence allowing the accumulation of a wealth of information on the system (see Section VIII). Furthermore, Cu_2Co_2SOD displays full enzymatic activity. Its crystal structure has been determined at 2.0 Å resolution (*76*). The crystals of Cu_2Co_2SOD belong to the space group $P2_12_12_1$ (see Table I), and despite the use of synchrotron radiation as the X-ray source, provide a 75.2% complete data set between 10.0 and 2.0 Å. The refinement has been carried out with a mix of molecular dynamics and conventional restrained least-squares methods, resulting in a model of almost ideal geometry and a final crystallographic R factor of 0.176. Again, the overall fold of SOD is preserved with only minor differences occurring in the loop regions. Despite the metal substitution, the active site structure shows small differences with respect to the native enzyme. The cobalt substitution does not perturb the active site. A water molecule has been clearly observed bound to Cu(II) at 2.38 Å, from which a network of H-bonded water molecules originates. The authors of the paper (*76*) note that most of the waters lie in the same positions as in the yeast enzyme, and propose that they help to stabilize the protein tertiary structure and may even have a role in catalysis.

G. Peroxynitrite-Modified Cu_2Zn_2SOD

The recent discovery that nitric oxide (NO) is a signaling molecule ubiquitous in tissue has raised the question that one of the pathways contributing to superoxide toxicity *in vivo* might be the formation of the highly reactive peroxynitrite anion ($ONOO^-$) produced by spontaneous reaction of NO with superoxide (*77*). It has been shown that peroxynitrite is a substrate of SOD (*78*). The interaction of SOD with peroxynitrite leads to a permanent modification of the enzyme at Tyr-108. The structural determination of the peroxynitrite-modified Cu_2Zn_2SOD has been conducted on monoclinic crystals (*79*). The structure confirms that peroxynitrite permanently modifies the Tyr-108 side chain with formation of 3-nitrotyrosine. The modification does not alter active site residues and the enzyme remains fully active.

H. Mutants of Cu_2Zn_2SOD

1. The Cys-6Ala Mutant of Bovine Cu_2Zn_2SOD

The crystal structure of the Cys-6Ala mutant of bovine SOD has been determined as part of a study aimed at investigating the role of this cysteine on the thermostability of Cu_2Zn_2SOD, and in an effort to understand and control the stability of the protein (*80*). The structure of the native enzyme shows that Cys-6 is buried in the β-barrel, where it makes hydrophobic interactions with neighboring chains. However, on heating it appears to form irreversible aggregates that prevent refolding. It appears that thermal inactivation occurs at a temperature lower than the melting temperature. The thermal scanning calorimetry profile of the mutant is consistent with either a two-step denaturation process or with the presence of two different species having different thermal stabilities (*80*). The mutation to Ala has proved effective in decreasing the rate of irreversible thermal denaturation, when incubated at 70°C for 180 min, despite causing the lowering of the melting temperature of the two putative components of the mutant enzyme with respect to the native enzyme. The crystal structure of the mutant has provided evidence for a concerted movement of the β-strand residues near the mutation site with respect to the native enzyme.

The authors propose that the observed shifts allow the enzyme to compensate for the energetic cost of the mutation by improving the packing and stereochemistry of the mutant molecule (*80*).

2. *The Cys-6Ala, Cys-111Ser Double Mutant of Recombinant Human Cu_2Zn_2SOD*

The double mutant Cys-6Ala, Cys-111Ser of human SOD gives crystals isomorphous with those of human SOD ($C222_1$) (see Section II,B). Alanine and serine are residues naturally occurring in other SODs at these positions. The double mutant is more stable than each of the single mutants to irreversible thermal denaturation, and all of them are more stable than the native enzyme, probably because of the removal of the reactive thiol groups.

The crystal structure shows that Ser-111 stabilizes the loop where it resides (the Greek key loop) by forming two H bonds with the carbonyl oxygen and the amide nitrogen of residues 106 and 113, respectively. In the wild-type human SOD crystal structure, Cys-111 is found to be involved in these H bonds in only 2 of the 10 independent subunits. The authors conclude that such intraloop side-chain to main-chain hydrogen bonds can thermodynamically stabilize the enzyme and, together with the zinc helix-dipole motif (see Section II,B), may provide a hint on how to modify the activity and the stability of human SOD and other β-barrel proteins.

I. Reduced Cu_2Zn_2SODs

One of the outstanding issues concerning the SOD mechanism involves the structure of the reduced enzyme. This point has been addressed by several authors attempting to provide a structural basis for Cu(I) as the catalytic species in SOD.

The first report of a reduced SOD structure was made in a preliminary announcement of the observation of a break in the histidinato bridge between copper and zinc, from studies on a reduced monoclinic form of bovine SOD (*81*). However, a full report has yet to appear in the literature, and the coordinates of the structure have not yet been released in the PDB.

1. *Reduced Bovine Cu_2Zn_2SOD at pH 7.5*

A second study reports two independent structural determinations on crystals obtained under anaerobic conditions from solutions of the reduced enzyme (*48*, *82*) at pH 7.5. The crystals are isomorphous with those of Cu_2Co_2SOD (*76*). In order to check the reproducibility of the experiment, two independent data sets were collected at

a synchrotron source on crystals from different batches. A third data set was obtained by merging the two experimental data sets so as to obtain a higher quality data set and hence a better final model. The refinement has been performed on all the three data sets. The metal centers were left unrestrained throughout all the refinement cycles. The final R factors were 0.166, 0.153, and 0.156 for the two independent and for the merged data sets, respectively. The reduced state of the copper in the crystals was proved by electron paramagnetic resonance (EPR) spectroscopy which shows no evidence of a Cu(II) signal in the crystal used for data collection nor in those from the same crystallization batch. The refinement procedure has provided a quite accurate model of the enzyme at 1.9 Å resolution in which, contrary to expectations, the copper coordination appears conserved with respect to the native oxidized form of the enzyme. Indeed, His-61 is found bridging copper and zinc in both subunits of the two independent structures. Only an overall increase in the Cu–ligand bond lengths has been observed. It should be noted that the difference in Cu–N bond length between Cu(II) and Cu(I) coordination compounds having the same coordination number is much less than 0.1 Å as observed in Schiff base, *N*-alkylpyrazole, phenantrolines, and tertiary amine copper complexes (*83a*). Only in chelating dioximes is a lengthening of 0.16 Å found on going from Cu(II) to Cu(I) (*83a*), which is about the estimated standard deviation in bond lengths found for the above SOD structures.

Apart from the His-61 bridge, the two structures reveal significant differences in the coordination geometry of the copper sites in the two subunits (A and B). In the A subunit the copper geometry can be described as a flattened tetrahedron with the water molecule interacting only weakly with it at 3.0 Å. In the B subunit the Cu(I) coordination is better respresented by a trigonal bipyramid having as the basal plane His-44, His-46, and the water molecule (at ~2.5 Å), with His-61 and His-118 in the axial positions.

A covalent modification of the Glu-119 side chain has been observed in this structure. An unexpected electron density of approximately 10 e^- has been found extending from one of the Glu-119 carboxylate oxygen atoms and could not be unambiguously assigned. The authors report that a similar density was also observed in the crystal structure of the oxidized enzyme so as to exclude a modification due to the dithionite used for reduction of the enzyme. The proximity of the modification to the active site suggests that it may affect the catalytic mechanism (*48*).

2. *Reduced Bovine Cu_2Zn_2SOD at pH 5.0*

The same research group has reported that crystal structure, at 2.0 Å resolution, of the reduced bovine enzyme obtained from crystals grown at pH 5.0 (*83b*). The crystals belong to the orthorhombic space group $C222_1$ with cell dimensions $a = 104.6$, $b = 197.5$, and $c = 50.8$ Å. This crystal form is characterized by a high solvent content, estimated at 73% from a $V_m = 4.5$ Å^3/Da. The packing of the Cu_2Zn_2SOD dimers is such that one of the two subunits makes very few intermolecular contacts with respect to the other in the crystal lattice. In other words, one subunit has a solution-like environment, being surrounded almost completely by water. This is reflected in an almost double average temperature factor for all the atoms of that subunit with respect to the other, indicating a larger mobility of the molecule.

The crystal structure shows a marked difference in the copper environments in the two monomers. In one of the subunits two electron density maxima are observed riding the cuprous ion in place of the usual density expected for the weakly bound water molecule. This is a two-center density that can be modeled with two water molecules at full occupancy, each being at coordinating distance from the metal ion, resulting in the unusual geometry shown in Fig. 11. The electron density could not be unambiguously interpreted because it can be modeled as well by a disulfide anion at about half occupancy. Such an anion may have been originated from the dithionite used for copper reduction.

On the contrary, the copper site in the solution-like subunit does

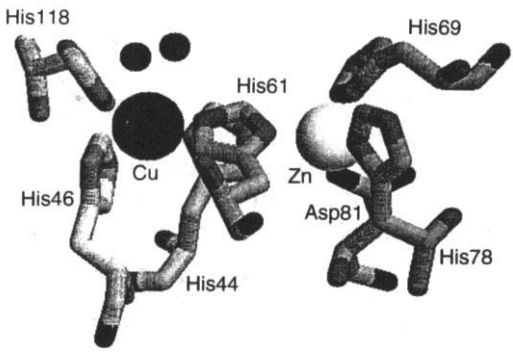

FIG. 11. The "anomalous" copper coordination sphere found in the crystal structure of reduced bovine Cu_2^I Zn_2SOD at pH 5.0. The metals and the two unknown atoms at bonding distance from Cu(I) are represented as spheres of arbitrary radius. The metal ligands are represented in full as sticks.

not show anything similar. Moreover, in this subunit the bridging ligand, His-61, is found disordered and away from the cuprous ion. It cannot be modeled properly because the electron density corresponding to the ring Nε2 nitrogen is missing. It appears to have moved away from the metal at about 3.0 Å. The metal appears to be disordered over two positions.

This finding indicates a possible detachment of the bridging His-61 in the structure and seems to confirm the flexibility of the copper site and its ability to shift between two different coordination geometries. The His-61 detachment from Cu(I) may be facilitated by the low pH, which favors protonation of the His-61 Nε2.

3. *The Reduced Yeast Cu_2Zn_2SOD at pH 7.7*

Three high-resolution tridimensional structures of a new crystal form of yeast Cu_2Zn_2SOD have been reported (*56*). Two independent determinations were conducted at room temperature and the third one at −180°C. The crystals belong to the rhombohedral space group *R*32 (see Table I). In this crystal form the SOD dimer sits on an exact crystallographic dyad axis so that the independent part of the molecule is made up by only one monomer. It is the first time that exact twofold symmetry has been observed for a dimeric SOD molecule. The crystals diffract to a limit of 1.70 and 1.73 Å at room temperature and to 1.55 Å at cryogenic temperature. However, in the last resolution shells the observed data cover between 41 and 55% of the theoretically possible reflections. The structures have been solved by molecular replacement, using as a starting model the yeast Cu_2Zn_2SOD previously reported or the A1A2 dimer of human Cu_2Zn_2SOD adequately modified to represent the primary structure of yeast SOD. The structures have been refined without stereochemical restraints for the active site atoms to *R* factors of 0.186 and 0.182 for the two room-temperature structures and 0.190 for the low-temperature structures.

All three structures show the unexpected result that the copper ion has shifted its position by about 1.0 Å with respect to the orthorhombic yeast SOD structure, leaving the bridging His-63 at 3.16 and 2.93 Å in the two independent room-temperature structures, respectively. The correctness of the copper position has been checked by using an anomalous scattering difference Fourier map (*84*). The movement of the metal also involves His-120 (opposite to His-63), which maintains the usual coordination distance from the copper. The result is that the copper ion appears to be tricoordinate by His-44, His-46, and His-120, and His-63 no longer bridges it with zinc. The authors conclude that despite the absence of any reductant in the

crystallization medium, the coordination of the copper in the three structures is indicative of its reduction to Cu(I), which displays such coordination in small molecule compounds.

The authors support this conclusion by showing the EPR spectra of a crystal compared with that of the original protein solution used for crystallization, with that of the same crystal dissolved in an equal volume of buffer and with the same solution 12 hr after the exposure to oxygen. All the spectra show the characteristic Cu(II) EPR lines but with intensities steadily decreasing from the crystallization solution to the crystal, thus indicating a decreasing amount of Cu(II) ions in the different systems.

The above observations deserve a comment about stereochemistry of the yeast SOD active site (which may hold also for the reduced bovine SOD at pH 5.0). The copper–His-63 Nε2 distances observed in the structures are in the range 2.93–3.16 Å, which is longer than the sum of the covalent radii of Cu (in either +2 or +1 oxidation state) and N. However, these distances still appear to indicate close contacts between the copper and the nitrogen. It is difficult to give a proper estimate for the contact distance of a Cu(I) or Cu(II) ion in coordination compounds. In small molecule complexes the intermolecular distances involving mononuclear copper ions are always large because the metals are buried in the ligand matrix. In the cubic $Fm3m$ lattice of metallic copper the second shell of copper atoms is at a distance of 3.61 Å. A safe estimate of the Cu contact distance in its lower oxidation state may hence be taken at about 1.8 Å. Becuase the van der Waals (vdW) radius of nitrogen is 1.55 Å (*85*), the reported positions of copper and His-63 Nε2 are closer than the sum of their contact radii, indicating that there are short contacts between the copper and His-63 in each of the three structures. Furthermore, if a proton (vdW radius = 1.2 Å) is built on the Nε2 of His-63, it points toward copper at a distance of about 2.7 Å, still making close contact with it.

The copper reduction and the following disruption of the Cu–His-62 bridge seem to occur on crystallization. However, analysis of the crystal intermolecular contacts shows there are only few strong protein–protein contacts (not water mediated), mainly occurring in the C-terminal region and in loop IV just before the disulfide bridge (residues 49–52). The latter, even if placed quite far from the metal site, may have an influence on it because they are located in the loop supporting the crucial His-63 ligand. On the other hand, the superposition of the reduced and oxidized yeast SOD structures shows that His-63 has remained in the same place and that detachment is caused by the copper movement.

The structural information available on the reduced state of Cu_2Zn_2 SOD provides a view of the copper site as a very flexible system, where the Cu(I) ion can shift between three- and four-coordination with a water molecule weakly interacting with it, giving rise to 4 + 1 coordination. The latter coordination is commonly observed in small molecule complexes [a recent example is provided by Lee *et al.* (*86*)]. It is noteworthy to point out that a concerted movement of the metal and of some of the ligands seems responsible for the coordination changes observed in the reduced yeast SOD and bovine SOD structures. In the case of yeast SOD it appears that reduction of the copper ion occurs on cyrstallization and that crystal packing does not play a role in the process. On the contrary, in the bovine SOD example, pH and the solution-like environment of one of the subunits seem to be responsible for the probable detachment of the His-61 from Cu(I).

J. Inorganic Anion Complexes of Cu_2Zn_2SOD

The structures of Cu_2Zn_2SOD complexes with small inorganic anions have been determined at different copper oxidation states.

1. *The Crystal Structure of the Cyanide Adduct of Cu_2Zn_2SOD from Xenopus laevis*

The crystal structure of cyanide-inhibited Cu_2Zn_2SOD from *X. laevis* has been determined at 98 K and refined at 1.7 Å to an *R* factor of 0.17 (*87*). Formation of the complex does not affect the overall structure of the protein. In both subunits the cyanide anion is found to be bound to Cu(II) through its C atom at about 2.2 Å. It interacts electrostatically with Arg-141 at 3.3 Å, pointing directly to it with its free end. On binding of the inhibitor the His-46 ligand moves 2.6–2.7 Å from copper, changing the metal coordination polyhedron into a distorted square pyramid. His-46 is at the apex and the cyanide is on the basal plane, confirming what was previously proposed after NMR experiments on Cu_2Co_2SOD (*88*, *89*).

2. *The Crystal Structure of the Azide Complex of Bovine Cu_2Zn_2SOD*

The azide complex crystals have been grown at pH 6.5 in the space group $P2_12_12_1$; the azide complex was prepared by soaking the crystals in a precipitant solution containing 1 *M* NaN_3. The data at 2.1 Å resolution have been refined to an *R* factor of 0.166 (*90*).

The competitive inhibitor azide makes strong coordination bonds of 1.97 and 2.18 Å, respectively, with the Cu(II) ion in the two subunits. Azide replaces the water molecule in the metal coordination and

makes an electrostatic interaction with the positively charged guanidinium group of the Arg-141 residue at a distance of about 3.6 Å. The binding of azide perturbs the copper coordination sphere by causing a shift of about 0.7–0.4 Å of the Cu(II) position with respect to the native enzyme, as is supported by spectroscopic studies (see Section VIII). The movement of copper is accompanied by that of His-118.

As in the cyanide complex, the His-46 coordination distance is lengthened by about 0.4 Å on average. The resulting copper coordination polyhedron is a distorted square pyramid with His-46 at the apical position and azide on the basal plane, paralleling the behavior observed in the cyanide complex. The above results allow rationalization of the previous spectroscopic data (*89*). The zinc coordination is left unaltered.

3. *The Crystal Structures of Azide and Thiocyanate Complexes of Reduced Bovine Cu_2Zn_2SOD*

The structures of the adducts of the competitive inhibitor azide and of the inhibitor thiocyanate with the reduced enzyme have been determined using the $C222_1$ crystal form obtained at pH 5.0 (*83b*). In both structures the inhibitors are found bound to Cu(I), replacing the water molecule(s) close to the metal site. However, their distances from Cu(I) are longer than those found in the oxidized enzyme, being in the range 2.7–2.9 Å. The coordination sphere of Cu(I) is left essentially unaltered by the interaction, as is that of Zn(II). In this case the anions extend in the cavity, having an electrostatic interaction with Arg-141 at 3.1–3.2 Å from its guanidinium group, stronger than in the oxidized enzyme. The thiocyanate anion appears to be bound to copper through the nitrogen atom.

The different behavior with respect to the oxidized enzyme reflects the different preference of Cu(II) and Cu(I) cations for five-coordination. Cu(I) prefers four-coordination, and the interaction with the negatively charged anions looks merely electrostatic, the two ends of the anions being almost equidistant from the two positively charged groups present in the cavity, namely Cu(I) and Arg-141.

The mechanistic implications of the observed anion binding modes in the two oxidation states of the enzyme are discussed in Section IX.

III. Activity

A. Activity Measurements

The ability of an enzyme to perform its function is appropriately measured by enzymatic activity, which follows the Michaelis–Menten

kinetics, i.e. by the parameters obtained using the Michaelis-Menten equation. If reference is made to the Michaelis–Menten reaction scheme [Eq. (7)],

$$E + S \underset{k_{-1}}{\overset{k_1}{\rightleftharpoons}} ES \overset{k_2}{\rightarrow} E + P, \tag{7}$$

saturation of the enzyme E, with the complete transformation into the enzyme–substrate complex ES, is never obtained for SOD (except in one case; see later) because the transformation of ES into free E and the product P is very fast and the amount of substrate is in general small. The rate constants k_1, k_{-1}, and k_2 are defined for single steps. The kinetics can be fitted to Eq. (8),

$$v = k_{cat}[E][S]/(K_m + [S]), \tag{8}$$

where v is the velocity, k_{cat} is the catalytic constant (or turnover number), and K_m is the Michaelis–Menten constant [$K_m = k_1/(k_{-1} + k_2)$]. With a low concentration of substrate (i.e., $[S] \ll K_m$), the velocity $v = k_{cat}[E][S]/K_m$ is referred to as a nonsaturating condition.

Superoxide can be generated by pulse radiolysis of aqueous solutions containing O_2 (*52*, *91–94*). The necessary irradiation is achieved with pulses of high-energy electrons (2–5 MeV), generated by a Van der Graaf linear accelerator. The irradiation also generates some radicals, i.e., OH radicals and H radicals are also formed. Formate, used as buffer (1–10 m*M*), converts all these radicals to superoxide according to reactions (9–11):

$$OH + HCO_2^- \rightarrow H_2O + CO_2^-, \tag{9}$$

$$H + HCO_2^- \rightarrow H_2 + CO_2^-, \tag{10}$$

$$CO_2^- + O_2 \rightarrow O_2^- + CO_2. \tag{11}$$

With formate and O_2 concentrations kept constant, it is possible to calibrate O_2^- concentrations by changing energy and pulse time. The oxygen aqueous solution containing formate is pulsed to generate O_2^- in the presence of varying amounts of enzyme. The decay of O_2^- is monitored spectrophotometrically at 245 nm (the maximum of absorbance of superoxide) as a function of the enzyme concentration, pH, and ionic strength. In the absence of enzyme the spontaneous

disappearance of O_2^- is a second-order process ($O_2^- + HO_2 \rightarrow O_2 + HO_2^-$) whose rate constant at pH 7.5 is $8.5 \times 10^7\ M^{-1}\ sec^{-1}$ (*93*). When superoxide dismutase is added to the solution the kinetics of the decay changes from a second-order process to a pseudo-first-order mechanism with respect to both the enzyme and the substrate concentrations (*92*, *93*). If the dose of O_2^- is constant, the rate of decay is proportional to the enzyme concentration. The rate constant, k_{cat}/K_m, for the bovine enzyme was determined to be $2.3 \times 10^9\ M^{-1}\ sec^{-1}$ at pH 7.0 and 25°C (*52*). Similar values were found for human SOD expressed in yeast and in *E. coli* (*95*, *96*) (Table III). There are no indications of saturation at the highest O_2^- concentration, and the measured rate constant is near the diffusion control. This method, besides the advantage of a direct determination of the catalytic constant, yields very high superoxide concentrations and is highly sensitive. Furthermore, it has been shown that the rate constants for the reduction of O_2^- by the reduced enzyme and for the oxidation of O_2^- by the oxidized enzyme are the same (*97*, *98*). By lowering the temperature to 5.5°C and raising the initial O_2^- concentration to about 5 m*M* (possible using a stopped flow apparatus), Fee and co-workers were able to saturate the enzyme and to determine the Michaelis–Menten parameters, K_m, and turnover number or k_{cat} (*99*). At pH 9.3, in H_2O, the turnover number is $0.9 \times 10^6\ sec^{-1}$ and K_m is $3.5 \times 10^{-3}\ M$. The saturative behavior is more pronounced in D_2O and decreases in the presence of acid, at variance with what happens in nonsaturating conditions when no isotopic effects are observed. These results suggest that, only in saturative conditions, proton transfer is rate limiting. In nonsaturating conditions the observed rate constant is probably determined by the rate of approach of O_2^- to the copper center [k_1 of reaction (7)]. Such a rate is controlled by the rate of substrate diffusion.

The polarographic method, another technique to measure the decay of superoxide, does not require special and expensive apparatus such as a Van der Graaf generator. A dropping mercury electrode works both as a source of superoxide and as a detector of superoxide dismutation products (*100*). The electroreduction of O_2 in aqueous solution can be a monoelectronic process that produces O_2^- ($O_2 + e^- \rightarrow O_2^-$) or a bielectronic process, with reduction to H_2O_2. The latter happens in the presence of protons: $O_2 + 2e^- + 2H^+ \rightarrow H_2O_2$.

The polarographic curves for the two processes are indicated in Fig. 12. Hydrophobic surfactants such as triphenylphosphinoxide (TPO) are used to cover the electrode surface and prevent proton transfer from occurring on the electrode surface. At pH 9.5 only the reduction of oxygen to superoxide is observable, whereas at lower pH two elec-

TABLE III

ACTIVITY OF SODs FROM DIFFERENT SOURCES AND OF SOME MUTANTS

Source	Activity	pH	$I(M)$	Ref.
Bovine SOD (erythrocyte)	3300 U/mg[a]	7.8	—	*2*
	$2.3 \times 10^9\ M^{-1}\ sec^{-1}$[b]	7.0	—	*52*
	$3.9 \times 10^9\ M^{-1}\ sec^{-1}$[b]	7.5	0.02	*128*
	$1.7 \times 10^9\ M^{-1}\ sec^{-1}$[b]	8.0	0.16	*118*
	32,180 U/mg[c]	7.4	—	*109*
Human SOD (erythrocyte)	3500 U/mg[a]	7.8	—	*103*
	6900 U/mg[a]	—	—	*61*
	120,500 U/mg[d]	—	—	*146*
Human SOD (*E. coli* cytoplasm)	7500 U/mg[a]	—	—	*61*
Human SOD (yeast)	6570 U/mg[a]	7.8	—	*104*
	$2.3 \times 10^9\ M^{-1}\ sec^{-1}$[b]	7.0	0.01	*95*
	$1.65 \times 10^9\ M^{-1}\ sec^{-1}$[b]	7.0	0.01	*342*
	$1.75 \times 10^9\ M^{-1}\ sec^{-1}$[e]	8.5	0.16	p.c.[f]
Human SOD (*E. coli*)	$2.3 \times 10^9\ M^{-1}\ sec^{-1}$[b]	7.0	0.01	*64*
Human SOD (*E. coli*)	$1.32 \times 10^9\ M^{-1}\ sec^{-1}$[e]	8.5	0.16	p.c.[f]
Human SOD (*E. coli*)	19,000 U/mg[c]	7.4	—	*119*
Ox SOD	$3.8 \times 10^9\ M^{-1}\ sec^{-1}$[b]	8.0	0.02	*116*
Pig SOD	$3.2 \times 10^9\ M^{-1}\ sec^{-1}$[b]	8.0	0.02	*116*
Sheep SOD	$3.3 \times 10^9\ M^{-1}\ sec^{-1}$[b]	8.0	0.02	*116*
Yeast SOD	$3.4 \times 10^9\ M^{-1}\ sec^{-1}$[b]	8.0	0.02	*116*
Extracellular human SOD	116,000 U/mg[d]	—	—	*146*
Extracellular recombinant human SOD	116,000 U/mg[d]	—	—	*146*
Shark (*Prionace glauca*) SOD	$3.75 \times 10^9\ M^{-1}\ sec^{-1}$[b]	7.5	0.02	*128, 343*
Bacillus abortus SOD (*E. coli*)	3800 U/mg[a]	7.8	—	*152*
Xenopus laevis SOD	$3.7 \times 10^9\ M^{-1}\ sec^{-1}$[b]	8.0	0.02	*329*
	$1.3 \times 10^9\ M^{-1}\ sec^{-1}$[b]	8.0	0.145	*329*
Thr-137IleHSOD (yeast)[g]	$1.20 \times 10^9\ M^{-1}\ sec^{-1}$[b]	7.0	—	*342*
Thr-137SerHSOD (yeast)	$1.25 \times 10^9\ M^{-1}\ sec^{-1}$[b]	7.0	—	*342*
Thr-137AlaHSOD (yeast)	$1.19 \times 10^9\ M^{-1}\ sec^{-1}$[b]	7.0	—	*342*
Thr-137ArgHSOD (yeast)	$1.04 \times 10^9\ M^{-1}\ sec^{-1}$[e]	8.5	—	p.c.[f]
Arg-143LysHSOD (yeast)	2840 U/g[a]	7.8	—	*104*
	$9.9 \times 10^8\ M^{-1}\ sec^{-1}$[b]	7.0	0.01	*95*
Arg-143IleHSOD (yeast)	708 U/mg[a]	7.8	—	*104*
	$1.8 \times 10^8\ M^{-1}\ sec^{-1}$[b]	7.0	0.01	*95*
Arg-143AlaHSOD (yeast)	$1.7 \times 10^8\ M^{-1}\ sec^{-1}$[b]	7.0	0.01	*95*
Arg-143GluHSOD (*E. coli*)	$3.5 \times 10^7\ M^{-1}\ sec^{-1}$[b]	7.0	0.01	*95*
Arg-143AspHSOD (*E. coli*)	$3.5 \times 10^7\ M^{-1}\ sec^{-1}$[b]	7.0	0.01	*95*
Cu_2E_2HSOD (*E. coli*)	$7.0 \times 10^8\ M^{-1}\ sec^{-1}$[b]	7.0	—	*96*
Asp-124AsnCu_2E_2HSOD (*E. coli*)	$5.2 \times 10^8\ M^{-1}\ sec^{-1}$[b]	7.0	—	*96*
Asp-124GlyCu_2E_2HSOD (*E. coli*)	$1.8 \times 10^8\ M^{-1}\ sec^{-1}$[b]	7.0	—	*96*
Glu-133GlnHSOD (*E. coli*)	$6.8 \times 10^9\ M^{-1}\ sec^{-1}$[b]	7.0	0.01	*64, 141*
Glu-132GlnHSOD (*E. coli*)	$4.2 \times 10^9\ M^{-1}\ sec^{-1}$[b]	7.0	0.01	*64, 141*
Glu-133Gln, Glu-132GlnHSOD	$7.0 \times 10^9\ M^{-1}\ sec^{-1}$[b]	7.0	0.01	*64, 141*

(*Continues*)

TABLE III (*Continued*)

Source	Activity	pH	$I(M)$	Ref.
Glu-133Lys, Glu-132GlnHSOD	$4.2 \times 10^9\ M^{-1}\ sec^{-1}$[b]	7.0	0.01	*64, 141*
Lys-120Leu *X. laevis* SOD	$2.1 \times 10^9\ M^{-1}\ sec^{-1}$[b]	8.0	0.02	*329*
	$1.0 \times 10^9\ M^{-1}\ sec^{-1}$[b]	8.0	0.145	*329*
Lys-134Thr *X. laevis* SOD	$2.1 \times 10^9\ M^{-1}\ sec^{-1}$[b]	8.0	0.02	*329*
	$1.0 \times 10^9\ M^{-1}\ sec^{-1}$[b]	8.0	0.145	*329*
Lys-120Leu, Lys-134Thr *X- laevis* SOD	$1.1 \times 10^9\ M^{-1}\ sec^{-1}$[b]	8.0	0.02	*329*
	$0.7 \times 10^9\ M^{-1}\ sec^{-1}$[b]	8.0	0.14	*329*
Glu-131Gln *X. laevis* SOD	$6.5 \times 10^9\ M^{-1}\ sec^{-1}$[b]	7.5	0.02	*175*
Asp-130Gln *X. laevis* SOD	$3.7 \times 10^9\ M^{-1}\ sec^{-1}$[b]	7.5	0.02	*175*
Lys-136ArgHSOD (*E. coli*)	30,400 U/mg[c]	7.4	—	*119*
Lys-136AlaHSOD (*E. coli*)	15,200 U/mg[c]	7.4	—	*119*
Lys-136GlnHSOD (*E. coli*)	22,800 U/mg[c]	7.4	—	*119*
His-63Ala yeast SOD (*E. coli*)	0.4% wild type[h]	—	—	*149*
His-63CysHSOD (*E. coli*)	<1% wild type[e]	7.4	0.16	*179*
	$3.8 \times 10^6\ M^{-1}\ sec^{-1}$[e]	8.5	0.02	*179*
Phe-50Glu, Gly-51GluHSOD	10 ± 5% wild type[a]	7.8	0.16	*60*
	$2.0 \times 10^7\ M^{-1}\ sec^{-1}$[e]	8.5	0.16	p.c.[f]
Phe-50Glu, Gly-51Glu, Glu-133GlnHSOD	$8.6 \times 10^7\ M^{-1}\ sec^{-1}$[e]	8.5	0.16	p.c.[f]

[a] Activity determined using the xanthine oxidase method (*2*).
[b] Activity determined using pulse radiolysis (*52, 91, 92, 112*).
[c] Activity determined using Paoletti's method (*108–110*).
[d] Activity determined using Marklund's method (*344*).
[e] Activity determined using the polarographic method (*100, 101*).
[f] p.c., Personal communication from Prof. E. Argese (University of Venice).
[g] HSOD, Human SOD.
[h] Activity determined by monitoring the autooxidation of 6-hydroxydopamine (*345*).

trons are transferred to O_2, leading to H_2O_2. The addition of superoxide dismutase converts part of O_2^- to O_2, increasing the limiting currents. The difference in the limiting currents measured in the absence and in the presence of SOD are related to the rate constant of SOD (*101*). In order to overcome the limitation of pH, connected to the bielectronic process, it was demonstrated that the use of a dropping mercury electrode with short drop time (s.d.t.m.e.) (0.1 sec versus 1–2 sec) allows minimization of the contribution of the reaction that leads to H_2O_2 (*101*). In such a way activity measurements are possible down to physiological pH and the method becomes competitive with the pulse radiolysis method.

These direct assays provide immediate answers about the rate of dismutation of superoxide by SOD. Activity assays performed on the same sample with different direct methods (i.e., pulse radiolysis and polarography) in most cases give similar dismutation rate constants

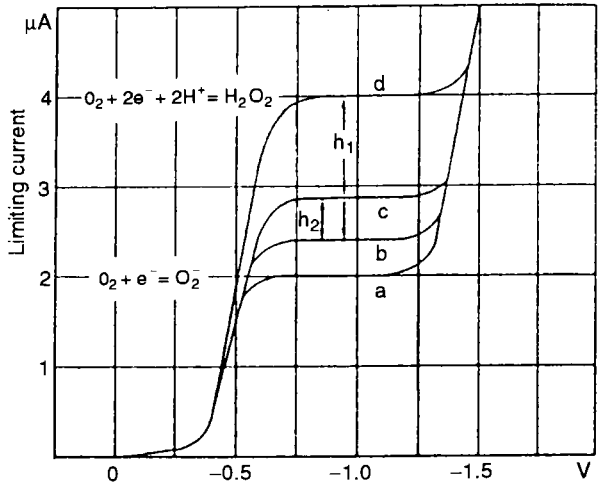

FIG. 12. Polarographic determination of oxygen and its derivatives. The cell current is plotted versus the potential for reduction of O_2^-. (a) pH 12.5, triphenylphosphinoxide (TPO) 0.9 m*M*; (b) pH 9.9, TPO 0.9 m*M*; (c) pH 9.9, TPO 0.9 m*M*, SOD 1.5×10^{-9} *M*; (d) pH 9.9, TPO 0.9 m*M*, SOD 1.5×10^{-7} *M*. The value of limiting current at −1.0 V is proportional to the concentration of O_2 in solution. Reprinted with permission from Ref. *100*.

(see Table III); some low-activity SOD mutants (in particular, monomeric mutants), however, show discrepancies for the two direct assays, discrepancies that we still do not understand (*102*).

In order to monitor SOD activity routinely, assays that require only instrumentation typical of a chemical or biochemical laboratory were set up. The assays consist of a reaction mixture that generates superoxide anion and a coupled redox reaction that scavenges the superoxide ion. The latter reaction is usually followed spectrophotometrically. The addition of superoxide dismutase destroys superoxide and inhibits the coupled reaction. The specific activity of the enzyme is determined on the basis of the amount of protein required to slow down to 50% the first-order coupled reaction, i.e., one enzymatic unit is the amount of protein that reduces the rate to 50% and the specific activity corresponds to the number of units per milligram of protein.

Following the method of McCord and Fridovich (*2*), the superoxide ion is generated through the oxidation of xanthine by oxygen, a reaction catalyzed by xanthine oxidase as shown in Fig. 13. O_2^- then reacts with oxidized cytochrome *c* and it is transformed into O_2. The disappearance of superoxide is monitored spectrophotometrically through the increase of the absorption band at 550 nm, as a consequence of

FIG. 13. Reaction between oxygen and xanthine, in the presence of the enzyme xanthine oxidase.

the reduction of oxidized cytochrome *c*. Superoxide dismutase, by successfully competing with cytochrome *c* for the oxidation of the superoxide ion, inhibits the reduction of oxidized cytochrome *c*. Activity values of 3300 and 3500 U/mg (*2*, *103*) were measured for the bovine and human enzymes, respectively, (Table III), corresponding to a kinetic rate constant of $2.3 \times 10^9\ M^{-1}\ sec^{-1}$, even though values of 6900 and 6600 U/mg have also been reported in literature (*104*). Such discrepancies were partially attributed to the different method for measuring protein concentration and to differences in homogeneity of the samples (*104*). Meaningful results are obtained when the activity of an isoenzyme or of a mutant is expressed relative to that of an isoenzyme taken as reference. However, the assay can be contaminated by the presence of other cytochrome *c* reducing agents (such as glutathione), or by impurities of superoxide dismutase in cytochrome *c*. Furthermore, the presence of anions that specifically bind to a residue in the SOD active cavity can inhibit the activity. This effect was first observed with phosphate, and Fridovich argued that the inhibitory power of the phosphate anion was an ionic strength effect (*105*); it was later proposed that phosphate interacts with Arg-143, a residue that is quite relevant for the attraction of superoxide in the cavity (*106*, *107*).

A relatively recent indirect assay was set up by Paoletti (*108*). The assay consists of a sequence of reactions that generate superoxide from molecular oxygen in the presence of EDTA, manganese(II) chloride, and mercaptoethanol (*108–110*). The reactions are monitored by following the oxidation of NAD(P)H by superoxide radicals through a decrease of absorbance at 340 nm, which corresponds to the maximum absorbance of NAD(P)H. The addition of SOD (scavenging superoxide) inhibits nucleotide oxidation (Fig. 14). At variance with the previous assays, whereby cytochrome *c* is reduced by superoxide, this method relies on the oxidation of NAD(P)H and, in theory, makes the detection less susceptible to aspecific reduction by common cellular components. The assay is very sensitive to the EDTA/Mn^{2+} ratio and to the mercaptoethanol concentration, both of which affect nucleotide

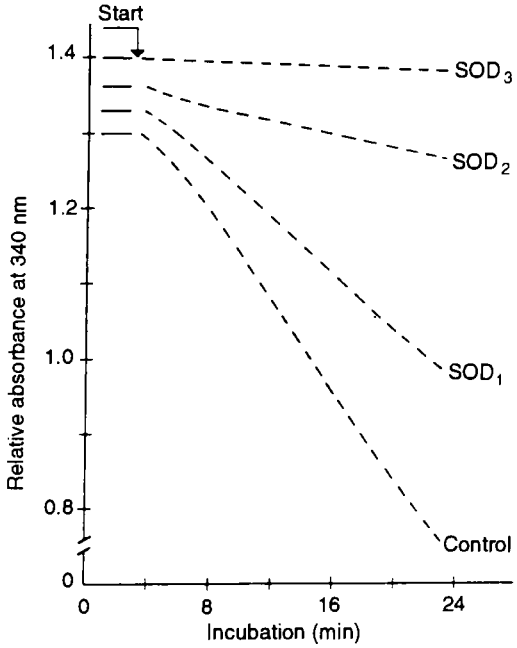

FIG. 14. Effect of superoxide dismutase on the rate of NADH oxidation. Decreases in absorbance are measured at 340 nm. Four assays are performed simultaneously in the absence (control) and in the presence of different amounts of SOD. Reprinted with permission from Ref. *108*. Copyright 1986, Academic Press.

oxidation rates (*109*). Therefore the presence of chelators, of endogenous Mn^{2+}, or of free thiols might alter the calibration curve.

The nitroblue tetrazolium assay (*111*) is another indirect method that is used especially for detecting SOD activity on gel electrophoresis. Superoxide radicals are generated by xanthine/xanthine oxidase or by the photoreduction of flavins (typically riboflavin), which oxidize H_2O to O_2^-. The gel on which SOD samples have been loaded is then stained with nitroblue tetrazolium chloride. This reagent is reduced by superoxide to the blue-colored formazan. SOD competes with nitroblue tetrazolium and produces colorless zones on the blue gels. This method, which is highly specific toward superoxide dismutase, is limited by its low reliability with respect to quantitative determinations.

The results obtained by indirect assay are hardly comparable, because the specific activity values are based on different types of reactions to induce the dismutation of superoxide. The results have different meanings, and only relative comparisons among different samples

can be made. Furthermore, indirect assays, which can be set up at a specific pH and buffer concentration, are not sufficiently versatile for SOD activity as a function of pH and ionic strength.

Activity measurements are made at low concentrations of SOD (typically micromolar). On the other hand, there is a concentration dependence equilibrium between monomeric and dimeric species. It has been suggested that bovine SOD at 25°C, pH 7.8, is only 50% in the dimeric form at a concentration 0.3–0.4 g/liter without any loss of activity (*33*).

All these assays can also be used to determine the activity of MnSOD and FeSOD. It should be noted that the nitroblue tetrazolium assay (*111*) allows differentiation of MnSOD, FeSOD, and Cu_2Zn_2 SOD. Indeed, these enzymes have different molecular weights and they run at different rates on acrylamide gel. In a mixture of the three proteins it is possible to resolve three spots representing Mn, Cu_2Zn_2, and FeSOD.

B. pH Dependence of Activity

In the pH range 5–9, activity is not influenced by pH. However, when pH exceeds 9, activity steeply decreases (*52*, *112*, *113*) (Fig. 15). This behavior cannot be ascribed to denaturation because NMR studies indicate no denaturation up to pH 12.5 (*114*). The rate constant curve versus pH shows an inflection at high pH, and for the human

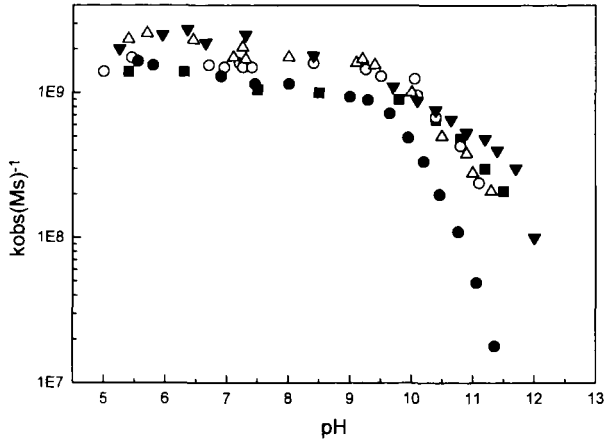

Fig. 15. Rate constant versus pH for bovine SOD (■), yeast SOD (○), mutant Cys-6Ala, Cys-111Ser of human SOD expressed in yeast (△), Thr-137Ile SOD (●), and Lys-136Ala SOD (▼).

enzyme an apparent pK_a of 10.7 ± 0.1 was calculated (*115*). This loss of activity at high pH has been matter of debate and many hypotheses have been proposed, including deprotonation of some residues belonging to the active site channel, such as Lys-136 (*116*, *117*) and Lys-122 (*117*, *118*), deprotonation of His-63 (*119*), which does not bridge the metal ions in the reduced species, and ionization of the water molecule, which is close to the copper ion (*119*). Mutations have shown that the lysines cannot be uniquely responsible for the drop in activity. By studying the Ile-137 mutant, which has the lowest apparent pK_a (*112*), it seems that the drop in activity is not related to changes involving the metal coordination sphere, but instead is related to changes in the electrostatic potential due to a deprotonation process (which could be represented by an OH^- group approaching copper) (*120*).

C. Ionic Strength Dependence of Activity

In wide-type Cu_2Zn_2SOD the activity decreases with ionic strength (*105*, *121*). Indeed, when ionic strength is increased from 0 to 150 m*M* (physiological ionic strength), the rate decreases by 30% (Fig. 16). This can be explained by taking into account two factors that moderate SOD activity: the overall negative charge of the dimeric protein

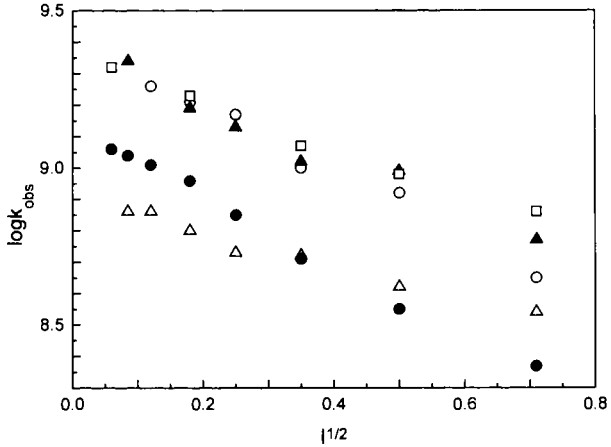

Fig. 16. Effect of ionic strength on dismutation rate of O_2^- by superoxide dismutase as measured experimentally by pulse radiolysis at pH 8. Ionic strengths were adjusted using NaCl. ○, Bovine SOD; ▲, human SOD expressed in yeast; □, mutant Cys-6Ala, Cys-111Ser of human SOD expressed in yeast; ●, Thr-137Ile SOD; △, Arg-143Lys.

(−4, at pH 7) and the positive active center. The former property determines a repulsive barrier for the negative superoxide; this repulsion is compensated by the electrostatic field generated by the positive copper and zinc ions and by the positively charged residues in the active site channel (*122*, *123*). In the presence of salt, the repulsive barrier is reduced; however there is a more substantial decrease in the positive target area. The combination of these effects yields, in wild-type SOD and also in most of the mutants, a decrease in activity as the ionic strength increases.

In the case of mutants such as the monomeric Phe-50Glu, Gly-51Glu, which has an overall charge of −4 (versus −2 of the wild-type SOD subunit), the activity is reduced to 10% and it is ionic strength independent. It is possible that the enhanced negative electric field strength of the monomeric mutant increases the repulsive barrier, causing a drastic decrease of activity. An increase in ionic strength reduces both the repulsive barrier and the steering effect of the positively charged residues of the active site, which apparently compensate each other. This produces catalytic rates that are ionic strength independent (*124*). Other monomeric mutants with the same charge density as the native protein, e.g., Phe-50Glu, Gly-51Glu, Val-148Lys, Ile-151Lys SOD (total charge, −2), show a dependence on the ionic strength qualitatively similar to wild-type SOD (*102*).

D. Computational Studies on Copper–Zinc SOD

Cu_2Zn_2SOD has been the subject of several theoretical studies aimed at predicting its structural and functional properties. The calculations performed to describe the catalytic process or to quantitate the experimental rates were essentially focused on the interaction and binding of the substrate. As discussed before, in nonsaturating conditions the diffusion of the substrate in the active site is the rate-limiting step of the catalytic process. This process is strongly determined by electrostatic forces due to the nature of the substrate. Consequently, electrostatic field calculations and Brownian dynamics simulations (*64*, *122*, *123*, *125–128*) have been extensively applied to SOD. On the contrary, no extensive studies are available for characterizing the subsequent steps, in which the electron transfer process occurs. Some preliminary calculations have been reported (*129*) whereby the energy for the process of transferring one electron from O_2^- to copper has been evaluated within a density functional approach.

Electrostatic calculations produced maps of the electrostatic forces in the active channel and enabled evaluation of the contribution of

each charged residue in the interaction with the substrate. Brownian dynamics calculations have been made for superoxide in order to estimate the rates of substrate–enzyme encounters for wild-type SOD and for the mutants (*130*). The results, compared with the experimental data on the mutants, pointed out that several residues make a large electrostatic contribution to the first step of the catalytic process, i.e., the binding of substrate. In a few cases the results disagree with the experimental data, indicating that other factors affect the reaction. The discrepancies have been rationalized, through molecular dynamics (MD) calculations, in terms of structural changes at the active site (see later).

Electrostatic field calculations have been also enabled rationalization of the dependence of catalytic rates on ionic strength (*122*, *126*, *131*). Due to the negative charges of SOD and the substrate, and to the diffusion-limited kinetidc rates, a positive dependence of catalytic rates on ionic strength would be expected, but the opposite is observed. This has been rationalized (*122*, *126*, *130–138*) taking into account that the diffusion of the charged substrate to the active site of SOD is determined by two competing effects: one is the repulsion between two species of the same charge, i.e., the substrate and the enzyme, after nonproductive collisions, and the other is the steering effect produced by the positive electrostatic field in the active site channel and at its entrance. The overall rate for the catalytic process, which is determined by the diffusion of the substrate, is the balance between these two effects, where the second is the dominant one. The first effect, which decreases the rates of collisions, is positively affected by an increase in ionic strength as the latter reduces the overall protein charge. The second effect, i.e., the steering of the substrate due to the positive charges of the channel, negatively affects the catalytic rates with increasing ionic strength because the attraction of the substrate would be reduced. Because the second effect in wild-type SOD is larger, an increase in ionic strength would reduce the productive collision rates and, for this enzyme, the catalytic rates.

Molecular dynamics studies have been particularly successful in rationalizing and predicting properties of SOD and its mutants (*139*, *140*). The different catalytic properties of the active site mutants have been interpreted as a result of structural and dynamic changes at the active site channel.

The overall protein structure and, in particular, the metal coordination sites and the active channel are quite stable when they are relaxed through MD calculations in the presence of explicit water. A striking result is the capability of these calculations to reproduce the

solvation properties of the metal sites and of the active channel. As will be discussed (see also Section VIII), the water molecule close to the copper ion is not coordinated to it and does not contribute to its ligand field. Consequently, in these calculations it was simply placed at its crystallographic position without any link to the protein by assigning it the force field parameters of the bulk water. During the MD trajectory on wild-type SOD and on all the mutants characterized by nuclear magnetic relaxation dispersion measurements (see Section VI) but Thr-137Ile, this water molecule maintains its position close to copper, as experimentally observed, despite the absence of any constraints. This indicates that the field produced at the active site by the residues of the channel is capable of maintaining the water molecule in its equilibrium position (*140*).

In the case of the Thr-137Ile mutant the same water molecule moves, after a few picoseconds of simulation, far from the metal site, and no other water molecule substitutes for it (Fig. 17). No other water molecules are present within 5 Å from copper, as is indeed observed experimentally (*112*). Replacing a hydrophilic residue with a hydrophobic residue at the active site destabilizes the structural

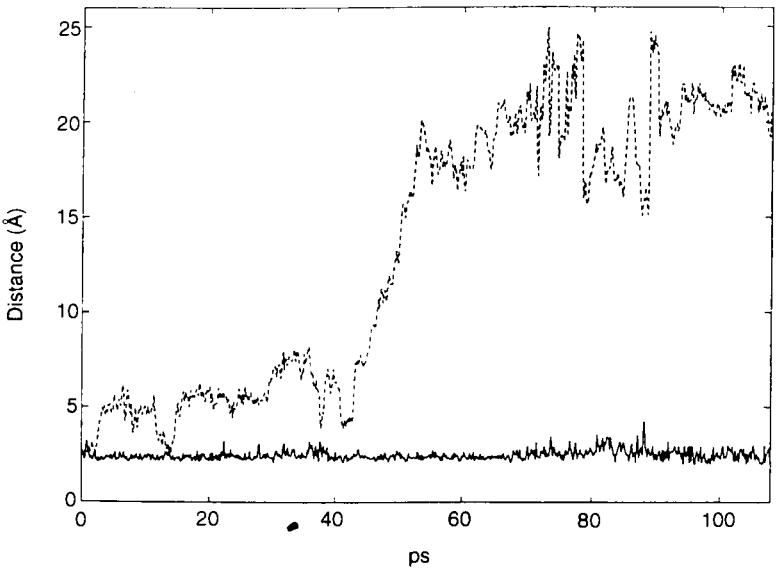

FIG. 17. Distance between copper and the oxygen of the closest water molecule to copper in wild-type SOD (solid line) and in Thr-137Ile SOD (dashed line) as a function of the simulation time. From Ref. *140;* Banci, L.; Carloni, P.; Orioli, P. L. *Proteins: Struct. Funct. Genet.* **1994** *18,* 216. Copyright © 1994 Wiley-Liss, Inc. Reprinted by permission of Wiley-Liss, Inc., a subsidiary of John Wiley & Sons, Inc.

water molecule and allows it to leave the cavity (*140*). This is a quite relevant result of these MD calculations, which are able to reproduce even fine details of the structural properties.

As expected on a pure electrostatic basis, neutralization of a negative residue in the channel would produce an increase in the catalytic rates, as has been indeed observed (*64*, *141*). The charge reversal from a negative to a positive residue is expected to produce an even larger increase in activity (*125*, *126*), but this does not occur (*64*, *141*). By analyzing the structural properties of the active channel in these mutants, as obtained by MD calculations, a large rearrangement of the electrostatic loop in the Glu-133Lys mutant has been observed. This could change the local electrostatic field, which could therefore not be enhanced by the charge reversal (*140*).

In addition to structural properties, the enzymatic activity is also modulated by the dynamic properties of the reaction site and of the channel. Mutation on Arg-143 produces, together with a decrease of the local positive field, a decrease of the flexibility of the bottleneck at the end of the active channel for the access to the copper site. The narrowest section of the active channel decreases in size on going from wild-type SOD to Arg-143Ile, to Arg-143Glu (*139*). Figure 18 shows the fluctuations of the distance between the residues at positions 143 and 137, which are the two groups determining the narrowest section of the active channel in SOD. This trend parallels closely the decrease in enzymatic activity observed for these mutants. The reduced size and mobility of the channel decrease the efficiency of the diffusion of the substrate in the channel, thus decreasing the number of encounters and therefore the enzymatic efficiency.

IV. Molecular Biology and Chemical Modifications

A. Expression Methods

Human SOD was one of the first types of Cu_2Zn_2SOD to be cloned and then expressed in different microorganisms. The human SOD gene was first isolated and sequenced. The wild-type human SOD proteins initiate with a methionine, which is then removed, followed by acetylation of the adjacent alanine to obtain the mature protein. In order to obtain a high transcription level of Cu_2Zn_2SOD in *E. coli*, the gene was cloned in a plasmid (ptac5) (Fig. 19) containing the *tac*1 promoter and transformed in an *E. coli* strain such as D1210 (*61*). Out of 500 colonies, 25 were able to produce SOD as 5% or more of the total soluble cell protein. Even if the activity of this recombinant

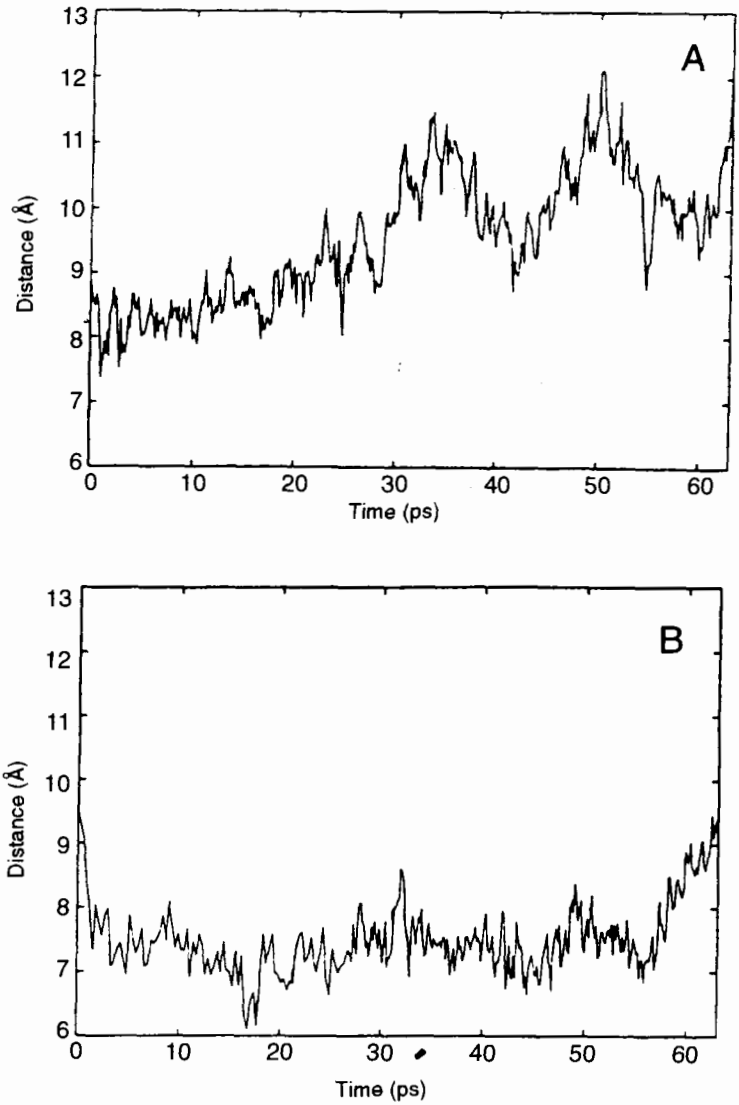

FIG. 18. Fluctuations of the distance between (A) Cζ Arg-143 and Cβ Thr-137 in wild-type SOD and (B) Cδ Glu-143 and Cβ Thr-137 in Arg-143Glu SOD. Reprinted with permission from Banci, L.; Carloni, P.; LaPenna, G.; Orioli, P. L. *J. Am. Chem. Soc.* **1992,** *114,* 6994. Copyright 1992 American Chemical Society.

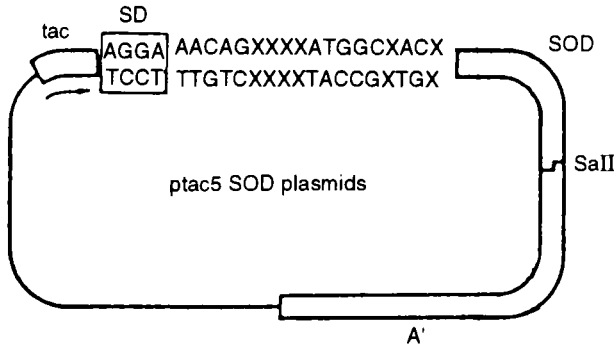

FIG. 19. Scheme of the ptac5 SOD plasmid, with the *tac*I promoter, the Shine–Dalgarmo sequence (SD), and the ATG-flanking sequence, with randomized positions, indicated by X, which contain all four bases. Reprinted from Ref. *61, Nucleic Acids Research,* **1985,** *13,* 2017, by permission of Oxford University Press.

protein is similar to that of purified human erythrocyte Cu_2Zn_2SOD (see Table III), the protein is not perfectly identical to the human protein because *E. coli* cells are unable to acetylate the exposed alanine. For this reason the expression of human SOD in yeast was also investigated. Human SOD was expressed in yeast using the yeast glyceraldehyde phosphate dehydrogenase promoter (*62*). The protein has a normal specific activity and it is indistinguishable from the human erythrocyte Cu_2Zn_2SOD.

Human SOD was also expressed in the periplasmic space of *E. coli* using a secretion vector that allows the protein to be accumulated in the periplasmic space. In 1988 the HSOD gene was cloned in a secretion vector pIN-III:OmpA (*142*) On induction of gene expression the protein was produced at a level of 10% of total cellular protein and was recovered through osmotic shock as the major component of the periplasmic fraction. Although the N-terminal alanine is not acetylated, it is practically indistinguishable from the acetylated form (see Table III).

Another periplasmic expression system (the plasmid pPHSOD1Iq) was constructed by Hallewell *et al.* (*64*); the plasmid contains a synthetic human SOD gene (*143*), joined to the leader sequence of *Photobacterium leiognathi* Cu_2Zn_2SOD (*144*), and the *lacIq* gene (*145*) in a pBR322 derivative containing the *tac*1 promoter (*61*). The synthetic SOD gene contains the Cys-6Ala, Cys-111Ser mutations, which are relevant for protein thermostability (*143*). In human SOD, Cys-6 and Cys-111 are the only free cysteines, the former buried and located adjacent to the dimer interface with the side chain pointed toward the interior of the β-barrel, whereas the latter is close to the dimer

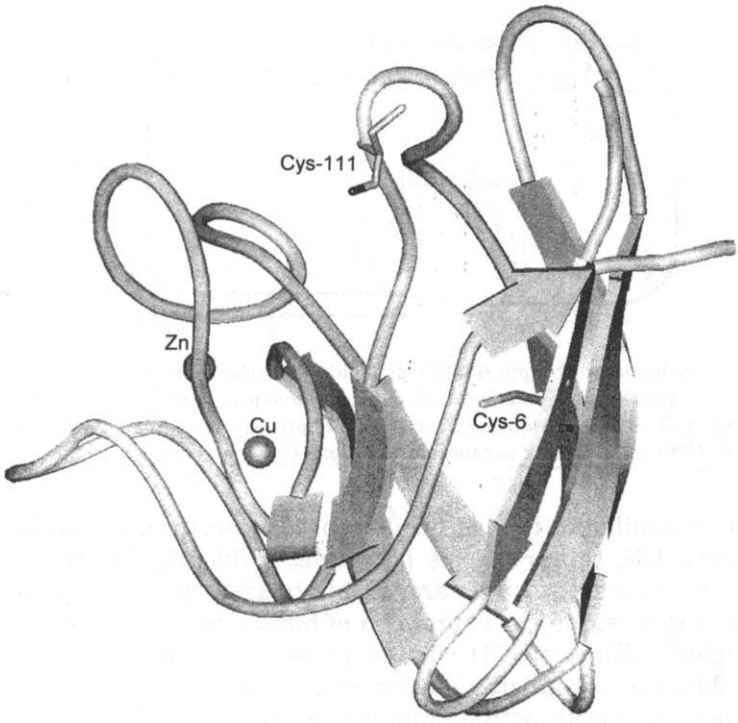

FIG. 20. Structure of human SOD indicating the position of the residues Cys-6 and Cys-111 (from Ref. *63*).

contact region but with its side chain pointed outward into the solvent (Fig. 20). Two mechanisms seem to be responsible for thermal inactivation of the cysteine-containing native enzyme: (1) hydrolysis of the backbone as happens for every cysteine-containing protein, and (2) incorrect formation of intermolecular disulfide bridges. Removal of Cys-6 and Cys-111 was demonstrated to increase protein thermostability (*143*).

Extracellular human SOD (EC-SOD), a tetrameric copper–zinc glycoprotein that is present in plasma, lymph, and synovial fluid, was expressed in Chinese hamster ovary cells (*146*, *147*). From cultures of these cells, recombinant EC-SOD was isolated in high yield with respect to native EC-SOD. Recombinant and native EC-SODs were compared and their properties were shown to be very similar (Table III).

Besides human SOD, other types of SOD were expressed in organisms different from those of the native species. Yeast SOD from *S. cerevisiae* was expressed in *E. coli* using the T7 RNA polymerase expression system (*148–150*). Cu_2Zn_2SOD from *X. laevis* was overex-

pressed from plasmid pKB under control of the *trc* promoter in *E. coli* (*151*). In *E. coli,* Cu_2Zn_2SOD from *Brucella abortus* was also expressed (*152*). The SOD gene was cloned in a pET3c vector containing the *T7* promoter. A leader sequence that directs secretion into the periplasmic space was also incorporated. The above plasmid was then inserted in the *E. coli* BL21 (DE3) strain, which carries the *T7* polymerase gene (*152*).

B. Chemical Modifications

Before the advent of biotechnology, in order to clarify the role of various amino acid residues in Cu_2Zn_2SOD, the first technique employed was chemical modification of specific residues.

Several α,β-diketones (phenylglyoxal, butanedione, and cyclohexanedione) inactivate the enzyme (the residual activity never exceeds 20%), interacting with and modifying one arginine/subunit (*153*). The inactivation, in the case of the bovine enzyme, is accompanied by some changes in the visible absorption spectrum of copper and by a small loss of copper, which, however, does not account for the inactivation and the spectral changes. Analysis of fragments obtained through treatment with CNBr demonstrated that the modified residue is Arg-143, whose presence was soon recognized to be very important for catalytic activity (*153*). In the case of the yeast enzyme the inactivation is complete and is not accompanied by any loss of copper(II) (*154*). Modification of the arginine residue affects the anion binding properties of the protein, lowering the affinity for CN^-, N_3^-, NCS^-, and CNO^-. The reduced affinity constants for these anions may be the result of modification of the copper coordination geometry or of neutralization of a positive charge in the active site, or both (*155*). Comparison of the rates of inactivation among Cu_2Zn_2SODs from different species indicate that bacterial enzymes are inactivated more rapidly by phenylglyoxal than are eukaryotic SODs (*156*).

Treatment of Cu_2Zn_2SOD with succinic anhydride led to full derivatization of all the lysine residues, indicating that all the lysines are accessible (*157*). The derivative has an increased negative charge that is reflected by a 10-fold decrease of activity, although the coordination geometry of the active site is not affected by succinylation (*157*). It was also proposed that this treatment might weaken the interactions between the two subunits (*157*). The lysine charge can also be neutralized through carbamylation and acetylation with a consequent decrease in activity and anion affinity (*105*, *158*).

The effect of chemical modifications on Arg-143 and lysines was also investigated for the reduced enzyme. It was observed that the

reduced, modified enzyme has a lower affinity for chloride than the reduced, untreated SOD, indicating that electrostatic interactions between positively charged groups and the substrate are present in the reduced state of the protein and play an important role in the catalytic mechanism (*159*) (see Sections II,A,J and IX,B).

Carboxylated polyethylenglycol (PEG, MW 5000) interacts with SOD through covalent binding with the protein amino groups (*160*, *161*) at the enzyme surface, resulting in a polymeric form with a molecular weight of 120,000 (*162*, *163*). This is confirmed by the line broadening of the ^1H NMR spectrum of the Cu_2Co_2 derivative (*163*). The structure of the active site geometry seems to be unaffected by PEG treatment, whereas the activity is reduced to 75%, and the affinity for N_3^- to 50%, with respect to the untreated enzyme. These results indicate that the lower activity must be ascribed to a decrease in the channeling of the O_2^- ion toward the active site, as a consequence of neutralization of positive charges.

Excess of hydrogen peroxide, one of the products of superoxide dismutation, at alkaline pH reduces copper(II) and inactivates the protein (*52*, *98*, *164*, *165*). Inactivation seems to be accompanied by changes in the visible and EPR spectra (*98*, *166*, *167*). The intensity of the EPR spectrum decreases with H_2O_2 concentration and with time, but it does not disappear completely (*167*). Kinetic studies in dilute solution indicated that inactivation is a first-order process with respect to enzyme and reagent (*98*). The effect of H_2O_2 was proposed to be related to the modification of the amino acid composition and to the destruction of one of the histidine ligands (*98*, *166*). The ^1H NMR investigation of the H_2O_2-treated Cu_2Co_2SOD derivative clearly shows that the coordinated residues are maintained, although there is evidence of some flexibility of the donor groups. Furthermore, His-48 (a copper-coordinated residue) is affected by the modification caused by H_2O_2 as far as its position with respect to the metal ion is concerned (*168*). Recent studies have provided evidence that treatment with H_2O_2 causes oxidation of histidine residues and that His-120 is selectively oxidized on the Cε1 atom and converted to 2-oxo-histidine (*169*).

The interaction of SOD with peroxynitrite has been investigated. Peroxynitrite is produced by the reaction between nitric oxide and superoxide, whose concentration increases in pathological conditions such as ischemia. It has been found that peroxynitrite is also a substrate for SOD and that the catalytic action of the enzyme permanently modifies Tyr-110 and converts it into 3-nitrotyrosine (*78*). The X-ray structure of the peroxynitrite-modified SOD has also been solved (see Section II,G).

C. The Mutants

From the very beginning of the investigation of superoxide dismutase it was noted that bovine SOD has an overall −4 charge and an isoelectric point at pH 5.2 (*170*). The protein should thus repel the anionic substrate. However, there is a positive charge on the surface of the active cavity and where the metal ion sits, which exerts a stronger and positive effect in guiding the substrate within the cavity. The ionic strength smoothens both effects with the result that it causes a decrease in activity, because the focused attraction has a larger effect on the enzyme activity than the overall repulsion (*122*).

The first mutation, according to this reasoning, was at position 143, where an Arg residue is strategically located (Fig. 21). When it is substituted with a Lys, which is still positive but has a different spatial location, the protein loses some of its activity. At pH 5 the latter is reduced to 10% when an Ile is present, and drops to 4% when there is a negative charge such as Glu or an Asp (Table III) (*95*, *104*). The pH dependence of the activity for these mutants is quite unique. Indeed, whereas wild-type SOD and most SOD mutants exhibit a constant rate in the pH range 5–9, with a drop at higher pH, the Arg-143Glu, the Arg-143Asp, and the Arg-143Lys mutants show drops at lower pH values, due to the deprotonation of the residue. This demonstrates that the presence of Arg at position 143 is crucial in keeping a stable positive charge up to pH 10 (*95*). The decrease in local positive charge on going from wild-type SOD to Arg-143Ile, to Arg-143Asp (or Glu) has a strong effect on the dependence of the catalytic rate on

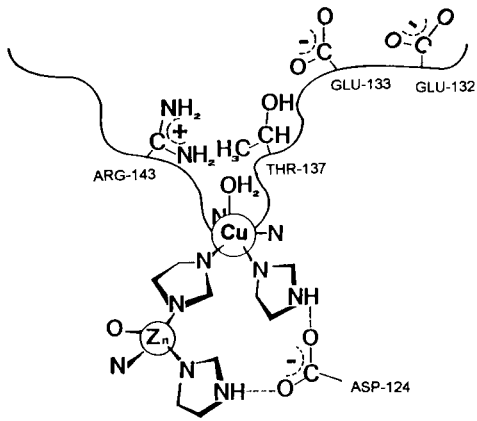

Fig. 21. Schematic drawing of the catalytic cavity of SOD.

ionic strength. Indeed, whereas the wild-type protein is greatly affected by ionic strength, the mutants, with negative residues at position 143, are almost unaffected by the increase in ionic strength (*95*). The ^1H NMR spectra of the Cu_2Co_2 derivative (see later) show that the ligands are not affected by these mutations. Interestingly, the affinity of N_3^- for the copper follows a pattern similar to that of activity. Because the dismutation of O_2^- by SOD is a very fast process and no saturation is observed at room temperature (see Section III) (*99*, *171*), the rate-limiting process of the catalytic rate of Cu_2Zn_2SOD is the binding of O_2^- to the active site. Therefore, whereas the activity is determined by k_{on} of O_2^- the affinity of N_3^- depends on the ratio k_{on}/k_{off}. If k_{off} is just determined by the barrier of the Cu–N bond breaking and is constant, then it is also reasonable that the patterns of k_{on} of O_2^- and the affinity constants of N_3^- are often similar.

If the Thr-137 residue is mutated the effects are also relatively large. The Thr-137Ile makes the cavity quite hydrophobic. Nuclear magnetic relaxation disperson studies (see Section VI) show that the semicoordinated water is now not present. Molecular dynamics calculations on the mutants have shown a high mobility of the water molecule close to the copper ion (see Section III,D). A rearrangement of the active site channel observed in this mutant is responsible for pushing out the water molecule and seems to produce a different electrostatic field with respect to wild-type SOD just on the coordination sphere of copper, but not to affect seriously its surroundings (*140*). Through spectroscopic investigation it was observed that the copper chromophore is more tetragonal than in wild-type SOD, with His-48 more firmly bound to copper in a more symmetrical environment (*112*) (see Table IV). A different effect on the hydrophilicity of the cavity is observed when Thr-137 is substituted by Ser or Ala: in the former case the hydrophilic residue stabilizes the water molecule more than in wild-type SOD, and in the latter case the small Ala, despite its hydrophobicity, slightly reduces the presence of water (*115*). The activity is not affected at all by the different stability of the water molecule close to copper (*115*). The Thr-137Arg mutant has a sizable activity but smaller than that of wild-type SOD (Table III), which, at low ionic strength, extrapolates at the same value of wild-type SOD. On the other hand, the affinity for anions such as azide is 20 times higher than is seen in wild-type SOD (*172*). A reasonable hypothesis for this behavior, confirmed by MD calculations (*112*), is that substitution of Thr-137 with Arg dramatically affects the loop formed by the side chains of Lys-136, Glu-132, and Glu-133, a loop that is implicated in electrostatic guidance of superoxide (Fig. 22). (*45*). In the case

TABLE IV

EPR PARAMETERS AND Hδ1 HIS-48 CHEMICAL SHIFTS OF THE Cu_2Co_2 DERIVATIVES FOR SOME Cu_2Zn_2SODs, SOME OF THEIR ADDUCTS WITH ANIONS, AND SOME OF THEIR MUTANTS[a]

Source[b]	$g_\parallel$	g	$A_\parallel$ (10^{-4} cm^{-1})	δ (ppm) Hδ1 His-48	Ref.
BSOD	2.26	2.07	143	34.5[c]	*207, 218, 242*
YSOB	2.26	2.08	141	34.1[d]	*243*
HSOD	2.26	2.07	140		*103*
HSOD (yeast)	2.28	2.09	145	34.6[d]	*346*
AS-HSOD (yeast)	2.28	2.09	142	34.6[d]	*346*
AS-HSOD (*E. coli*)	2.26	2.09	138	35.0[c]	*208*
BSOD + F^-	2.26	2.06	143	31.3[e]	*89*
BSOD + NCS^-	2.25	2.06	148	27.7[e]	*89*
BSOD + NCO^-	2.26	2.05	158	19.8[e]	*89*
BSOD + N_3^-	2.21	2.05	157	15.9[e]	*89*
BSOD + CN^-	2.21	2.06	188	13.0[e]	*89*
BSOD + HS^-	2.21	2.03	180	—	*278*
Cu_2E_2BSOD	2.27	2.04	148	—	*207, 243*
Cu_2E_2BSOD + N_3^-	2.24	2.06	164	—	*244*
Cu_2E_2BSOD + CN^-	—	2.06	181	—	*244*
Cu_2Hg_2BSOD	2.26	2.05	141	—	*243*
Cu_2Cd_2BSOD	2.26	2.05	138	—	*243*
Thr-137IleHSOD	2.25	2.04	162	38.6[d]	*89*
Thr-137AlaHSOD	2.26	2.07	140	36.3[c]	*115*
Thr-137SerHSOD	2.26	2.07	140	34.5[c]	*115*
Thr-137ArgHSOD	2.26	2.06	141	38.3[c]	*172*
Arg-143IleHSOD	2.26	2.08	137	34.6[d]	*270, 342*
Arg-143GluHSOD	2.28	2.09	148	36.2[d]	*270, 342*
His-80CysYSOD	2.26	—	139	—	*176*
His-46CysYSOD	2.23	—	151	—	*178*
His-120CysYSOD	2.27	2.05	175	—	*178*

[a] The data were collected between pH 5.0 and 7.5; in this range no spectroscopic changes are observed for the species cited. In rhombic systems $g_\parallel$ represents the reading at zero intensity on the left side of $g_x + g_y$.

[b] BSOD, Bovine SOD from erythrocytes; YSOD, yeast SOD; HSOD, human SOD; AS-HSOD, human SOD with the following modifications: Cys-6Ala, Cys-111Ser.

[c] Measured at 300 K.

[d] Measured at 303 K.

[e] Measured at room temperature.

of the Thr-137Arg mutant these residues are much further from the copper ion and point toward the surface of the protein, breaking the hydrogen bonding network that stabilizes the active channel (*112*, *172*).

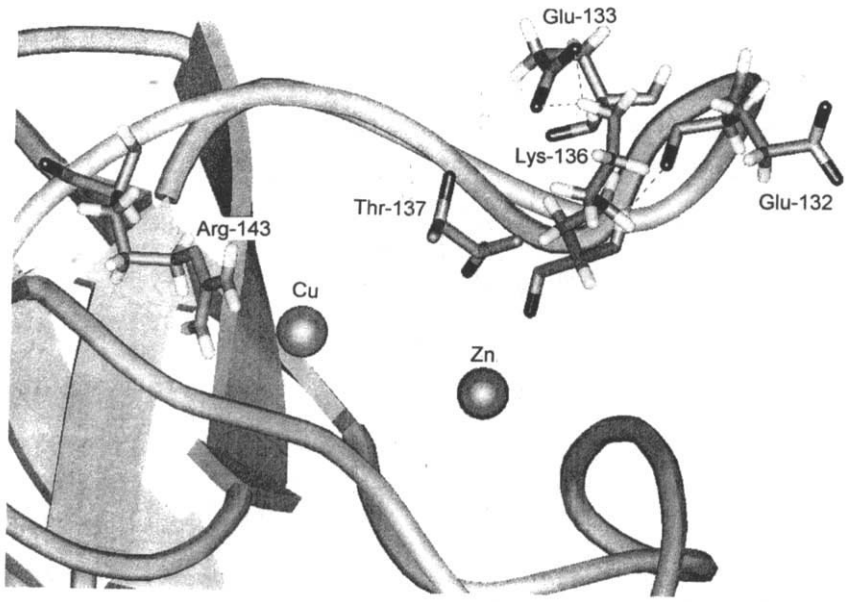

FIG. 22. The active site channel of human SOD with the hydrogen bond network among side chains of Glu-132, Glu-133, Lys-136, and Thr-137.

Asp-124 is responsible for a long-range bridge between the copper domain and the zinc domain, connecting, through hydrogen bonds, His-46 and His-71. Substitution of the residue with Asn, Gly, or Gln produces mutants that do not bind zinc. The mutants are stable at high pH whereas in the native zinc-deprived enzyme the copper ion, at high pH, moves to the zinc site to form a 50% dicopper derivative (*173*). The zinc-free Asn-124Asp mutant, at low pH (5–6), has about the same activity as wild-type SOD (Table III), and allows determination of the activity of a Cu_2E_2SOD derivative at high pH (Fig. 23) (*96*).

Through site-directed mutagenesis it was possible to design and obtain mutants that are significantly more active than the native protein (*174*). The substitution of the negative Glu-133 and/or Glu-132 with Gln, which gives rise to an increase in local positive charge while maintaining the orienting network, produces a two- to threefold more active protein (Fig. 24 and Table III). The decrease of activity on increase of ionic strength is stronger than for the native protein. These two effects corroborate the important role played by electrostatic interactions. However, electrostatic effects alone are insufficient to explain the activity behavior of SOD: the Glu-133Lys, Glu-132Gln mutant, which has a further increase in local positive charge, is less

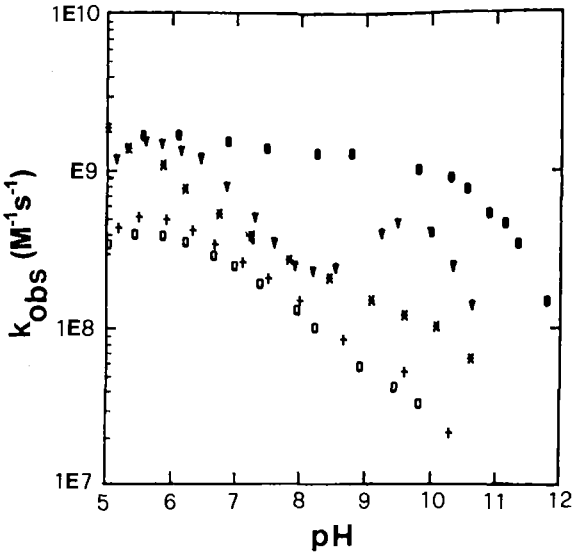

FIG. 23. Rate constant versus pH of Cu_2Zn_2 human SOD (●), Cu_2E_2 human SOD (▼), Cu_2E_2 Asp-124Asn SOD (★), Cu_2E_2 Asp-124Gly SOD (○), and Cu_2E_2 Asp-124Asn, Asp-125Asn SOD (+). Reprinted from Ref. *96*.

active than the Glu-133Gln, Glu-132Gln mutant, showing that the positive charge of Lys can disrupt the orienting network (*64*, *141*).

A similar enhancement of catalytic rate was observed with the Glu-131Gln mutant of *X. laevis* Cu_2Zn_2SOD, which corresponds to the Glu-133Gln of the human isoenzyme. However, the Asp-130Gln mutant differs from the corresponding mutant of the human enzyme: the mutant from *X. laevis* has a catalytic rate comparable to that of the native enzyme, indicating that some residues occupying the same position in the sequence of SODs from different organism might have a different role (*175*).

The role of Lys-136 is still a matter of debate. Its deprotonation has been related to the loss of activity observed at high pH (*116*). However, in the case of the human isoenzyme, the spectroscopic characterization, as a function of pH, of three mutants on this position (Arg-136, Ala-136, Gln-136), show the same pK_a values (within experimental error) as the native protein, both for the reduced and oxidized forms of the enzyme. These data ruled out Lys-136 as being responsible for the spectroscopically observed high-pH pK_a values (*119*). The activity of the Lys-136Gln and Lys-136Ala mutants at neutral pH is similar to that in the wild-type protein, whereas the Lys-136Arg de-

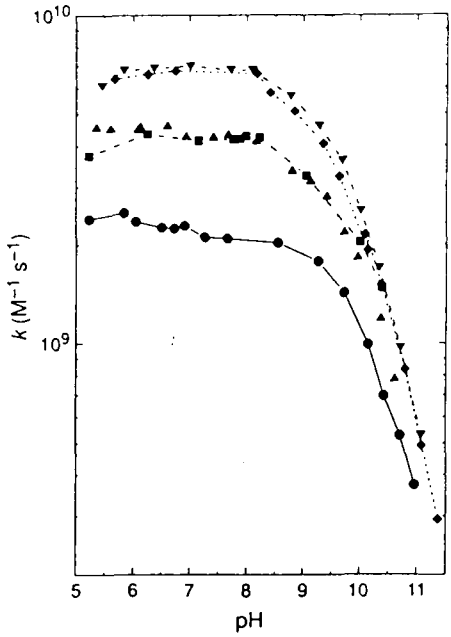

FIG. 24. Rate constant versus pH, at ionic strength = 0.01 *M*, for human SOD (●) and for the mutants Glu-132Gln, Glu-133Gln SOD (▼), Glu-133Gln SOD (◆), Glu-132Gln, Glu-133Lys SOD (■), and Glu-132Gln SOD (▲). Reprinted with permission from *Nature*; Getzoff, E. D.; Cabelli, D. E.; Fisher, C. L.; Parge, H. E.; Viezzoli, M. S.; Banci, L.; Hallewell, R. A.; **1992,** *358,* 347. Copyright 1992 Macmillan Magazines Limited.

rivative shows an increase of 1.5 times (Table III) (*119*). Activity profiles obtained through pulse radiolysis techniques on the same mutants indicate that the pK_a is essentially maintained, therefore Lys-136 does not seem to affect the activity profile (D. E. Cabelli, personal communication).

The role of the lysines of the active site channel, Lys-120 and Lys-134 (which correspond to positions 122 and 136 of the human isoenzyme) was investigated for the enzyme isolated from *X. laevis*. It was demonstrated that these lysines contribute to the steering of the superoxide anion toward the copper ion (*175*). Indeed, the activity of mutants at positions 120 and 134 is 60–65% with respect to wild type (*117, 175*). Furthermore, the pH dependence of the activity was investigated and the best fit of the experimental data was obtained with two pK_a values, $pK_1 = 9.3$ and $pK_2 = 11.3$, in the wild-type enzyme (*117*). The authors propose that pK_1 is mainly governed by Lys-120

and Lys-134 (*117*), even if the differences in pK_1 values for wild types and mutants are within experimental error.

In an attempt to redesign the metal binding site of SOD in order to convert it to a type 1 copper center, some mutants of yeast SOD, in which histidyl ligands in the metal sites were replaced by cysteines, were prepared (*150*, *176–178*). The mutant obtained substituting His-80 with Cys in the zinc site, and then replacing zinc(II) with copper(II), shows spectroscopic features typical of type 1 copper, as far as electronic, magnetic circular dichroism (MCD), electron paramagnetic resonance (EPR), and Raman spectra are concerned (*150*, *176*, *177*). On the other hand, when the newly introduced cysteine ligands bind copper(II) in its site, as in the case of His-46Cys and His-120Cys analogues, the properties of type 1 centers are not observed. Investigations on model complexes and on naturally occurring type 1 copper proteins have demonstrated that an essential feature is the presence of a trigonal N_2S site, whereas type 2 copper proteins tend toward tetragonal rather than trigonal geometries. Apparently the geometry around the metal, which is determined by the protein, is a determining factor as far as the type of copper is concerned. An interesting difference between His-46Cys and His-120Cys mutants is that the imidazolate bridge between copper and zinc remains intact in the His-46Cys mutant but is not present in the copper–cysteinate His-120Cys mutant (*177*, *178*).

In order to investigate the role of the imidazolate (His-63) that bridges copper and zinc ions, mutants on residue 63 have been prepared and characterized. The substitution of alanine in place of the bridging histidine ligand, in yeast SOD, perturbs the metal binding properties of the protein. The mutant His-63Ala shows significant changes in the geometry of the zinc site with respect to wild-type SOD, the pH independence of the spectral properties up to pH 12, typical of wild-type protein, is not maintained, and a pK_a of 9.3 was observed. In addition the activity of the His-63Ala mutant is pH dependent and, at physiological pH, is 250-fold less than that of wild type (*149*) (Table III).

The His-63Cys mutant seems to have the Cys bound to zinc, thus leaving copper(II) coordinated to three histidines and to solvent. Two water molecules have been proposed to interact with copper. Now water is regularly coordinated. The enzyme has no activity (Table III), although the reduction potential is still in the correct range to function. It has been proposed that a water bound to copper causes a decrease in the activity because the electron transfer has to occur through a water molecule rather than directly (*179*).

If we look at the interface of the dimer, a hydrophobic patch is noted that is responsible of the existence of the dimeric entity (Fig. 10). As mentioned in Section II, transformation of two neutral groups of the human isoenzyme (Phe-50 and Gly-51) into negative charged residues (two Glus) produces a monomeric species (*60*). This is checked through gel filtration experiments and through ^{1}H NMR of both the reduced derivative species and the oxidized paramagnetic CuCo derivative. The line width of the NMR signals is fully and unequivocally consistent with monomeric species. The ^{1}H NMR spectra show that the ligand assignment is similar to that of wild-type SOD and that the geometry of the chromophore is closest to that of the Ile-137 mutant (Table IV) (*60*). The enzyme is only 10% active (Table III) and its catalytic rate is not dependent on ionic strength. The reduction in activity has been ascribed to some structural changes in the active site channel, changes that may indirectly derive from the solvation of the newly exposed dimer interface or to its distortion (*60*). As far as the behavior with ionic strength is concerned, we should take into account that in this mutant the net protein charge is -4 (vs. -2 of the wild-type SOD subunit). As a consequence, the protein–substrate repulsion is higher than for wild-type SOD, which balances the steering effect of the positively charged residue in the active site channel. An increase in ionic strength, which reduces both electrostatic effects, seems to produce compensating effects in this case, thus producing catalytic rates that are ionic strength independent.

With the goal of increasing the catalytic activity a monomeric mutant (Phe-50Glu, Gly-51Glu), in which the negative Glu-133 is neutralized, was prepared. The mutant, Phe-50Glu, Gly-51Glu, Glu-133Gln, has an enhanced catalytic rate, and in contrast to Phe-50Glu, Gly-51Glu is ionic strength dependent. In this case the net protein charge is -3, compared to -4 of the Phe-50Glu, Gly-51Glu mutant, the protein–substrate repulsion is decreased, and the increased salt concentration again causes a decrease in catalytic rate (*124*).

V. Metal Substitutions

At low pH values SOD tends to lose the metal ions (*180*) and below pH 3 it exists almost entirely in a random coil form (*181*). Either the native metal ions or combinations of various metal ions can be readded to apoSOD at high pH to form a variety of metal-substituted SODs, which have been the subject of extensive physical measurements. ApoSOD is prepared by dialysis versus EDTA solution at pH

3.8 (*2*) or 1,10-phenathroline at pH 3.2 for 24 hr, at room temperature (*182*). In order to reobtain the holoenzyme or metal-substituted derivatives the pH is increased. The holoSOD was reconstituted from apoSOD for the first time in 1974 (*183*). A scheme to obtain metal-substituted derivatives is shown in Fig. 25.

It appears that Cu_2Zn_2SOD (and also Cu_2Cu_2SOD and Cu_2Co_2SOD) loses the metal at the zinc site between pH 4.5 and 3.0, and indeed all the spectral data indicate the formation of Cu_2E_2SOD[5] (*184*). The metal is rapidly rebound when the pH is raised. It is also suggested that a protein conformational change is involved rather than a simple competition between metal ions on one side and protons on the other. At pH below 4, the copper binding site is the only strong binding site. At pH 3.6, 95% of zinc is removed by dialysis, versus only 5% of copper (*180*). Below pH 3, copper is also lost from the protein (*184*). E_2Zn_2SOD can be obtained by reacting reduced SOD with CN^-, at pH 6 (Fig. 25).

For spectroscopic determinations of the amounts of protein material it should be noted that SOD absorbs, in the UV region, with a maximum at 265 nm. Different extinction coefficients were found for various isoenzymes, as a consequence of the different primary sequence. For example, ε_{max} is 15,900 M^{-1} cm^{-1}, for the human enzyme, and 10,300 M^{-1} cm^{-1} for the bovine enzyme (*2*, *103*). In the visible region of the electronic spectrum the holoenzyme has an absorption maximum at 680 nm [ε = 300 M^{-1} cm^{-1} (2)]. The Cu_2E_2 enzyme has a typical absorption with λ_{max} at 700 nm, at pH 6 (*183*). The two metal binding sites in SOD are largely determined by the tertiary structure of the protein, so that a number of M_2N_2SOD derivatives can be prepared (Fig. 25) with coordination properties similar to those seen for $Cu_2^{II}Zn_2^{II}SOD$ and $Cu_2^{I}Zn_2^{II}SOD$.

At the copper site there may be Ni^{2+}. This is obtained after addition of nickel at pH 7.5 to E_2N_2SODs that are obtained by adding the metal ion N to E_2E_2SOD at pH 6 (*185*) (Fig. 25). Nickel(II) is a reasonable probe for copper(II) because both tend, whenever possible, to give rise to square planar coordination geometries (*186*). Nickel(II) is five-coordinated, with a water molecule probably coordinated. When there is cobalt(II) in the copper site, the coordination number is again five, as in the case of nickel(II). However, when phosphate is present, it binds Arg-143 and cobalt. The latter would be displaced from its original place, causing detachment from the bridging histidine. Cobalt(II) is

[5] M indicates the metal ion in the copper site, N is the metal ion in the zinc site, and E means "empty."

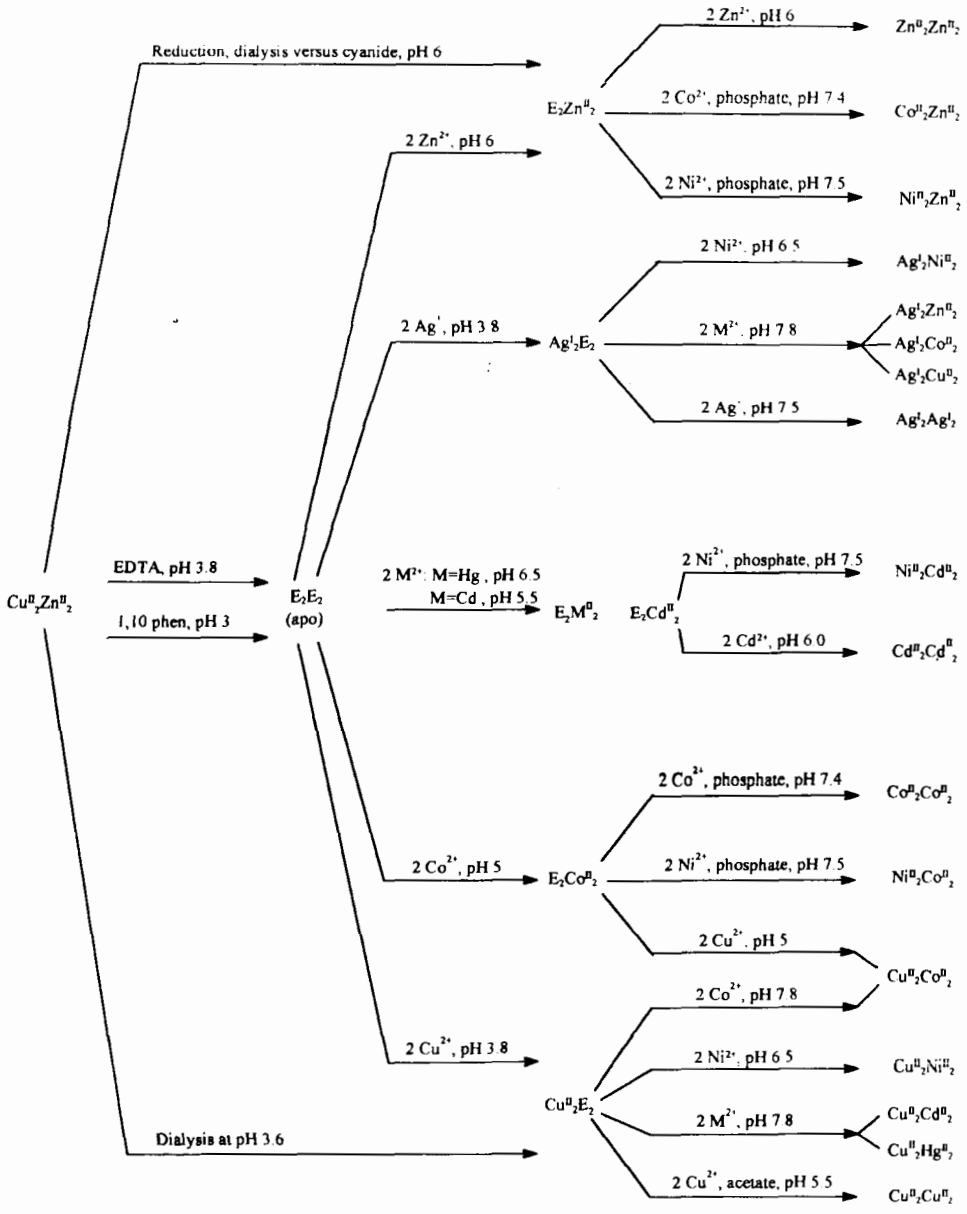

FIG. 25. Metal substitution procedures for Cu_2Zn_2SOD: E_2Co_2 (*289*); Cu_2Co_2 (*189, 350*); Cu_2Ni_2 (*258*); Cu_2Cu_2 (*252*); Cu_2Hg_2 (*243*); Cu_2Cd_2 (*243*); Cu_2E_2 (*243, 350*); Ag_2Zn_2 (*188*); Ag_2Co_2 (*188, 244*); Ag_2Ni_2 (*258*); Ag_2Cu_2 (*188*); Ag_2Ag_2 (*188*); Ag_2E_2 (*188*); Zn_2Zn_2 (*251, 351*); Ni_2Zn_2 (*185*); Ni_2Co_2 (*185*); Ni_2Cd_2 (*185*); Co_2Zn_2 (*185, 259*); Co_2Co_2 (*185, 259*); Cd_2Cd_2 (*197*).

tetrahedral with the three His nitrogens and a phosphate ion. Only above pH 10 is the bridge reestablished (*187*).

Ag^+ is a good probe for reduced copper, and has high affinity for the copper site. It may bind to the zinc site but only in the absence of other metal ions (*188*). When two Ag^+ and Cu^{2+} ions are present, only Ag_2Cu_2SOD is obtained, independently of the order of addition of the metal ions (*188*). The presence of Zn^{2+} in the zinc site increases the affinity of Ag^+, and thus it is proposed that zinc stabilizes the reduced enzyme. The only difference between Ag^+ and Cu^+ is that at high pH His-63 bridges Ag^+ and the metal at the zinc site, whereas Cu^+ remains coordinated to three His residues at every pH.

There may be a variety of metal ions in the zinc site (Fig. 25). The most important substitution (for spectroscopic studies) is that of zinc by cobalt (*189*). The coordination chemistry of cobalt is similar to that of zinc and the derivative is quite similar to the native enzyme. The affinity of zinc and other metal ions (*173*, *190*) for the zinc site at pH > 7.5 increases when copper(II) is bound to SOD. It seems that copper organizes the zinc site. Indeed, Cu_2E_2 transforms into Cu_2Cu_2 and E_2E_2SOD at pH higher than 7 (*173*).

For the E_2Co_2SOD derivative, a pH-dependent Co^{2+} migration from the zinc site to the empty copper site was observed, forming subunits containing Co^{2+} in both metal binding sites. The presence of phosphate was observed to facilitate the cobalt migration process, presumably due to the fact that the anion causes an enhancement of Co^{2+} binding to the copper site (*191*). Every time there is migration from E_2N_2SOD or M_2E_2SOD to MNSOD and EESOD, the problem remains of whether the M-His63-N moiety is randomly distributed or whether there is cooperativity within the dimeric unit of SOD.

An anticooperative behavior within the same subunit was proposed when copper binds E_2Co_2SOD at acidic pH (5.5). When the zinc site is partially occupied by cobalt, copper ions preferentially bind the subunits lacking cobalt. This can be explained by taking into account that the binding of copper to a site where the bridging His is already bound to cobalt requires a second deprotonation (*192*). An asymmetric behavior of the two subunits has been also proposed (*193*, *194*), but this hypothesis was shown to be wrong by Valentine *et al.* (*195*).

Cd^{2+} has been added either at the copper site or at the zinc site (*196*, *197*). Its properties have been investigated by perturbed angular correlation (PAC) studies and by ^{113}Cd NMR. The PAC coordination number may be higher than that usually proposed or found (*198*, *199*).

Differential scanning calorimetry has been used to compare the thermally induced unfolding of native SOD and apoSOD. The results

clearly demonstrate that metal ions play a significant role in enhancing the thermal stability of SOD (*31*). Some apparent affinity constant measurements are available for copper(II) and apoSOD (*200, 201*). The rate constant of metal release has been studied at low pH values (*182*).

The stability of the MNSOD derivative (indicated as such for this purpose) can be derived as follows: The first metal ion binds EESOD according to Eq. (12) with an apparent equilibrium constant K_M:

$$M + EESOD \rightleftharpoons MESOD. \tag{12}$$

The second metal ion binds according to Eq. (13) with apparent equilibrium constant K_N:

$$MESOD + N \rightleftharpoons MNSOD. \tag{13}$$

The overall stability is given by Eq. (14):

$$S_{MN} = \log K_M + \log K_N. \tag{14}$$

Table V gives the S_{MN} values that have been reported for several real and hypothetical derivatives of SOD at pH 6.25 (*188*). The data are instructive and show that the native enzyme is the most stable form.

From the early investigation of SOD (*202*) it was recognized that apoSOD was more labile toward a variety of inactivating stresses than was the holoenzyme. Addition of Cu^{2+}, besides restoring the ac-

TABLE V

RELATIVE SOLUTION STABILITIES OF METAL-SUBSTITUTED DERIVATIVES OF SOD AT pH 6.25[a]

M, N (in M_2N_2SOD)	$S_{M,N}$	M, N (in M_2N_2SOD)	$S_{M,N}$
Cu, Zn	24.9	Zn, Zn	18.15
Cu, Cu	24.5	Zn, Cu[b]	18.0
Ag, Zn	23.1	Ag, Ag	17.05
Ag, Cu	21.3	Zn, Ag[b]	14.15
Cu, Ag[b]	20.65		

[a] Reprinted with permission from Roe, J. A.; Peoples, R.; Scholler, D. M.; Valentine, J. S. *J. Am. Chem. Soc.* **1990,** *112,* 1538. Copyright 1990 American Chemical Society.

[b] Theoretical values: these species have not been observed.

tivity, enhanced the thermostability of the enzyme. Such stability further increases on addition of metal ions to the zinc site.

VI. Water in the Active Site Cavity

X-Ray crystallography has always shown the presence of water in the active cavity. Often, one molecule is about 2.2–3.0 Å from copper and another is a little farther (see Section II) (*41*, *44*, *63*, *75*).

Extended X-ray absorption fine structure (EXAFS) studies in aqueous solutions have shown that a water molecule in wild-type bovine SOD is 2.5 Å (Cu–O distance) from the metal (*203*). From ^{1}H NMR studies the same distance is proposed (see later). Ligand field calculations have shown that the water molecule essentially does not affect the energy levels (*89*, *204*).

The interaction of water with the paramagnetic copper(II) ion of oxidized SOD has been monitored through nuclear magnetic relaxation dispersion (NMRD) (*114*, *205–208*). The interaction of water protons with the unpaired electron of copper(II) causes an enhancement on the proton NMR relaxation. Usually the water proton T_1^{-1} measurements are performed at proton Larmor frequencies between 0.01 and 50 MHz. The profiles are of the type shown in Fig. 26. In a simplified model of the electron–nucleus coupling in macromolecules the T_1^{-1} enhancements are inversely proportional to the sixth power of

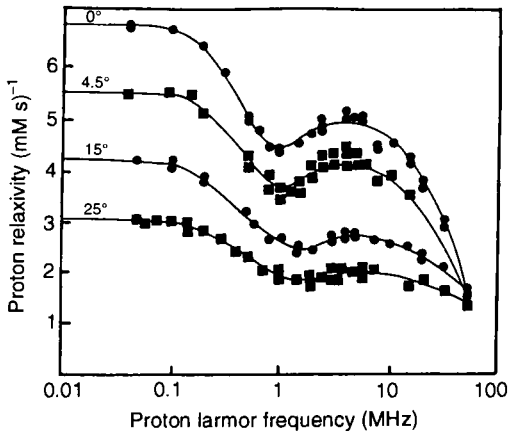

FIG. 26. ^{1}H T_1^{-1} values, as a function of the proton Larmor frequency for Cu_2Zn_2SOD at different temperatures (*205*). The lines are best-fit curves obtained with the inclusion of the effect of hyperfine coupling with the metal nucleus (*212*) (from Ref. *295*).

the average proton–copper distance and depend on the external magnetic field with an equation (*209*) of the type

$$T_1^{-1} \propto a\tau_s/(1 + \omega_s^2\tau_s^2) + b\tau_s/(1 + \omega_I^2\tau_s^2), \quad (15)$$

where ω_s and ω_I provide the energy of the split Zeeman levels for the electron and the nucleus, respectively, τ_s is the electron relaxation time, and a and b are constants containing the copper–proton distance. The drop of T_1^{-1} values at high field depends on the electronic relaxation time. If such time is the same, the T_1^{-1} values before the high-field decrease are proportional to the number of exchangeable protons sensing the unpaired electrons and to the reciprocal sixth power of the proton–copper distances. In general, a single water molecule is assumed to be responsible for the T_1^{-1} enhancement, so that analysis of the plots provides a copper–water distance.

The theory necessary for the analysis was developed in the 1980s (*207*, *210–213*) and a general computer program is now available (*214*). The program requires, besides the water proton T_1^{-1} values, the hyperfine coupling constants relative to the coupling between the copper nucleus and the unpaired electron. The program then provides the electronic relaxation times, the water–copper distance, and the angle between the copper–proton and the molecular z axis. In Table VI such values are reported for the native bovine SOD, human SOD, some mutants, and some adducts with inhibitors. The water–proton distance for bovine SOD is the same as proposed from EXAFS studies in aqueous solution (*203*).

In Fig. 27 the water ^1H T_1^{-1} profiles of Cu_2Zn_2SOD and of its Thr-137Ser, Thr-137Ala, and Thr-137Ile mutants are reported. The Ser derivative appears to have a water molecule closer to the metal ion (*115*, *208*, *215*). The Ala-137 derivative, as a consequence of the hydrophobicity of this residue, has a water molecule at a distance slightly longer than wild-type SOD (*115*, *208*, *215*). The NMRD profile of the Thr-137Ile mutant suggests that there is no water closer to copper(II) in the cavity, as there is in wild-type SOD, probably because of the bulkiness of the residue and the hydrophobicity of the cavity (*112*, *115*). As discussed in Section III,D, molecular dynamics simulations are capable of reproducing the presence of water in wild type SOD and its absence in the Ile mutant (*140*). The Thr-137Ile mutant is largely active (Table III), indicating that copper-bound water is not important for catalysis.

In the His-63Cys mutant (see Section IV,C) copper(II) is coordinated to three histidines and to solvent. Two water molecules have

TABLE VI

BEST-FIT PARAMETERS FOR THE WATER PROTON NMRD DATA ON Cu_2Zn_2SOD, SOME MUTANTS, AND SOME INHIBITOR DERIVATIVES

System[a]	τ_s (nsec)	r_{Cu-H} (Å)[b]	θ (deg)[c]	$A_\parallel$ (10^4 cm^{-1})	Ref.
BSOD	2.8	3.4	19	143	*207*
HSOD (yeast)	2.2	3.5	20	145	*208*
Cu_2E_2BSOD	3.6	3.2	24	148	*207*
Cu_2Cu_2BSOD	4.2	3.4	29	143	*207*
Arg-143GluHSOD	2.5	3.4	22	148	*208*
Arg-143IleHSOD	2.5	3.8	15	137	*208*
Thr-137AlaHSOD	1.5	3.7	—	140	*115*
Thr-137SerHSOD	2.1	3.2	—	140	*115*
Thr-137IleHSOD	3.8	4.7	20	162	*115*
His-63CysHSOD	1.5	2.8[d]	—	142	*179*
His-63CysHSOD + N_3^-	1.5	2.8	—	123	*179*
BSOD + 0.5 *M* P_i	3.2	3.3	36	143	*219*
BSOD + 0.5 *M* NCO^-	3.2	3.9	32	158	*219*
BSOD + 0.5 *M* NCS^-	2.3	3.6	19	—	*219*
BSOD + 2.0 *M* NCS^-	3.1	3.9	13	148	*219*
BSOD + 0.1 *M* N_3^-	3.9	4.8	37	157	*219*
BSOD + 2.0 *M* CN^-	7.7	5.2	53	188	*219*

[a] Abbreviations: BSOD, bovine SOD from erythrocytes; HSOD, human SOD.

[b] Calculated by assuming a single water molecule interacting with Cu^{2+} in the copper site with its protons equidistant from the ion.

[c] θ is the angle between the r_{Cu-H} direction and the unique axis of the hyperfine tensor for the interaction of a Cu^{2+} ion with its nucleus.

[d] Calculated by assuming two water molecules interacting with Cu^{2+}.

been proposed to be coordinated to copper on the basis of NMRD measurements. One of the water molecules is removed on azide binding (*179*).

Despite the indication that the water molecule close to copper in the native enzyme and in the mutants, not involving the metal ligands, has no effect on activity, it has some fine effects on some spectroscopic parameters. This appears true when the low-field water proton T_1^{-1} values are reported together with the values of $A_\parallel$ (between the copper ion and its unpaired electron) (see Tables IV and Table VI). In turn, large values of $A_\parallel$ are taken to indicate a deviation of the CuN_4 chromophore toward planarity (*216*). It has also been suggested that this is achieved through a displacement of copper. Of course, the effects described in Table VI are the results of fine structural changes sometimes not observable as optical transitions.

The water proton relaxivity of the native enzyme was found to in-

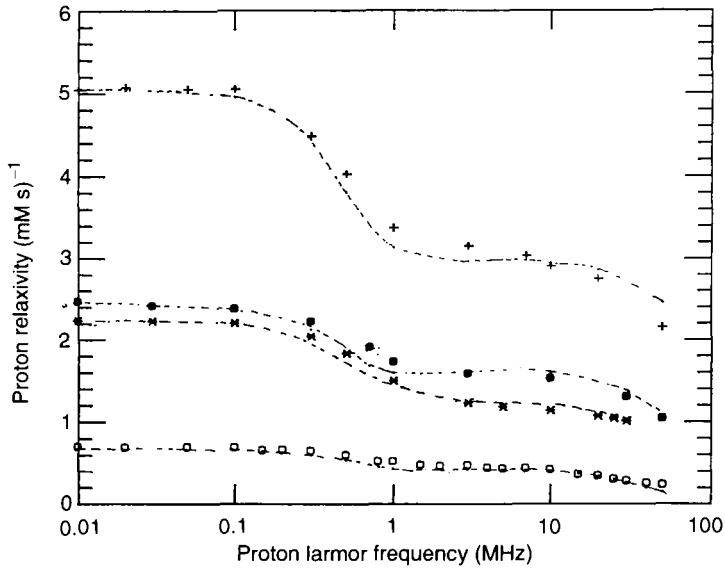

FIG. 27. ^1H T_1^{-1} values, at 298 K, as a function of the proton Larmor frequency for Cu_2Zn_2SOD (●), Thr-137Ser SOD (+), Thr-137AlaSOD (★), and Thr-137Ile SOD (○). T_1^{-1} values are subtracted from the bulk solvent and diamagnetic contribution and normalized to 1 m*M* copper concentration. Dashed lines are the best fits of the experimental data. Reprinted with permission from Banci, L.; Bertini, I.; Cabelli, D.; Hallewell, R. A.; Luchinat, C.; Viezzoli, M. S. *Inorg. Chem.* **1990,** *29,* 2398. Copyright 1990 American Chemical Society.

crease with pH, with a pK_a of 11.5 (*114*). A deprotonation of the water molecule interacting with copper was taken as explanation of this effect: indeed, the hydroxide proton was believed to experience a higher relaxation rate, with respect to water protons, as a consequence of a shorter Cu–H distance (*114*). Boden *et al.* suggested that the above behavior can be explained taking into account that, at high pH, an OH^- binds the copper ion, likely displacing a coordinated histidine (*206*). This hypothesis was partly confirmed by ^{17}O NMR studies of $H_2{}^{17}O$ solutions of bovine Cu_2Zn_2SOD: the large increase in T_{2p}^{-1} values, which is observed from neutral to alkaline pH, can be explained only by the addition of a hydroxide anion interacting with Cu^{2+} (*217*). The ^1H NMR spectra of the Cu_2Co_2SOD Ile-137 mutant show that all histidines are coordinated even at high pH (*120*).

The interaction of water with the copper ion in the presence of some anions that bind copper was monitored through NMRD (Fig. 28). In the case of N_3^- and CN^-, the water molecule is moved far away from

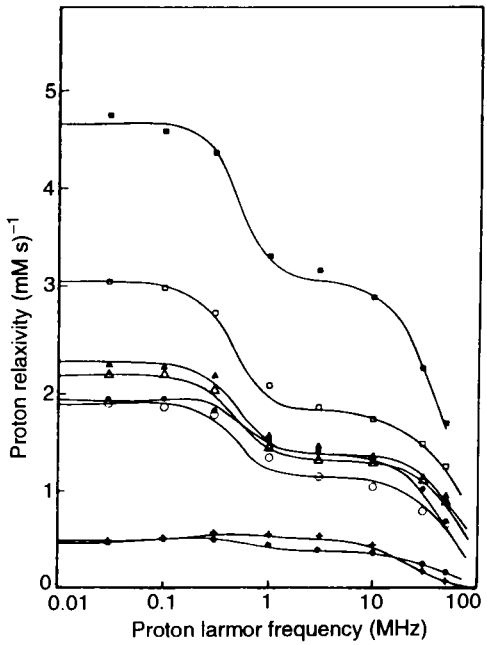

FIG. 28. ^1H T_1^{-1} values, at 298 K, as a function of the proton Larmor frequency for Cu_2Zn_2SOD solutions at pH 5.5 in the presence of 0.5 *M* $H_2PO_4^-$ (■), 0.5 *M* NCS^- (▲), 1.0 *M* NCS^- (△), 2.0 *M* NCS^- (○), 0.5 *M* NCO^- (●), a slight stoichiometric excess of CN^- (+), and 0.1 *M* N_3^- (★). The best-fit parameters are reported in Table VIII. Reprinted with permission from Bertini, I.; Banci, L.; Brown III, R. D.; Koenig, S. H.; Luchinat, C. *Inorg. Chem.* **1988,** *27,* 951. Copyright 1988 American Chemical Society.

the chromophore (*218*, *219*). In the case of NCO^-, there is a closer water molecule. In the presence of 0.5, 1.0, and 2.0 *M* NCS^-, which has a very low affinity constant, the water proton relaxivity decreases from the starting value toward those of NCO^-, with the largest effect between 0 and 0.5 *M* NCS^- (*219*). Phosphate, which was proposed to bind Arg-143 and not copper (Cu–P distance = 5 Å) (*106*), dramatically increases the relaxivity, probably because the acidic phosphate protons interact with the water molecule, increasing the number of exchangeable protons feeling the paramagnetic center (*219*).

Cu_2E_2SOD shows a more planar structure than the native enzyme. The profile for Cu_2E_2SOD has a higher relaxivity, attributable to a shortened Cu^{2+}–proton distance (*207*, *220*). The effect of N_3^- and NCS^- on Cu_2E_2SOD is similar to that observed on the native enzyme for the same anions (*220*). It is interesting to note that the T_1^{-1} values decrease down to about one-half by adding copper(II) until Cu_2Cu_2SOD

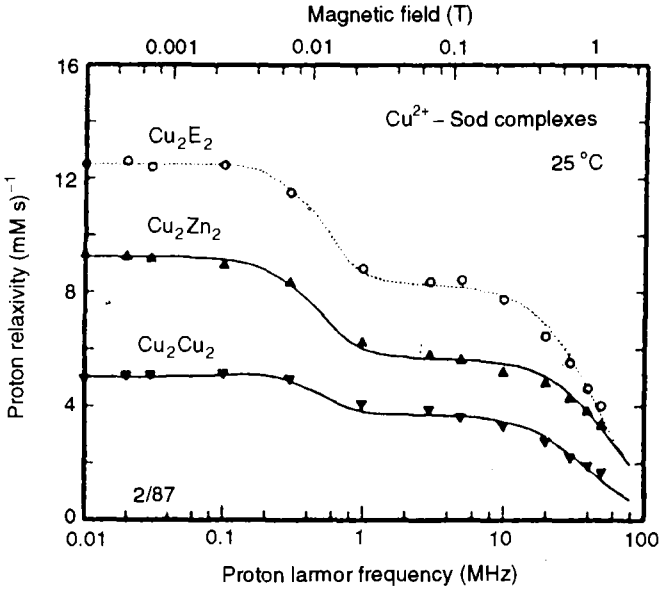

FIG. 29. ^1H T_1^{-1} values, at 298 K, as a function of the proton Larmor frequency for Cu_2Zn_2SOD, Cu_2E_2SOD, and Cu_2Cu_2SOD. T_1^{-1} values are subtracted from the bulk solvent and diamagnetic contribution and normalized to 1 mM copper concentration. Reprinted with permission from Banci, L.; Bertini, I.; Luchinat, C.; Monnanni, R.; Scozzafava, A. *Inorg. Chem.* **1988,** *27,* 107. Copyright 1988 American Chemical Society.

is formed (Fig. 29). The decrease in T_1^{-1} values is the result of magnetic coupling between the two metal ions whereas the electron relaxation values and copper–water distances are essentially not changed.

VII. Redox Properties

A. Reduction Potentials

Determination of the reduction potential of proteins is important when they perform redox reactions. Because SOD is a dismutase, its redox potential should be intermediate between that of the two semireactions [Eqs. (16) and (17)]:

$$O_2 + e^- \rightarrow O_2^- , \tag{16}$$

where $E^\circ = -0.33$ V vs. NHE (pH 7, $P_{O_2} = 0.101$ MPa), and

$$O_2 + 2H^+ + 2e^- \rightarrow H_2O_2, \tag{17}$$

where $E^\circ = 0.89$ V vs. NHE (pH 7).

Various values of reduction potentials for Cu_2Zn_2SOD are available, from 120 to 420 mV around neutrality. Values of 403 (*221*), 350 (*222*), 280 (*222*), and 400 mV (*223*) versus NHE at pH 7.0 and 120 mV at pH 7.5 (*224*) are reported in the literature. The variability of the values is largely due to the slow electron exchange rate, which is typical of nonelectron transfer proteins, especially if of large size. This reflects the experimental difficulties in such measurements. This aspect has been discussed in classical papers (*225*, *226*). If titrations are performed, the reactant should not interact with the protein by altering its potential. Potentiometric measurements, i.e., those methods based on the measurements of the reduction potential of systems containing various ratios of oxidized and reduced forms at equilibrium, need a redox partner that interacts weakly with the protein and reaches equilibrium fast. The latter condition is critical. Generally, the mediators that are used are capable of exchanging electrons with the protein and the partner. Direct methods, e.g., voltammetry, are very dependent on the protein–electrode interaction, which in turn depends on the applied potential and on the cleanliness of the electrode surface. Sometimes a promoter that is preferentially absorbed on the electrode is used. The hydrophilic nature of the promoter film prevents protein denaturation.

An extensive investigation of SODs and mutants has been performed by Luchinat *et al.* (*227*). The absolute values were later questioned by Hagen *et al.* (*224*). Still, the Luchinat investigation is the only one that allows comparison of the redox potentials among isoenzymes and mutants that have been treated with the same type of approach.

A typical cyclic voltammogram is shown in Fig. 30 for 10^{-3} *M* human SOD. 1,2-Bis(4-pyridyl)ethene has been used as a promoter. The working electrode was a gold electrode. The E° value has been taken as $E^\circ = (E_1 + E_2)/2$, where E_1 and E_2 are the anodic and cathodic peak potentials. The values are reported in Table VII. In 1973 Fee and Di Corleto (*223*) noted that the reduction of copper(II) is accompanied by the uptake of a proton from the medium. The reaction therefore is

$$\mathrm{ECu(II)} + e^- + \mathrm{H^+} \rightleftharpoons \mathrm{HECu(I)}. \tag{18}$$

The pH dependence of E° for human SOD is shown in Fig. 31. E° linearly decreases with increasing pH from 5 to 9. The slope is 55 mV/pH. The whole curve can be fitted with Eq. (19),

$$E^\circ = E^\circ_{\mathrm{lim}} + 2.3RT/F \log(1 + [\mathrm{H^+}]/K_a), \tag{19}$$

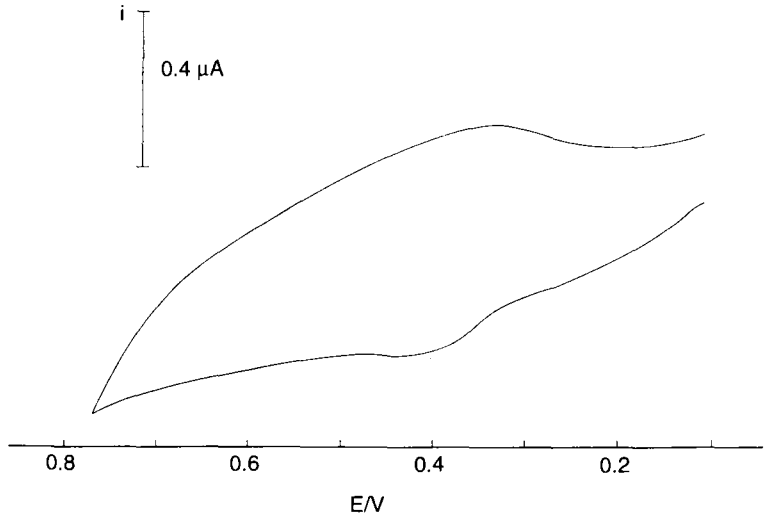

FIG. 30. Cyclic voltammogram of 10^{-3} *M* human SOD in the presence of 10^{-4} *M* 1,2-bis(4-pyridyl)ethene as a promoter and 0.1 *M* $NaClO_4$ as base electrolyte. Conditions: scan rate, 200 mV sec^{-1}, pH 7.42, 298 K. Reprinted with permission from Azab, H. A.; Banci, L.; Borsari, M.; Luchinat, C.; Sola, M.; Viezzoli, M. S. *Inorg. Chem.* **1992,** *31,* 4649. Copyright 1992 American Chemical Society.

where E°_{lim} is the high pH value (280 mV) and K_a is the constant of the single acid–base equilibrium. Its value is found to be 8.9 ± 0.6. The authors have discussed the meaning of this value in the light of the debate (*228*) on the deviation of pK_a obtained from electrochemical measurements with respect to the thermodynamic value. They concluded that this value could be consistent with that of 10.8 found from NMR measurements for the deprotonation of His-63, as shown in Fig. 32 (*227*). In this experiment the shift of the His-63 Hε1 proton is taken as a sensor of the protonation of His-63, according to the equilibria shown in Fig. 33.

The E° of the mutants so far investigated are lower than that of wild-type SOD (Table VII). Furthermore, substitution of Lys-136 has no effect on the pH dependence of E°, thus showing that its deprotonation is not involved in the pH dependence of E°. The Asp-124Asn mutation (see Section IV), which leads to a decrease in the affinity of the zinc site for metal ions and thus remains as Cu_2E_2SOD at every pH, has an E° value close to E_{lim} and is pH independent. The E° values for Cu_2E_2SOD, which undergoes the reaction given by Eq. (20),

$$2\,Cu_2E_2SOD \xrightarrow{pH} Cu_2Cu_2SOD + \text{apoenzyme}, \qquad (20)$$

TABLE VII

ELECTROCHEMICAL POTENTIALS FOR SOME ISOENZYMES AND AS-HUMAN SOD MUTANTS[a]

Derivative[b]	pH	$E°$ (V)	Ref.
BSOD	7.4	0.32	*227*
BSOD	7.0	0.40	*221*
BSOD	7.5	0.12	*334*
BSOD	7.0	0.28	*222*
BSOD	7.0	0.35	*222*
HSOD	7.4	0.36	*227*
AS-HSOD	7.4	0.37	*227*
Thr-137AlaHSOD	7.05	0.35(0.40)[c]	*227*
Thr-137SerHSOD	6.92	0.38(0.41)	*227*
Lys-136AlaHSOD	7.04	0.35(0.40)	*227*
Lys-136GlnHSOD	7.01	0.29(0.40)	*227*
Glu-133GlnHSOD	7.37	0.33(0.38)	*227*
Glu-132Gln, Glu-133GlnHSOD	7.45	0.30(0.37)	*227*
Cu_2E_2 AS-HSOD	5.11	0.28(0.51)	*227*
Cu_2E_2 AS-HSOD	7.50	0.25(0.37)	*227*
Cu_2E_2 AS-HSOD	9.15	0.23(0.30)	*227*
Cu_2E_2 AS-HSOD	10.55	0.22(0.29)	*227*
Cu_2E_2 Asp-124AsnHSOD	5.42	0.31(0.49)	*227*
Cu_2E_2 Asp-124AsnHSOD	7.21	0.30(0.39)	*227*
Cu_2E_2 Asp-124AsnHSOD	8.88	0.31(0.31)	*227*
Cu_2E_2 Asp-124AsnHSOD	10.45	0.29(0.29)	*227*

[a] AS-human SOD, Human SOD with the mutations Cys-6Ala, Cys-111Ser (see Section IV,A).

[b] BSOD, Bovine SOD from erythrocytes; HSOD, human SOD.

[c] The corresponding $E°$ values for human SOD-AS, obtained by interpolation from Fig. 31, are given in parentheses.

with a pK_a around 8, are similar to those of the Asp-124Asn mutant with the exception of a further decrease between pH 7 and 8, when migration starts to occur.

CN^- and N_3^- dramatically alter the $E°$ values (Table VIII). The measurement on the former derivative is performed at high pH. However, the low value is consistent with potentiometric measurements performed with methyl viologen (*222*) and with spectrophotometric titrations with $[Fe(CN)_6]^{4-}$ (*229*). With both anions, the oxidized form is so highly stabilized that SOD is no longer able to disproportionate O_2^- from the thermodynamic point of view.

As expected, Cu_2Co_2SOD behaves similarly to the native enzyme (Table VIII) (*227*).

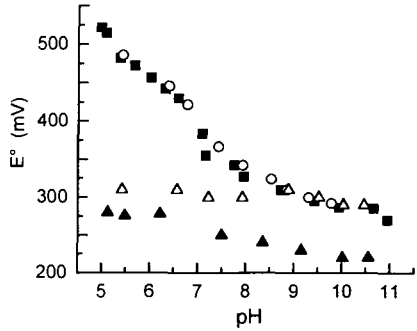

FIG. 31. The pH dependence of the redox potential for human SOD (■), human SOD-AS (○), Cu_2E_2 human SOD (△), and Cu_2E_2Asp-124Asn human SOD (▲). Reprinted with permission from Azab, H. A.; Banci, L.; Borsari, M.; Luchinat, C.; Sola, M.; Viezzoli, M. S. *Inorg. Chem.* **1992,** *31,* 4649. Copyright 1992 American Chemical Society.

B. ELECTRON TRANSFER BETWEEN $[Fe(CN)_6]^{4-}$ AND CU_2Zn_2SOD

The reduction potential of $[Fe(CN)_6]^{3-}$ is known (0.358 V) and that of SOD decreases with increasing pH. Therefore, the reaction given

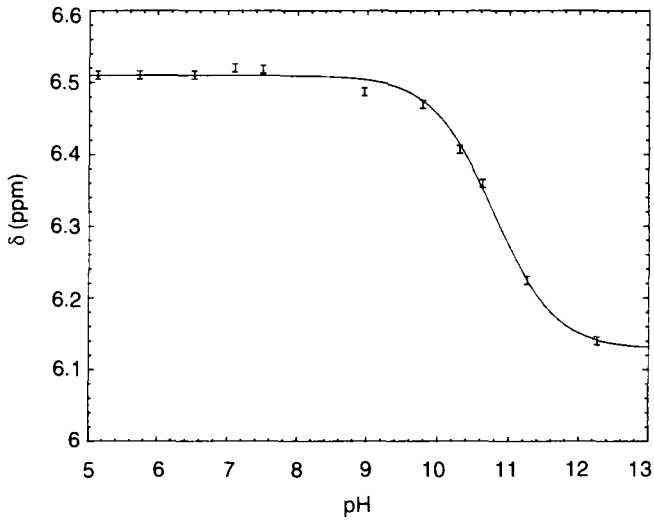

FIG. 32. Plot of the ^1H NMR chemical shift (600 MHz, 300 K) versus pH of the Hε1 of His-63 in reduced Cu_2Zn_2SOD. Reprinted with permission from Azab, H. A.; Banci, L.; Borsari, M.; Luchinat, C.; Sola, M.; Viezzoli, M. S. *Inorg. Chem.* **1992,** *31,* 4649. Copyright 1992 American Chemical Society.

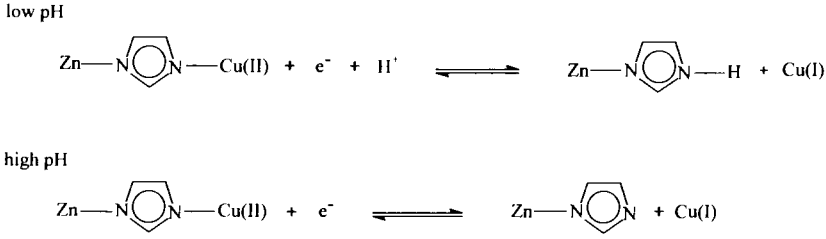

FIG. 33. Scheme of the deprotonation equilibria of the bridging His-63.

by Eq. (21)

$$ECu^{2+} + [Fe(CN)_6]^{4-} \underset{k_{-1obs}}{\overset{k_{1obs}}{\rightleftharpoons}} ECu^{+} + [Fe(CN)_6]^{3-} \qquad (21)$$

proceeds completely to the right in the pH range 5–7.2, starting with only the reactants (ECu^{2+} is the oxidized enzyme). The reaction is an overall second-order reaction and its rate is described by Eq. (22) (*229*):

$$d[ECu^{+}]/dt = k_{obs}[ECu^{2+}] = k_{1obs}[Fe(CN)_6]^{4-}[ECu^{2+}], \qquad (22)$$

where k_{obs} is the pseudo-first-order rate constant and k_{1obs} is the second-order rate constant for the reduction of ECu^{2+} by $[Fe(CN)_6]^{4-}$.

The reaction can be easily followed by monitoring, at 420 nm, the appearance of a band typical of $[Fe(CN)_6]^{3-}$. In Fig. 34 the linear relationship between k_{obs} and the concentration of the $[Fe(CN)_6]^{4-}$ is shown. The values of k_{-1obs} have also been obtained by measuring the rate of reaching the chemical equilibrium of the above reaction under

TABLE VIII

ELECTROCHEMICAL POTENTIALS FOR Cu_2Co_2 BOVINE SOD AND SOME ADDUCTS OF BOVINE SOD WITH ANIONS[a]

Derivative[b]	pH	$E°$ (V)
Cu_2Co_2BSOD	7.20	0.34(0.32)[c]
BSOD + N_3^-	7.32	−0.22(0.31)
BSOD + CN^-	10.18	−0.59(0.25)

[a] Reprinted with permission from Azab, H. A.; Banci, L.; Borsari, M.; Luchinat, C.; Sola, M.; Viezzoli, M. S. *Inorg. Chem.* **1992,** *31,* 4649. Copyright 1992 American Chemical Society.

[b] BSOD, Bovine SOD from erythrocytes.

[c] The corresponding $E°$ values for bovine SOD, obtained by interpolation, are given in parentheses.

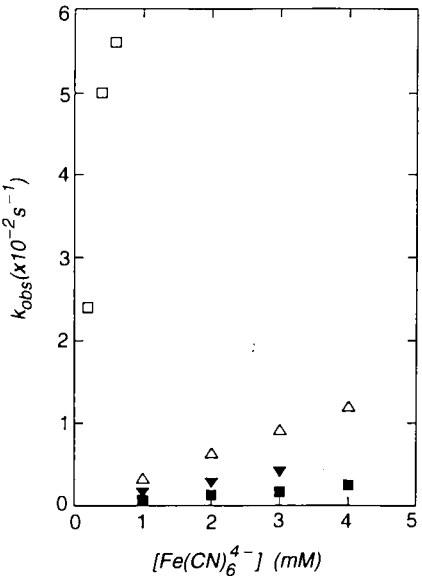

FIG. 34. Relationship between k_{obs} and concentration of $[Fe(CN)_6]^{4-}$ for human SOD (△) and some mutants: Glu-133Gln (□), Lys-136Gln (■), and Thr-137Ser (▽). Reprinted with permission from Bertini, I.; Hiromi, K.; Hirose, J.; Sola, M.; Viezzoli, M. S. *Inorg. Chem.* **1993,** *32,* 1106. Copyright 1993 American Chemical Society.

certain conditions. It has also been verified that the apparent equilibrium constant K is given by

$$K = k_{1obs}/k_{-1obs}. \tag{23}$$

The values of the three constants are reported in Fig. 35. It appears that k_{1obs} increases with increasing pH above pH 6, providing the pH dependence of K (*223*).

It is possible that, as for the substrate, the rate of approach determines k_{1obs} because the following step, electron transfer, may be quite fast. The approach of the anion may be regulated by the charge in the active cavity. Indeed, the kinetic values (Table IX) indicate a dramatic decrease when the positive Arg-143 is substituted by an Ile and a dramatic increase is observed when the negative Glu-133 residue is neutralized. The change in activity (Table IX) is qualitatively parallel, but not quantitatively, probably on account of the different charges of the two anions (i.e., $[Fe(CN)_6]^{4-}$ and O_2^-), which magnify the effect of the electrostatic charges in the active cavity in the case of $[Fe(CN)_6]^{4-}$ (*230*).

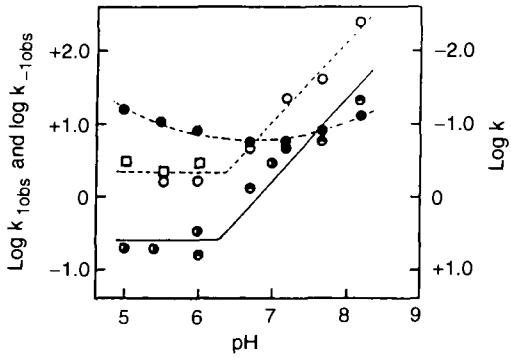

FIG. 35. The pH dependence of k_{1obs}, k_{-1obs}, and K: k_{1obs} (●) and k_{-1obs} (○) were directly obtained by kinetics; k_{-1obs} (□) was indirectly obtained by k_{1obs}/K; the apparent equilibrium constant K (◑) was obtained by the equilibrium method of Fee *et al.* (*223*); the apparent equilibrium constant K (◓) was obtained by the kinetic method. Reprinted with permission from Ozaki, S.; Hirose, J.; Kidani, Y. *Inorg. Chem.* **1988,** *27,* 3746. Copyright 1988 American Chemical Society.

A temperature dependence of the reduction potential allowed the calculation of the thermodynamic parameters (*221*): $\Delta G^{\circ\prime} = -9.31$ kcal/mol, $\Delta H^{\circ\prime} = -21.4$ kcal/mol, and $\Delta S^{\circ\prime} = -25.1$ eu (pH 7.0, I = 0.1 M) (*221*). The large negative $\Delta H^{\circ\prime}$ is attributed to strong Cu(I)–Im bonds and to the protonation of the bridging Im. It is proposed that

TABLE IX

REDUCTION RATE CONSTANTS AND ACTIVITIES FOR O_2^- DISMUTATION OF HUMAN SOD AND SOME OF ITS MUTANTS WITH $[Fe(CN)_6]^{4-}$[a]

Derivative	k_{1obs} (M^{-1} sec^{-1})	Activity (%)
Human SOD	2.88	100
Arg-143IleHSOD	0.018	11[b]
Thr-137SerHSOD	1.44	70[c]
Glu-133GlnHSOD	108	222[d]
Lys-136GlnHSOD	0.63	65[e]
Asp-124AsnHSOD	No reduction	81[f]

[a] Reprinted with permission from Bertini, I.; Hirami, K.; Hirose, J.; Sola, M.: Viezzoli, M. S. *Inorg. Chem.* **1993,** *32,* 1106. Copyright 1993 American Chemical Society.

[b] From Ref. *104.*

[c] From Ref. *115.*

[d] From Ref. *64.*

[e] From Ref. *119.*

[f] From Ref. *96.*

zinc(II) binding at the zinc site stabilizes a protein configuration at the copper site that is particularly favorable for Cu(I) binding. The negative entropy implies an increase in order on breaking the His-63 bridge. This may be not surprising if it is considered that the latter has not much freedom, that the proton comes from the solvent, and that water is indeed not bound to copper(II). The changes in the thermodynamic parameters account for the high reorganization energy associated with electron transfer; such reorganization energy makes SOD a poor electron transfer carrier.

VIII. The Spectroscopic Properties of Metal Ions

Spectroscopy is used to study metalloproteins whose X-ray structure is available in order to obtain further information on fine effects that generally escape detection with X-ray analysis or to provide additional evidence about electronic structure, dynamics, and reactivity. In the absence of X-ray analysis, spectroscopy becomes a challenge and represents a means to figure out structural information. In the case of SOD spectroscopic investigations have been very numerous because (1) metal substitution provides a unique wealth of derivatives and (2) the structural data were few until 1982, when the first structure became available and the scientific community was eagerly expecting the structure of other derivatives. It was not until after 1992, however, that several groups started producing X-ray structures. Therefore, most of the spectroscopic data preceded pertinent X-ray analysis, and now it may be useful to revisit the early work. A thorough review on the spectroscopic properties of SOD up to 1990 is available in the literature (*231*).

It may be appropriate to comment about the rigidity of the donor groups in SOD. In M_2N_2SOD, the geometry of the ligands of M is fixed by the protein frame and there is only a minor effect of the metal ion, which, however, may have preference for a certain stereochemistry. Therefore M^{2+} is generally bound to four His and sometimes to a water molecule. N^{2+} is bound to three His and an Asp. The possibility that the Asp behaves as bidentate with some metal ions has been mentioned (*232*) but never proved. Anions bind M^{2+} and, depending on the donor strength, may displace copper from the original position and loosen a metal–His bond. When M = M^+, His-63 is not bridging (*233*) except in one crystalline form (*82*) (see Section II,I).

A. Copper(II) in Native Protein

The copper(II) ion as a d^9 ion has a d–d spectrum, often with a single broad band that contains several transitions. The electronic

spectrum is reported in Fig. 36 (*2, 234–239*). The maximum at 14,700 cm^{-1} is responsible for the green color of the protein. There are other transitions in the UV region. The CD spectrum of the human enzyme shows a better resolution with bands at 13,300, 16,700, 22,400, 29,600, and 33,000 cm^{-1} (Fig. 37) (*204*). The first two bands belong to *d–d* transitions. A further weak positive CD band has been proposed by Valentine *et al.* to be present at 18,800 cm^{-1}, which would again be a *d–d* transition (*239*). The weak band at 22,400 cm^{-1} has been assigned to the lowest ligand metal charge transfer (LMCT) band. This band disappears whenever the bridge is removed and then is reasonably assigned to the bridging His to copper charge transfer (CT) (*239*). The last two bands are LMCT (*239*). This assignment is supported by model complexes having tetragonal Cu–imidazole and Cu–imidazolate compounds (*240, 241*). The spectra are essentially pH independent in the range pH 4–10. At pH below 4 the bridge is broken on the side facing zinc (*181*). What happens at high pH values will be discussed together with the role of anions (see later).

The EPR spectrum is rhombic at every temperature from 77 K to room temperature (*218, 242–244*) (Fig. 38). The $A_{\parallel}$ of the bovine enzyme is 141×10^{-4} cm^{-1}. The A_x and A_y values are obtained by simulating the spectra and are 35×10^{-4} and 52×10^{-4} cm^{-1}, respectively (*245*). The EPR spectra are shown in Fig. 38. In Table IV the relevant

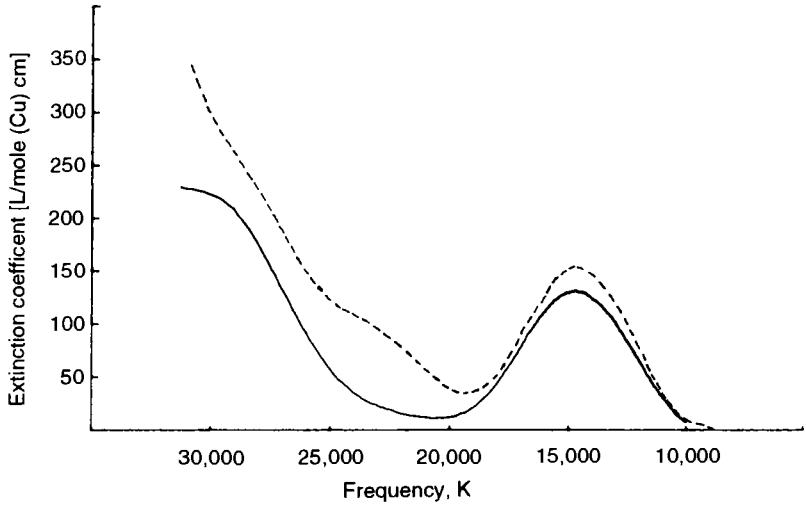

FIG. 36. Visible and near-IR absorption spectrum of $Cu_2^{II}Zn_2^{II}$ bovine SOD (---) and $Cu_2^{II}E_2$ bovine SOD (—) at pH 6.1. Reprinted with permission from Pantoliano, M. W.; Valentine, J. S.; Nafie, L. A. *J. Am. Chem. Soc.* **1982,** *104,* 6310. Copyright 1982 American Chemical Society.

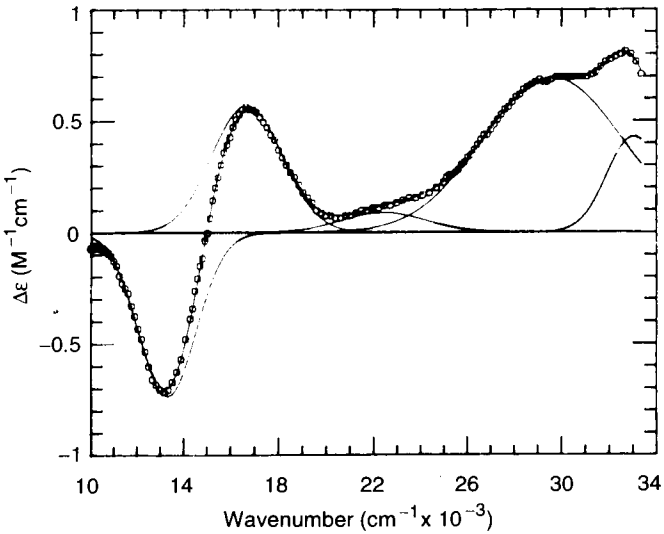

FIG. 37. Visible and near-IR circular dichroism spectrum of $Cu_2^{II}Zn_2^{II}$ human SOD with the individual Gaussian lines in the fitting of the experimental data. Reprinted with permission from Ref. *204*.

EPR data are reported for a series of isoenzymes, mutants, and anion derivatives. Single-crystal studies have led to two possible orientations of the g tensor (*245*). The d–d transitions, g values, and g orientations have been reproduced through an angular overlap model (*204*). The best fitting of the electronic transitions was achieved with nitrogen ligand parameters $e_\sigma^N = 7600$ cm^{-1}, $e_\pi^N = 1000$ cm^{-1}, and the water parameter $e_\sigma^O = 0$ cm^{-1}. With the same parameters the computed g values are $g_x = 2.03$, $g_y = 2.08$, and $g_z = 2.28$, which fit quite well with the data obtained from single-crystal studies ($g_x = 2.03$, g_y

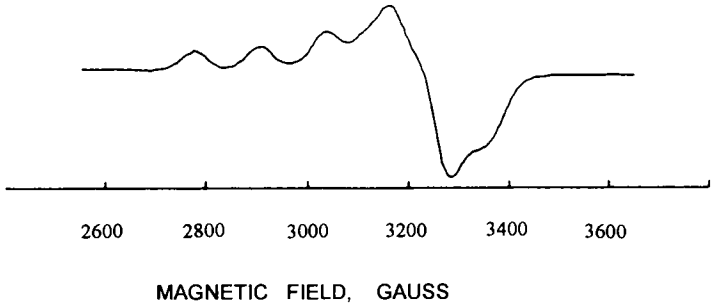

FIG. 38. EPR spectrum of $Cu_2^{II}Zn_2^{II}$ bovine SOD at pH 5.6 (303 K). Reprinted with permission from Pantoliano, M. W.; Valentine, J. S.; Mammone, R. J.; Scholler, D. M. *J. Am. Chem. Soc.* **1982,** *104,* 1717. Copyright 1982 American Chemical Society.

= 2.09, g_z = 2.26) (*245*). It appears that the water molecule does not contribute to the ligand field splitting. This is in agreement with the model that requires a free approach site for O_2^- (*246*).

Through electron spin echo spectroscopy, a splitting of the low-field lines was observed, arising from the interaction of copper(II) with the remote ^{14}N atoms of the coordinated imidazoles. This splitting, which disappears at low pH, was attributed to the presence of a divalent metal linked by an imidazolate bridge (*247*).

Electron and nuclear double resonance (ENDOR) studies at 5 K have led to the assignment of all protons of histidines bound to copper (*248*, *249*) and to the factorization of the coupling constants into a dipolar and an isotropic part. This has been possible through irradiation of a frozen sample at different g values. Figure 39 shows ENDOR spectra of bovine Cu_2Zn_2SOD, obtained at five working points of the

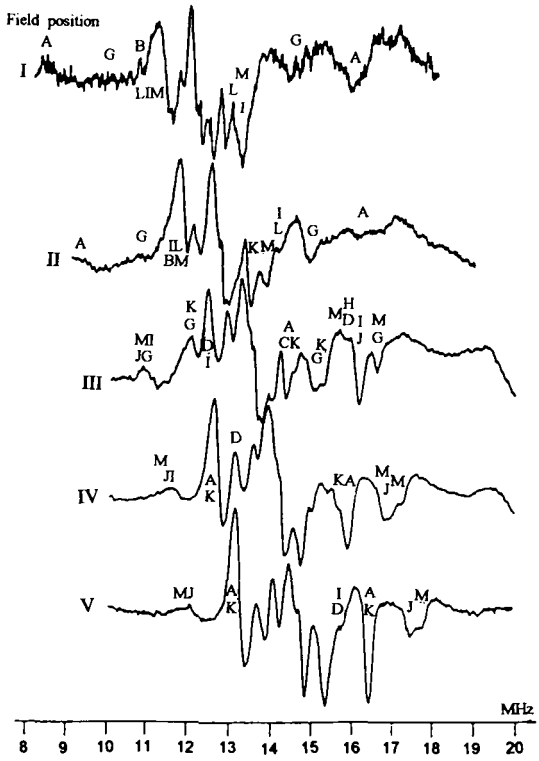

FIG. 39. ENDOR spectra of bovine SOD obtained at the five working points across the EPR spectrum. The letters indicate assigned resonances (see Table X). Reprinted with permission from Reinhard, H.; Kappl, R.; Hutterman, J.; Viezzoli, M. S. *J. Phys. Chem.* **1994,** *98,* 8806. Copyright 1994 American Chemical Society.

EPR spectrum. In Table X the assignment of some resonances is reported together with the isotropic hyperfine coupling constants. In all cases but three, the values are the same as those calculated from NMR contact shifts of the Cu_2Co_2 derivative at room temperature (see Section VIII,M). It is possible that these discrepancies may derive from slight geometrical distortions of the copper–histidine system at low temperature. The ^{14}N and ^{15}N hyperfine parameters of the coordinated nitrogens are also available, with the quadrupolar splitting of the former (*249*). Coupling with the distal nitrogens was observed through electron spin echo envelope modulation (ESEEM) of the ^{15}N enriched protein (*250*), though not specifically assigned.

^1H NMR experiments cannot be performed in this protein if interest is focused on the copper ligands, because the large electronic relaxation times broaden the lines beyond detection in a sphere about 6 Å from copper. Actually, the disappearance of histidine signals from reduced to oxidized state allowed the first proposal to be made about the coordinated His (*251*).

TABLE X

ISOTROPIC COUPLING CONSTANTS OF THE HISTIDINE PROTON SIGNALS IN THE ENDOR SPECTRA OF BOVINE SOD[a]

Protons[b]	Line assignment	a_{iso} (MHz)[c]
Hβ1 (His-44)	A	0.6118(0.350)
Hβ2 (His-44)	B	0.6118
Hδ2 (His-44)	C	0.8132
Hε1 (His-44)	D	0.4788
Hε2 (His-44)	E	1.0450
Hδ1 (His-46)	F	1.6492
Hδ2 (His-46)	G	0.6954
Hε1 (His-46)	H	1.2844
Hδ2 (His-61)	I	0.8740
Hε1 (His-61)	J	0.8740(1.440)
Hδ1 (His-118)	K	1.8810
Hδ2 (His-118)	L	0.6498
Hε1 (His-118)	M	1.2198(1.900)

[a] Reprinted with permission from Reinhard, H.; Kappl, R.; Huttermann, J.; Viezzoli, M. S. *J. Phys. Chem.* **1994,** *98,* 8806. Copyright 1994 American Chemical Society.

[b] His numbering follows the bovine SOD sequence.

[c] Isotropic coupling constants are in agreement with those obtained from the NMR contact shifts within experimental error except for three coupling constants, for which the corresponding values from the NMR contact shifts are given in parentheses for comparison.

The ^1H nuclear magnetic relaxation dispersion is discussed in Section VI.

B. Copper(II) in the Cu_2E_2 Enzyme

The electronic spectra show a small shift toward the high frequencies with respect to the native state (Fig. 36) (*239*, *243*). A similar shift is observed in the CD spectrum at low pH for the d–d transitions (*239*). Furthermore the weak band at 22,400 cm^{-1}, assigned to the lowest LMCT band (*239*), disappears because of the absence of the imidazolate bridge. In the EPR spectrum the $A_\parallel$ values is somewhat larger ($A_\parallel = 148 \times 10^{-4}$ cm^{-1}) than that in the native protein (Table IV) (*184*, *243*). It seems that the removal of the constraint due to the bridge relaxes the coordination sphere, providing a more tetragonal environment. This is more evident at low pH than at neutral pH. As a result of this minor rearrangement, according to NMRD measurements, the water close to copper is moved further away (see Section VI). Electron spin echo spectra of Cu_2E_2SOD show lines of 0.7, 1.5, and 4 MHz, which resemble the spectra of a model compound containing an imidazole ligand [Cu(II)–diethylenetriamine–imidazole] (*247*).

At pH > 7, Cu_2E_2SOD transforms into Cu_2Cu_2SOD and apoSOD (see Section V) (*173*).

C. Copper(II) with Other Metal Ions in the Zinc Site

Several copper derivatives have been prepared with Cu, Co, Ni, Cd, and Hg in the zinc site. The Cu_2Cu_2SOD shows magnetic exchange coupling effects between the two metal ions through the histidinato bridge. In a classical experiment copper(II) was added to apoprotein at pH 5.5 and the titration was followed by EPR. At the beginning the EPR of copper in the copper site developed and eventually the spectrum of the Cu–Cu dimer appeared, with simultaneous disappearance of the EPR spectrum of the monomer (Fig. 40). If the hamiltonian is written as

$$H = J\hat{S}_1 \cdot \hat{S}_2, \tag{22}$$

and the EPR parameters are explained with $J = 26$ cm^{-1} and the $S' = 0$ ground state (*252*). Such a J value has been obtained through the temperature dependence of the intensity of the EPR signal, which depends on the population of the excited $S' = 1$ level (*252*). The spectrum, which was first reported in 1973 (*253*), was subsequently shown to be due to the Cu–Cu moiety (*173*, *252*). The hyperfine values are about one-half of the monomeric species, as expected (*252*, *254*). The

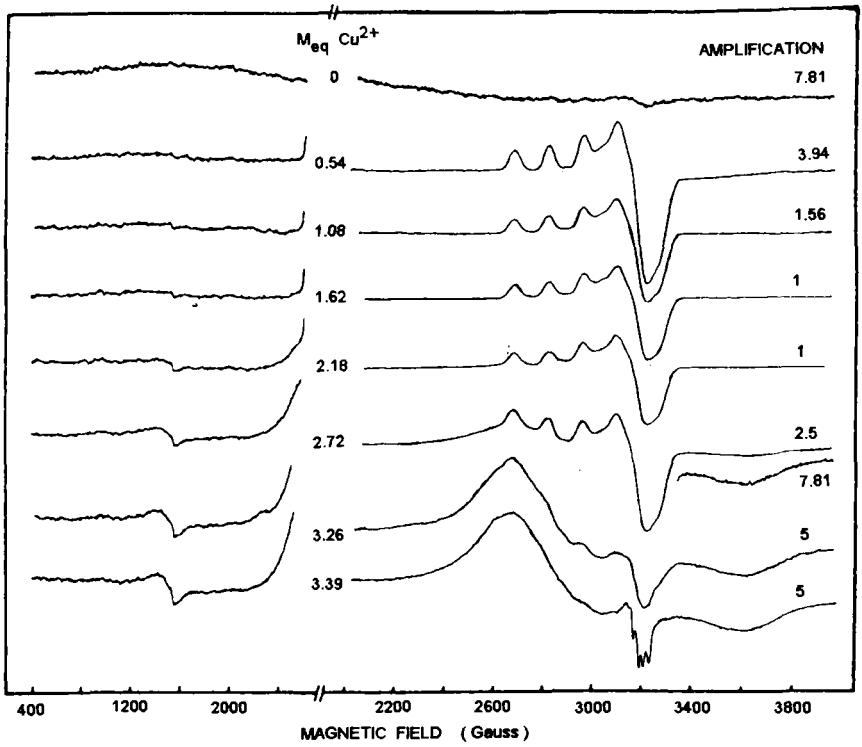

FIG. 40. EPR titration of apoSOD with Cu^{2+}. The spectra were recorded near 1090 K. Reprinted from *Biochim. Biophys. Acta,* Vol. 400; Fee, J. A.; Briggs, R. G.; p. 439, Copyright 1975, with kind permission of Elsevier Science–NL, Sara Burgerhartstraat 25, 1055 KV Amsterdam, The Netherlands.

interaction between the ground state of one copper and the excited levels of the other has been proposed to be significant with respect to the energy separation between $S' = 0$ and $S' = 1$ (*255*). In the lyophylized state the imidazole bridge is broken and the EPR of the two copper sites appears (*256*). This shows that some tension is experienced by the copper site. The visible absorption spectrum shows a very broad band with a maximum at 12,500 cm^{-1} (*173, 243*).

Copper(II) also experiences magnetic exchange coupling with cobalt(II) and nickel(II) when they occupy the zinc site. In the former case J has been estimated to be 17 cm^{-1} (*257*). The electronic spectra of copper(II) are barely affected by the presence of cobalt(II) or nickel(II) instead of zinc(II) (*243, 258*). The same holds when cadmium and mercury are in the zinc site (*243*).

D. Nickel(II) in the Copper Site

The electronic spectrum of Ni^{2+} in Ni_2N_2SOD is shown in Fig. 41 (*185*). It shows absorptions at 14,815 and 25,600 cm^{-1} with molar extinction coefficients of 14 and 85 M^{-1} cm^{-1} per subunit, respectively. The low intensity indicates the *d–d* nature of these transitions. The former band is attributed to the highest $^3F \rightarrow {}^3F$ transition and its value has been sensibly attributed to five-coordination. It is proposed, as in the case of cobalt, that the coordination donors are four His nitrogens (*185*). Although not clearly stated, it is probable that a water oxygen is the fifth ligand. The ^1H NMR spectra are well resolved, as shown in Fig. 42. The signals A, B, and G, which are due to exchangeable protons, are assigned to the three NH protons of the coordinated His and signal H is assigned to the metalike proton of His-46 (*185*).

E. Cobalt(II) in the Copper Site

If cobalt(II) is added to E_2N_2SOD, in the presence of acetate buffer, a five-coordinated complex is obtained (*259*) with four His nitrogens and a water oxygen as donors. Consistently, the electronic spectrum has a low absorbance (Fig. 43) (*259*) and the ^1H NMR spectrum gives sharp and well-spread signals (*260*) as a result of fast electronic relaxation times and large magnetic anisotropy (Fig. 44). The EPR spectra (Fig. 45) can be recorded at liquid helium as long as N is a diamag-

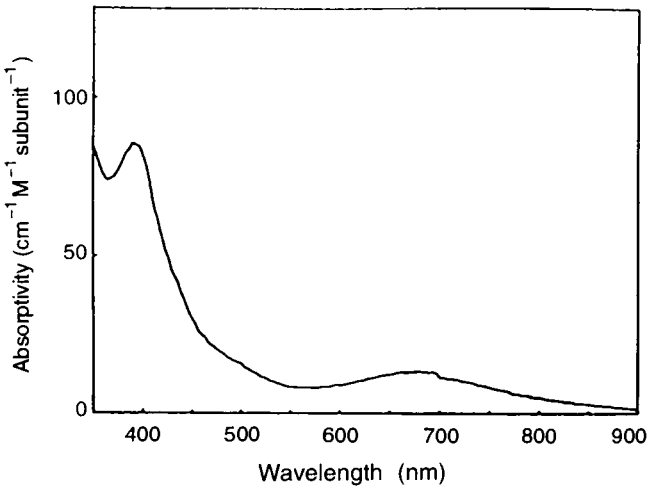

FIG. 41. Electronic spectrum of Ni_2Zn_2SOD in 50 m*M* phosphate buffer, pH 7.5. Reprinted from Ming, L. J.; Valentine, J. S. *J. Am. Chem. Soc.* **1990,** *112,* 6374. Copyright 1990 American Chemical Society.

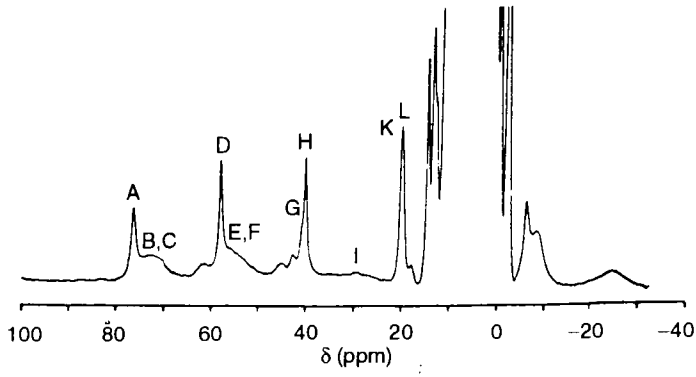

FIG. 42. The 200-MHz ^{1}H NMR spectrum of Ni_2Zn_2SOD in 50 m*M* phosphate buffer, pH 7.5. Reprinted from Ming, L. J.; Valentine, J. S. *J. Am. Chem. Soc.* **1990,** *112,* 6374. Copyright 1990 American Chemical Society.

netic metal (i.e., Zn^{2+}, Cd^{2+}) (*259*). The interaction of N_3^- with Co_2Zn_2-SOD was studied in the presence and in the absence of phosphate: EPR, NMR, and optical titrations demonstrated that different adducts are obtained depending on the presence of phosphate, at variance with what happens with CN^-, indicating a different mechanism of binding for different anions (*261*). If N is paramagnetic, magnetic exchange coupling occurs between cobalt(II) and N. On magnetic coupling, the total spin is either zero or an even number, and no EPR spectra are detected under the usual conditions. In Co_2Co_2SOD, the magnetic coupling and the fast electronic relaxation rates of five-coordinated cobalt induce fast electron relaxation in tetrahedral cobalt (i.e., that at the zinc site), and the NMR signals of the latter (Fig. 46a) are much sharper than in M_2Co_2SOD with M diamagnetic (*187, 191, 260*). The chemical shifts of the signal of tetrahedral cobalt are

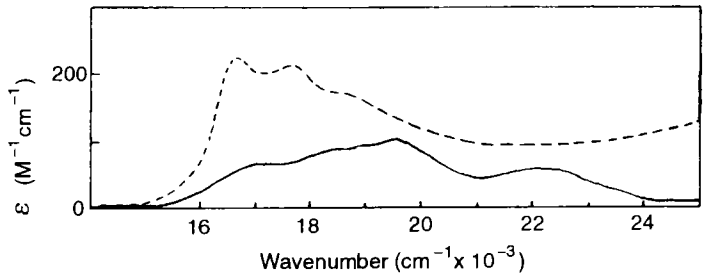

FIG. 43. Electronic spectra in the visible region of Co_2Zn_2SOD in the absence of phosphate (—) and Co_2Zn_2SOD in the presence of phosphate (---). Adapted with permission from Banci, L.; Bertini, I.; Luchinat, C.; Monnani, R.; Scozzafava, A. *Inorg. Chem.* **1987,** *26,* 153. Copyright 1987 American Chemical Society. Also adapted from Ref. *260.*

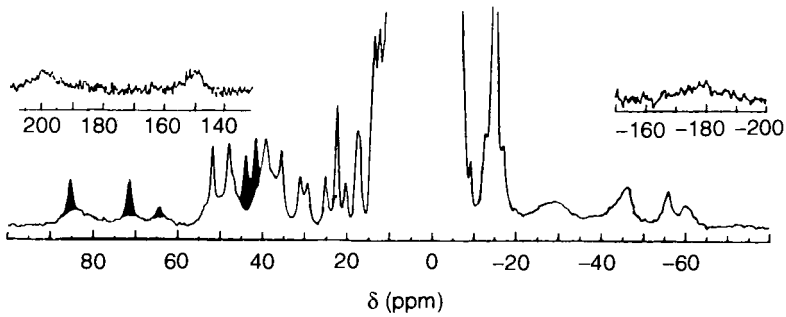

FIG. 44. The 90-MHz ^1H NMR spectrum of Co_2Co_2SOD. The filled signals belong to exchangeable protons. Reprinted with permission from Ref. *260*.

different depending on whether there is or is not a five-coordinated cobalt(II) at the copper site. In fact, the latter cobalt causes some pseudocontact shifts on the signals of the tetrahedral cobalt domain.

When cobalt(II) is added to E_2N_2SOD in phosphate buffer, an absorption spectrum typical of tetrahedral cobalt is displayed (Fig. 43). The EPR spectrum of cobalt(II) can be observed at liquid helium when N is diamagnetic (*259*) (Fig. 45a). It is suggested (*187*) that phosphate bridges the Arg-143 and the cobalt ion, thus moving the latter toward the outside of the cavity and breaking the imidazolate bridge (Fig. 47). The ^1H NMR spectra are typical of tetrahedral species, with little spreading of the signals and large line width (Fig. 46b) (*187*). At pH values greater than 10 the bridge is reestablished (*191*).

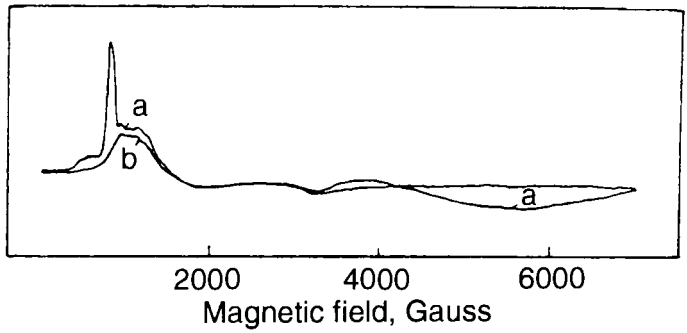

FIG. 45. EPR spectra of (a) Co_2Zn_2SOD in the presence of phosphate and (b) Co_2Zn_2-SOD in the absence of phosphate. Spectra are recorded at 10 K, pH 7.4. Reprinted from *FEBS Letters*, vol. 166. Calabrese, L.; Cocco, D.; Desideri, A.; p. 142. Copyright 1979 with kind permission of Elsevier Science–NL, Sara Burgerhartstraat 25, 1055 KV Amsterdam, The Netherlands.

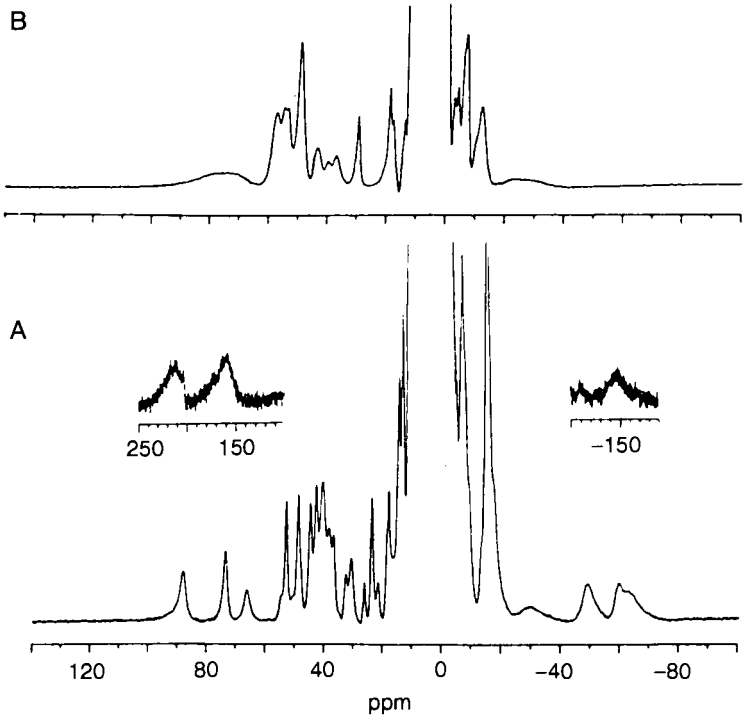

FIG. 46. The 200-MHz ^1H NMR spectra of Co_2Co_2SOD in the absence of phosphate (a) and in the presence of phosphate (b). Reprinted with permission from Ming, L. J.; Valentine, J. S. *J. Am. Chem. Soc.* **1990,** *112,* 4256. Copyright 1990 American Chemical Society.

F. ANION DERIVATIVES

Do anions bind copper(II) or other metal ions at the copper site? This was an important question before the appearance of pertinent X-ray data, because O_2^- is an anion. In the presence of N_3^-, SOD displays a CT at 28,200 cm^{-1} (*164, 262*), which shows the N_3^- binds copper(II). By looking at the CD spectra (Fig. 48) it appears that CN^- and NCO^- also bind copper(II) because the spectra indeed change, even if no CT

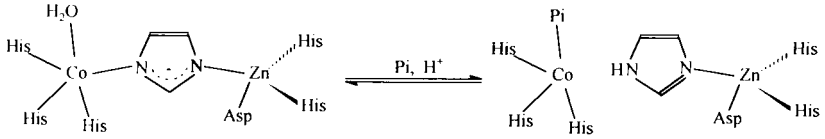

FIG. 47. Schematic representation of the breaking of the imidazolate bridge in Co_2Zn_2SOD in the presence of phosphate.

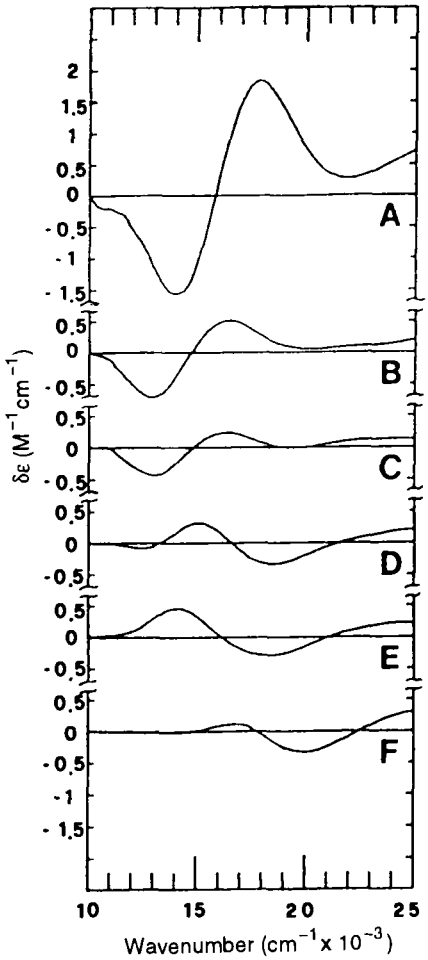

FIG. 48. Circular dichroism spectra of Cu_2Zn_2SOD (B) and of its derivative with thiocyanate (C), cyanate (D), azide (E), and cyanide (F). The CD spectrum of the Ile-137 mutant (A) is also shown. Reprinted with permission from Banci, L.: Bencini, A.; Bertini, I.; Luchinat, C.; Piccioli, M. *Inorg. Chem.* **1990,** *29,* 4867. Copyright 1990 American Chemical Society.

band are observed. The most well-studied anions are N_3^- and CN^-. The latter binds quantitatively and tends to reduce copper(II). The affinity of N_3^- for SOD is small and depends on the conditions. Spectrophotometric titrations provide an affinity constant of 138 ± 4 M^{-1} at pH 5.6 (*262*).

CN^- (*263*), N_3^- (*264*), and F^- (*264*) are competitive inhibitors. NCO^- and NCS^- have not been reported to be inhibitors (*229, 264, 265*). The EPR spectra show that CN^- and N_3^- provide an essentially tetragonal

structure, which contrasts with the rhombic structure of the native enzyme (*245*, *266*, *267*) (Table IV). It has been suggested that the three His plus the anion give rise to a tetragonal structure, which may have the fourth His as a fifth ligand more or less loosely bound. The binding of CN^- to copper was also proved by infrared (IR) and Raman spectroscopy: a band at 2137 cm^{-1} was attributed to the stretching frequency of the bound cyanide (*268*). The ^1H NMR spectrum of the copper–cobalt derivatives with different anions indicates that the protons of His-48 experience hyperfine coupling with the unpaired electron to a different extent. In the case of the CN^- derivative, negligible hyperfine coupling with the electrons of the copper ion is observed (Table IV) (*88*, *89*). The nuclear Overhauser effect (NOE) data with and without N_3^- show that the position of His-48 does not change appreciably within the protein framework (*89*). How then can the detachment of His-48 be reconciled with the NOE data? Movement of the copper ion satisfies the new requirements (*89*). This has been confirmed by X-ray studies (*90*, *269*). The water molecule close to copper is removed by CN^- and N_3^- (see Section VI). The X-ray data also show that the anions bind copper and interact with Arg-143. The affinity of anions for the enzyme decreases if Arg-143 is substituted through site-directed mutagenesis (*270*) or if the enzyme is treated with glyoxal, which reacts with the Arg residue (*163*). ^{14}N and ^{15}N NMR studies on the binding of N_3^- have provided copper–nitrogen hyperfine values that are consistent with an equatorial binding of the anion (*271*).

Ligands such as NCO^-, NCS^-, and F^- have also been extensively investigated and the interpretation of the data is rather intriguing. It has been proposed that their ability to move copper(II), as previously discussed, decreases in the order $NCO^- > NCS^- > F^-$. The electronic spectra of F^- and NCS^- are very similar to those of the native enzyme (Fig. 48). The same trend is observed in the chemical shifts of His-48 protons, in the case of the copper–cobalt derivative (Table IV).

The addition of NCO^- to a water solution of Cu_2Zn_2SOD causes a change in the electronic spectrum (*272*), the maximum of the absorption shifting from 14,700 to 15,100 cm^{-1}. The EPR spectra become more axial (*218*) (Table IV), whereas the ^1H T_1^{-1} values of water protons are only slightly affected (*267*). The binding of NCO^- to copper without displacing the water molecule is consistent with ^{13}C and ^{14}N NMR spectra (*267*). An affinity constant of $51 \pm 1\ M^{-1}$ was measured by CD spectroscopy (*262*).

NCS^- gives rise to a LMCT at 28,200 cm^{-1}, which shows direct binding (*273*). This is consistent with ^{13}C, ^{14}N, and ^{15}N NMR data (*266*, *267*). An affinity constant of $22 \pm 3\ M^{-1}$ has been measured at $I = 0.2$ M, pH 7.0. Under the same conditions the affinity constant of N_3^- is

88 ± 2 M^{-1} (*273*). However, it is proposed (*267*, *273*) that there is more than one binding site, as the apparent affinity constant decreases with increasing concentrations of NCS^-. The temperature dependence of the constant shows that the binding of NCS^- is entropy driven whereas it is disfavored from the enthalpic point of view. The thermodynamic parameters of NCS^- and N_3^- binding are reported in Table XI together with the analogous values of the diethylentriamine–copper complex (*273*).

Even the behavior of F^- is quite complex. ^{19}F NMR measurements show that F^- interacts with copper(II) (*274*, *275*). However, the electronic structure is hardly affected, as shown by the electronic and EPR spectra (*267*, *274*). F^- does not affect the relaxivity of water and has little effect on the NMR of Cu_2Co_2SOD (*275*).

These anions, which bind weakly to the metal ion, may have comparable affinity for the charged groups in the cavity. The binding at these groups affects the affinity of the anion for the metal ion, thus providing a spectral behavior difficult to understand in any detail. This holds also for phosphate, which reduces the affinity of Cu_2Zn_2 SOD for azide and cyanide (*107*). Phosphate was shown to interact with bovine Cu_2Zn_2SOD, but no changes in the electronic and EPR spectra were observed (*107*, *164*, *259*, *265*). The interaction of phosphate has been investigated through the paramagnetic effects caused by Cu(II) ions on the ^{31}P phosphate resonance. The ^{31}P NMR signal of phosphate shows a paramagnetic contribution to T_1^{-1} that is consistent with its binding at a site about 5 Å from the copper, whereas the contribution to T_2^{-1} is too large. At pH 6.3 two binding sites were observed, one at a distance >7 Å and another at approximately 5 Å from the copper. The latter could be the guanidinium group of Arg-143, located 5 Å from the copper (*106*). The idea of two binding

TABLE XI

THERMODYNAMIC PARAMETERS FOR LIGAND SUBSTITUTION REACTIONS IN SOD AND ONE MODEL SYSTEM[a]

Reaction[b]	K_{eq} (M^{-1})	$\Delta H°$ (kJ/mol)	$\Delta S°$ [J/(mol K)]	$\Delta G°$ (kJ/mol)
SOD + N_3^-	88 ± 2	−4.0 ± 1.0	28 ± 2	−11.0 ± 1.0
SOD + SCN^-	22 ± 3	11.7 ± 1.2	64 ± 4	−7.4 ± 2.4
$Cu(dien)^{2+}$ + N_3^-	75 ± 2	−10.6 ± 0.7	−2 ± 2	−10.0 ± 1.0
$Cu(dien)^{2+}$ + SCN^-	36 ± 2	−9.5 ± 1.0	−3 ± 3	−8.6 ± 1.0

[a] Reprinted with permission from Dooley, D. M.; McGuirl, M. A. *Inorg. Chem.* **1986**, *25*, 1261. Copyright 1986 American Chemical Society.

[b] dien, Diethylentriammine (1,4,7-triazaheptane).

sites could account for all these results (including T_2^{-1}) if the exchange of one site with bulk phosphate were relatively slow.

The overall model of anion binding is also consistent with the high-pH form of the enzyme. At pH > 10 the ^1H NMRD values increase (*114*), thus showing that at least a proton becomes closer to copper, and the ^{17}O relaxation values also increase (*217*). This behavior is followed best for the Ile-137 mutant, which is stable at high pH values (*120*). A hypothesis is that OH^- binds copper in a way similar to the other anions (*120*). Indeed, some signals of the ^1H NMR spectrum of the Cu_2Co_2 derivative, at high pH, experience variations in shift similar to those observed on addition of anions (*120*, *262*).

ENDOR studies on some anion adducts of SOD are available at low temperature. Hyperfine interactions of ^1H and ^{14}N with the Cu(II) site have been measured (*248*, *276*). From these data it appears that at 4.2 K CN^- loosens the coupling with His-48, whereas little change occurs on N_3^- binding (*248*). ESEEM spectra of ^{15}N SOD with cyanide (*250*) indicate that the inhibitor substitutes one of the histidines with the larger hyperfine constant (His-46 or His-48), producing a square planar configuration with the other three histidines.

Binding of formate to Cu_2Zn_2 and Cu_2Co_2SOD has been investigated by NMR spectroscopy. Formate belongs to a class of anions (such as chloride, acetate, and phosphate) that do not coordinate to copper. The formate binding occurs via hydrogen bonding of the carboxylate ion to the NHs of the side chain of Arg-143, without displacement of the water molecule (*277*).

Hydrogen sulfide (HS^-) is reported to bind copper(II), without inhibiting the enzyme. The visible and EPR spectra are strongly affected by HS^- binding, as with other anions (Table IV); however, the activity is slightly enhanced. A hypothesis of this behavior is that the HS^- ligand may improve the access of O_2^- to the catalytic site, displacing a water molecule (*278*).

Tetramer vanadate is also reported to bind SOD (*279*). It is proposed, on the basis of site-directed mutagenesis, that it binds to two lysines (positions 122 and 136) with an affinity constant of 2×10^7 M^{-1}, which is higher than that of CN^- (2×10^6 M^{-1}) (*107*). The affinity is drastically reduced when Arg-143 is mutated (*279*).

The interaction of Cu_2E_2SOD with azide produces effects on the EPR parameters similar to those observed for the native Cu_2Zn_2SOD (Table X) (*244*). Nevertheless, the binding of N_3^- to the copper ion was monitored in Cu_2E_2SOD (*244*) through ^{14}N electron spin echo spectroscopy. No appreciable effect was detected in the echo envelope spectrum with addition of ^{15}N azide, nor with ^{15}N cyanide, indicating that the binding of these anions to the Cu_2E_2 derivative does not alter the

magnetic coupling of the metal ion to ^{14}N of the ligated imidazoles (*247*). The interaction of Cu_2E_2SOD with azide and thiocyanate has been investigated through water ^1H NMR relaxation measurements (see Section VI) (*220*).

G. Other Metals at the Zinc Site

Zn^{2+} is not a great spectroscopic probe! However, because its d^{10} configuration ensures diamagnetism, it has been investigated by ^1H NMR (*280–282*).

1. Cobalt at the Site of Zinc

The visible absorption spectrum of E_2Co_2SOD (E = empty), with cobalt(II) in the zinc site, has an absorption maximum at 583 nm and an extinction coefficient of 370 M^{-1} cm^{-1} (Fig. 49). The CD spectrum possesses two negative bands at 585 and 530 nm. The EPR spectrum is observable below 100 K and shows $g_\perp = 4$ and $g_\parallel = 2.16$ (*189*). The ^1H NMR spectrum shows seven signals in the region between 35 and 55 ppm and two signals upfield that should belong to the residues (three His and one Asp) coordinated to cobalt(II) (Fig. 50a). The assignment of the spectrum, first proposed in 1985 (*262*), was completed through the investigation of the derivative, which was selectively deuterated at the Cε1 position of the imidazole rings (*283*).

The $Cu_2^ICo_2^{II}$ derivative is obtained through reduction of $Cu_2^{II}Co_2^{II}$ SOD. The electronic spectrum of this species shows a shift of the cobalt absorption maximum to a shorter wavelength (from 598 to 588), which renders the spectrum very similar to that of E_2Co_2SOD (Fig.

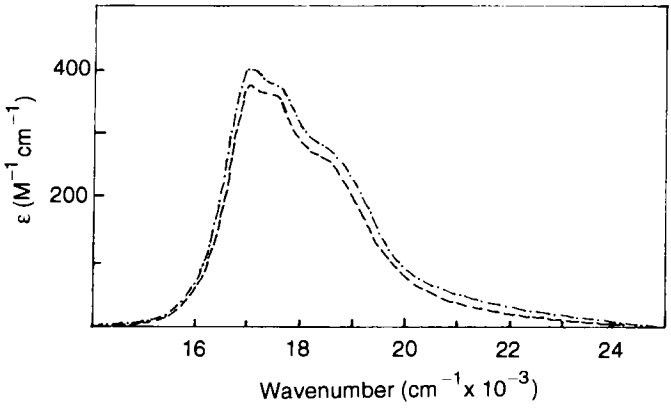

FIG. 49. Electronic absorption spectra of E_2Co_2SOD (-·-) and $Cu_2^ICo_2SOD$ (---). Reprinted with permission from Ref. *260*.

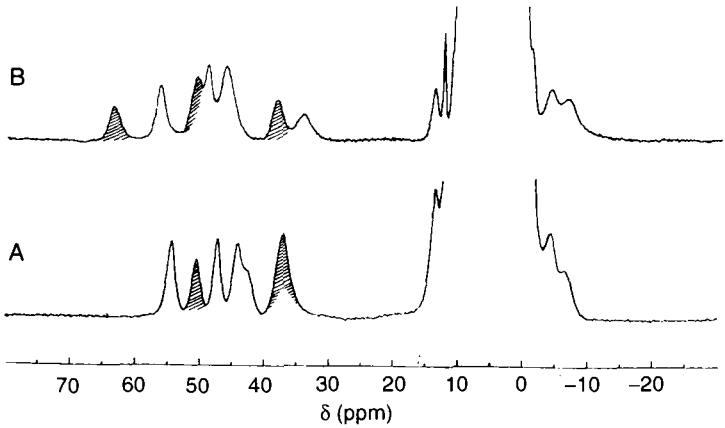

FIG. 50. The 300-MHz ^{1}H NMR spectra of (A) E_2Co_2SOD and (B) Cu^I_2 Co_2SOD. The shaded signals belong to exchangeable protons. Reprinted with permission from Ref. *168*.

49) (*284*, *285*). This result was related to the breaking of the imidazole bridge on reduction (*284*, *285*). It was later confirmed by the ^{1}H NMR spectrum of the same derivative, which clearly shows the presence of three exchangeable NH′ protons belonging to His-71, His-80, and His-63 (Fig. 50b). Therefore, His-63 is regularly coordinated to the Co(II) but no longer to Cu(I) (*233*). An extensive assignment of the resonances belonging to the residues coordinated to the metal ions and to some residues near the copper(I) ion was obtained (*286*). The dipolar shift induced by cobalt(II), on signals not belonging to cobalt-coordinated residues, was determined and used to determine the orientation of the magnetic susceptibility tensor (*286*). Evidence for breaking of the imidazolate bridge on reduction of copper was also given in the crystalline state through polarized absorption spectra (*287*).

The $Ag^I_2Co^{II}_2$ derivative has electronic and ^{1}H NMR spectra similar to the $Cu^I_2Co^{II}_2$ derivative. Also in this case, the presence of three solvent-exchangeable signals is strong evidence that His-63 is not a bridging ligand (*191*).

2. *Nickel at the Site of Zinc*

The electronic spectra of the nickel chromophore at the zinc site in the compounds Ag_2Ni_2 and $Cu^I_2Ni_2SOD$ are shown in Fig. 51. The band at 750 nm is the highest $F \rightarrow F$ transition and is on the high side of the energy range for pseudotetrahedral compounds (*258*). Distortions and ligand strength may account for it. Evidence of a possible bidentate binding of Asp-83 has been proposed by EXAFS (*232*).

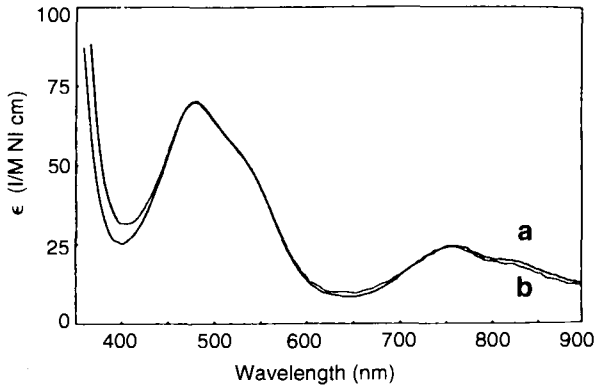

FIG. 51. Electronic absorption spectra of (a) $Cu_2^{I}Ni_2^{II}SOD$ and (b) Ag_2Ni_2SOD. Reprinted with permission from Ming, L. J.; Valentine, J. S. *J. Am. Chem. Soc.* **1987,** *109,* 4426. Copyright 1987 American Chemical Society.

The ^1H NMR spectra of the two derivatives show a number of isotropically shifted signals, in both the upfield and downfield regions, very similar to each other, indicating similar metal binding environments in both derivatives. Because Ag^+ and Cu^+ are diamagnetic, the isotropically shifted signals have been assigned to protons of the three His and one Asp residue coordinated to Ni^{2+}. The presence of three solvent-exchangeable signals, which account for three histidine NH, indicates that, in these derivatives, the His-63 bridging ligand is detached from the copper site and protonated (*258*, *288*).

3. *Copper at the Site of Zinc*

The two derivatives $Ag_2^{I}Cu_2^{II}$ and $Cu_2^{I}Cu_2^{II}SOD$ [the latter obtained through semireduction of $Cu_2^{II}Cu_2^{II}SOD$] show quite similar visible absorption and EPR spectra (*244*, *252*). The spectra are characteristic of Cu(II) in the zinc site without interference from paramagnetic ions in the copper site. The hyperfine coupling constant of 105×10^{-4} cm^{-1} is typical of copper(II) tetrahedral complexes (*244*, *252*). Experiments based on linear electric field effect (LEFE) in pulsed EPR also support the conclusion that Cu(II) in the zinc site retains the pseudotetrahedral coordination geometry. Furthermore, ENDOR and ESEEM experiments on $Ag_2^{I}Cu_2^{II}SOD$ pointed out that Cu(II) forms inequivalent bonds to the three coordinated imidazoles (*289*).

H. CADMIUM AT BOTH COPPER AND ZINC SITES

^{113}Cd NMR is a very sensitive tool to identify coordination number and donor atoms (*290*). ^{113}Cd NMR experiments on cadmium at the

copper (*197*) and zinc site (*196*) indicate (1) that the two subunits are identical and (2) that the coordination at the zinc site is similar in the case of E_2Cd_2SOD and $Cu_2^{II}Cd_2^{II}SOD$ (*196*, *197*). The chemical shifts are ≅320 ppm for Cd at the zinc site and 185 ppm for Cd at the copper site. For the former case there are two earlier reports (*291*, *292*). One of them agrees with the above values (*291*). It was also noted that the observed shift is much lower than that predicted on the basis of a simple additive model (*293*).

Experiments based on perturbed angular correlation (PAC) of γ rays, performed on the Cu_2Cd_2SOD derivative, demonstrated that His-63 bridges the two metal sites (*199*, *294*).

I. ^{1}H NMR Spectra of Cu_2Co_2 and Cu_2Ni_2SOD

The magnetic coupling between copper(II) and cobalt(II), or copper(II) and nickel(II), is responsible for the fast electronic relaxation times of copper(II), which become similar to those of the cobalt(II) or nickel(II) ions (*295*, *296*). As a consequence, ^{1}H NMR spectra can be performed as for any cobalt(II) or nickel(II) protein. This is absolutely a peculiarity as far as the NMR of copper(II) proteins is concerned. The spectra are shown in Fig. 52 (*262*, *288*). N_3^-, if added, is in fast exchange with the bulk anion and thus the signals can be followed on increasing addition of the anion. It appears that a set of protons

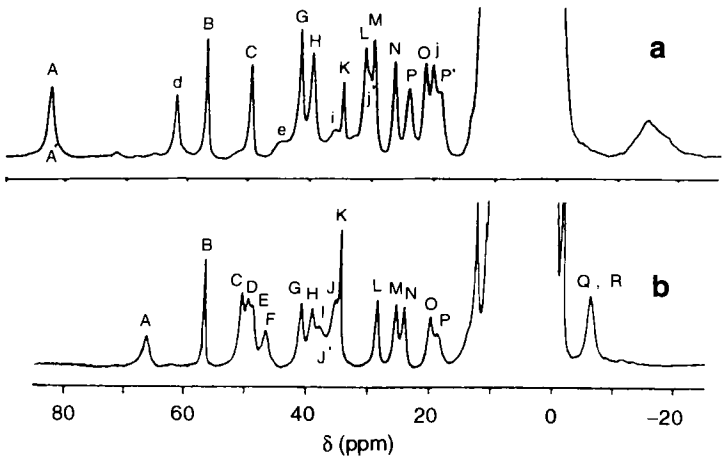

Fig. 52. The 300-MHz ^{1}H NMR spectra of (a) $Cu_2^{II}Ni_2^{II}SOD$ and (b) $Cu_2^{II}Co_2^{II}SOD$ at pH 6.5. Reprinted with permission from Ming, L. J.; Banci, L.; Luchinat, C.; Bertini, I.; Valentine, J. S. *Inorg. Chem.* **1988,** *27,* 4458. Copyright 1988 American Chemical Society.

corresponding to a His decreases its coupling with the unpaired electron of copper(II). When these studies were done it became historically important to be successful with the assignment. These systems were used to pioneer the procedure for the assignment of proton signals in paramagnetic molecules. A definitive assignment of the Cu_2Co_2 derivative was achieved through 1D NOE measurements (*297*) first and then confirmed through 2D NOESY spectroscopy (*298*, *299*) (Table XII). Rotilio *et al.* first misassigned the spectra (*300*) but eventually confirmed the above assignment (*301*).

A polyethyleneglycol (PEG) derivative, with large molecular weight, was investigated and a sizable Curie relaxation was observed (*163*).

The ^1H NMR spectra of the Cu_2Co_2SOD anion derivatives indicate that the protons of His-48 experience hyperfine coupling with the unpaired electrons to different extents: the hyperfine shifts decrease in the following order: $F^- > NCS^- > NCO^- > N_3^- > CN^-$ (Table IV) (*89*). ^1H NOE experiments on the Cu_2Co_2 adduct with N_3^- show that the interproton distances involving the histidines coordinated to copper(II) are similar to those measured in the absence of azide. All these results account for an increase of the copper–nitrogen (His-48) distance as a consequence of a movement of the copper ion (*89*). The decrease in hyperfine shifts of the His-48 protons can be taken as a qualitative estimate of the above movement. The Thr-137Ile mutant has the largest His-48 hyperfine shifts, which are indicative of a strongest Cu–His-48 bond (Table IV).

The assignment of the Cu_2Ni_2SOD ^1H NMR spectra was another significant achievement (*288*, *302*). It should be noted that tetrahedral nickel(II) has shorter electronic relaxation times than does tetrahedral cobalt(II), and consequently the ^1H NMR spectra are sharper in the former case.

J. ^1H NMR Spectra of the Reduced Enzyme

Because the reduced enzyme is diamagnetic, it was studied using NMR from the early days of application of this technique to biological systems (*251*, *280*, *303*, *304*). The recent results allow a complete assignment of the His protons bound to both copper(I) and zinc(II) (Table XIII). It appears that the bridge is broken on copper reduction. Indeed, an NH proton signal at 12.44 ppm could be assigned to the HNε2 of His-63 (Table XIII). This finding is consistent with the pH dependence of the reduction potential, which requires a proton together with the reducing electron (see Section VII,A). It is also consistent with the ^1H NMR spectrum of cobalt(II) in $Cu_2^ICo_2^{II}SOD$, which is

TABLE XII

ASSIGNMENT OF ^1H NMR SIGNALS OF METAL-COORDINATED RESIDUES IN Cu_2Co_2SOD[a]

Shift (ppm)	Assignment
67.4	His-63 Hδ2
57.0	His-120 HNδ1
50.3	His-46 HNε2
49.6	His-71 Hδ2
49.0	His-80 Hδ2
46.7	His-80 HNε2
41.0	His-46 Hδ2
39.5	His-120 Hε1
38.7	Asp-83 Hβ1
37.0	Asp-83 Hβ2
35.6	His-71 HNε2
34.7	His-48 HNδ1
28.4	His-48 Hδ2
25.7	His-46 Hε1
24.3	His-120 Hδ2
19.8	His-48 Hε1
18.7	His-46 Hβ1
−6.2	His-71 Hβ2
−6.2	His-46 Hβ2
12.30	His-48 Hβ2
11.21	His-120 Hβ2
8.44	His-120 NH[b]
6.40	His-48 Hβ1
4.43	His-120 Hα
3.73	His-48 Hα
3.13	His-120 Hβ1
1.23	Ala-140 β-CH_3
0.56	Val-118 γ_1-CH_3
−0.28	Arg-143 H-γ_1
−1.51	Val-118 γ_1-CH_3

[a] At 298 K, pH 5.5.

[b] Tentatively assigned on the basis of a single dipolar connectivity.

sensitive to the bridging/terminal character of His-63 (see Section VIII,G,1).

Several NMR studies indicate that there is binding of anions to the reduced species (*159*, *282*, *305*, *306*). However, the most significant information comes from X-ray studies (*83b*) (see Section II,J,3).

TABLE XIII

PROPOSED ASSIGNMENT OF HISTIDINE–IMIDAZOLE PROTONS OF HUMAN $Cu_2^{I}Zn_2^{II}$ SOD[a]

	ppm			
Residue	Hε1	Hδ2	HNδ1	HNε2
His-43[b]	8.64	7.14	12.9	14.07
His-80	8.57	6.86	—	12.70
His-110[b]	8.54	—[c]	—[d]	—[d]
His-48	8.52	—[c]	12.54	—
His-120	8.29	6.64	—[d]	—
His-71	7.78	6.82	—	15.40
His-46	6.78	7.11	—	13.42
His-63	6.57	6.05	—	12.44

[a] At 300 K, pH 5.5.
[b] His not associated with the active site.
[c] Not assigned.
[d] Not observed.

Monomeric species are now available with only 153 amino acid residues (*60*, *102*, *124*). A fully ^{13}C- and ^{15}N-labeled sample has been prepared and should lead to the solution structure. At the moment the full backbone assignment is available (unpublished results from this lab).

IX. Mechanistic Aspects of Cu_2Zn_2SOD

A. NONCATALYZED DISPROPORTIONATION OF O_2^-

The superoxide anion is produced in living cells of aerobic organisms mostly as an unwanted by-product of oxidative metabolism (*307*). The intrinsic toxicity of superoxide has been the subject of a passionate debate in past years (*308–310*). It seems that O_2^- toxic effects are not due to direct interaction of the O_2^- species with biological substrates, but rather to the likely products of chemical reactions involving superoxide.

Thermodynamic and chemical data support this point of view. The radical character of O_2^- can be estimated from the $H-OO^-$ bond energy. This amounts to the relatively small value of 301 kJ, indicating that the superoxide anion has a limited radical character (*311*). Indeed, the O_2^- anion is not able to produce homolytic cleavage of even

the weakest C—H bond present in the allylic carbons of linoleic acid (≈311 kJ) (*311*). On the contrary, its conjugate acid, HOO·, can break C—H bonds, because the radical character of HOO· is given by the bond energy of the H—OOH bond, which is ≈344 kJ.

Extensive reviews of the chemical properties of the superoxide anion are in Sawyer and Valentine (*308*) and in Sawyer (*311*).

Besides the effects of the HO_2 radical, the indirect toxicity of superoxide may also be due to the fact that superoxide may originate hydroxyl radicals through reaction (23) or even singlet oxygen through reactions (23) and (24) (*312*, *313*):

$$O_2^- + H_2O_2 + H^+ \rightarrow O_2 + H_2O + OH\cdot \tag{23}$$

where $k_{23} < 10^{-4}\ M^{-1}\ \text{sec}^{-1}$ (*312*, *314*), and

$$O_2^- + HO_2 + H^+ \rightarrow O_2 + H_2O_2 \tag{24}$$

where $k_{24} \approx 1 \times 10^8\ M^{-1}\ \text{sec}^{-1}$ (*308*, *315*).

The generation of singlet oxygen ($^1\Delta O_2$ or $^1\Sigma_g O_2$) in reactions (23) and (24) has been proposed on the basis of thermodynamic calculations (*313*), but direct experimental evidence is lacking.

The O_2^- disproportionation equilibria

$$2O_2^- + 2H^+ \underset{}{\overset{K_{25}}{\rightleftharpoons}} H_2O_2 + O_2 \tag{25}$$

$$2O_2^- + H_2O \overset{K_{26}}{\rightleftharpoons} HO_2^- + O_2 + OH^- \tag{26}$$

are shifted to the right: at pH 7.0 $K_{25} = 4 \times 10^{20}$ and even at pH 14 $K_{26} = 9.1 \times 10^8$ (*311*). Because of this proton-driven equilibrium, and not for its intrinsic Brønsted base properties ($pK_b = 9.2$), O_2^- can be seen as a strong Brønsted base able to abstract protons from very weak acids (up to $pK_a > 23$) to form HO_2^-. In other words, the addition of O_2^- to aqueous solutions results in the quantitative formation of the strong bases HO_2^- and OH^-.

The maximum rate of O_2^- disproportionation occurs at pH = pK_a of the HO_2^- weak acid and decreases with increasing pH. At pH 4.8 $k > 10^8\ M^{-1}\ \text{sec}^{-1}$. Thus O_2^- reacts with protic substrates to yield products that are consistent with an apparent one-electron oxidation of the substrate and the production of H_2O_2. However, it has been shown that there is not direct one-electron transfer to O_2^-. The process consists instead of the abstraction of a proton from the substrate:

$$HA + O_2^- \rightarrow A^- + HO_2 \tag{27}$$

in weak acids and in water; $k_{27} = 10^4$–$10^{-3}\ M^{-1}\ sec^{-1}$, depending on pH (*308*). In strong acids reaction (27) is extremely rapid.

Only after the protonation step [Eq. (27)] the reaction

$$HO_2 + O_2^- + H^+ \rightarrow H_2O_2 + O_2 \tag{28}$$

or

$$HO_2 + HO_2 \rightarrow H_2O_2 + O_2 \tag{29}$$

may occur; k_{28} and $k_{29} > 10^7\ M^{-1}\ sec^{-1}$.

It has been proposed that the actual oxidant of the A^- substrate is the newly formed oxygen, as indicated by the quantitative yields of the nonoxidized substrate when O_2 from dismutation is continuously purged from the reaction vessel (*311*, *313*).

The direct reaction of O_2^- with H_2O_2 to give OH · radicals [Eq. (23)] is unlikely ($k < 10^{-4}\ M^{-1}\ sec^{-1}$) (*314*), but complexes of redox-active metal ions such as Fe(III) may catalyze the reaction (*312*):

$$Fe(III)L + O_2^- \rightarrow Fe(II)L + O_2 \tag{30}$$

and then

$$Fe(II)L + H_2O_2 \rightarrow Fe(III)L + OH\cdot + OH^-. \tag{31}$$

On the other hand, the peroxidation reaction

$$M(II) + O_2^- \rightarrow M(III)\text{–}O_2^{2-} \tag{32}$$

may also occur. The latter reaction has been proposed to explain the unique *in vivo* toxicity of superoxide (*316*).

Whatever the actual reagents might be, it has been shown that O_2^- can oxidize sulfite and initiate a free-radical chain reaction, or oxidize iron-containing clusters present in enzymes, such as aconitase and fumarases, freeing Fe(II), which in turn initiates a Fenton-like chemistry by interacting with hydrogen peroxide (*317*). Fe(II) release from transferrin has also been observed following O_2^- secretion by stimulated human neutrophils (*318*).

B. Some Pertinent Facts about Cu_2Zn_2SOD Catalysis

Studies on Cu_2Zn_2SOD performed over the past 25 years have produced an enormous amount of information on the system. Nevertheless, several aspects of the mechanism of action of Cu_2Zn_2SOD toward O_2^- dismutation are still unclear. In this section we will summarize the facts that have been ascertained about Cu_2Zn_2SOD chemistry and with which any mechanistic proposal should be consistent.

1. Superoxide spontaneously disproportionates in water to dioxygen and hydrogen peroxide. As discussed in Section I, the uncatalyzed reaction is pH dependent and has a maximum rate at a pH equal to the pK_a of the $HO_2 \rightleftharpoons O_2^- + H^+$ equilibrium; namely, when $[O_2^-] = [HO_2]$ ($K_a = 1.6 \times 10^{-5}$ M, pKa = 4.8) (*315*, *319*) this means that the reaction given by Eq. (2)

$$O_2^- + HO_2 \rightarrow O_2 + HO_2^-$$

is fast, and even at pH 7.5 its rate constant k is equal to 8.5×10^7 M^{-1} sec^{-1}, compared to $k = 10^2$ M^{-1} sec^{-1} for the disproportionation among O_2^- radicals ($O_2^- + O_2^-$) (*97*, *320*).

2. Cu_2Zn_2SOD catalyzes the O_2^- dismutation to dioxygen and hydrogen peroxide in a first-order reaction with respect to both the enzyme and substrate and with a pseudo-second-order rate constant of about 2×10^9 M^{-1} sec^{-1}. The same catalytic efficiency is observed for copper in both +2 and +1 oxidation states (*52*, *91*, *97*). At steady state, the blue color of Cu_2Zn_2SOD is bleached by about 30% on reaction with O_2^- generated by pulse radiolysis. The bleaching is independent of the enzyme concentration and does not alter the superoxide disproportionation rate (*91*, *321*). The reduced $Cu_2^IZn_2SOD$ is not readily reoxidized by air oxygen at room temperature (*223*), but hydrogen peroxide oxidizes it. These observations suggest that the superoxide dismutation in Cu_2Zn_2SOD proceeds by a cyclic oxidation and reduction of the copper ion by two successive O_2^- molecules, as shown in the following scheme:

$$ECu(II) + O_2^- \rightarrow ECu(I) + O_2$$

$$ECu(I) + O_2^- + 2H^+ \rightarrow ECu(II) + H_2O_2.$$

3. Copper is essential for catalysis; removal of Cu(II) or its replacement with other metals results in the complete loss of catalytic activity (*2*) with the exception of Ag(I), for which catalytic activity up to

about 5% of the native enzyme has been claimed (*244*). On the contrary, the Zn(II) ion can be replaced by Co(II), Cu(II), or Cd(II), or by an empty site with none or limited loss of activity (*173*, *183*, *252*, *322*).

4. The dismutase reaction is reversible (*323*). Indeed, Cu_2Zn_2SOD is reduced by H_2O_2 (*98*, *164*, *321*). However, the fast Cu(II) reduction is followed by a slow irreversible inactivation of the enzyme, which has been attributed to a Fenton-like chemistry involving Cu(I) and H_2O_2 (*324*).

5. There are conflicting reports about the substrate K_m values. Evidence of a first-order rate-limiting step was provided by a polarographic method resulting in a K_m value of 0.5 m*M* (*263*). However, kinetics measured using the stopped-flow method do not show saturative behavior at 25°C and indicate that $K_m > 5$ m*M* (*325*). By lowering the temperature to 5.5°C at pH 9.3 and with an initial O_2^- concentration of ≈ 5 m*M*, Fee and Bull were able to observe saturative behavior in Cu_2Zn_2SOD (*99*) and to measure a K_m value of 3.5 m*M*.

6. Studies conducted in nonsaturating substrate conditions ($K_m \gg [O_2^-]$) show that the rate of catalyzed superoxide dismutation is independent of pH in the range 5.0–9.5 (*52*, *91*, *118*) even though the isoelectric point of Cu_2Zn_2SOD around 5 suggests a pH-dependent activity. This fact, together with the observation that the reaction is not slowed down if performed in D_2O (pH 10.0) (*99*, *324*), indicates that, under such conditions, proton transfer is not a rate-limiting step. It is worth noting that in the pH range 5.0–9.5 the EPR and visible spectra of the enzyme are also invariant, indicating that the copper site is unperturbed by the pH change. On the contrary, in the pH range 9.0–12.0 a reversible decrease of Cu_2Zn_2SOD activity is observed with concomitant changes in the chromophore (*114*, *120*, *206*). It has been proposed that the rate-limiting step is the diffusive approach of O_2^- to copper (*231*).

7. In nonsaturating conditions the rate-limiting step is the apparent binding of the substrate to copper (*99*). This means that the encounter rate of the superoxide with the enzyme is slower than the electron transfer process. The Marcus theory of electron transfer predicts that fast processes, such as that observed in SOD, occur only when the distance between the components of the redox couple is of the order of few angstrøms (*326*). Hence, the observation that in Cu_2Zn_2SOD the electron transfer is not the rate-limiting step implies that the superoxide substrate must dock close to the copper ion before the electron transfer and the consequent copper reduction occur. However, the theory does not require that a $Cu–O_2^-$ coordination bond should actually be formed, because the electron jump in a vacuum

could work as well. Under saturating conditions ($K_m \ll [O_2^-]$) (at 5.5°C and pH 9.3) a first-order rate constant of $k_{cat} = 1 \times 10^6$ sec^{-1} and $K_m = 3.5 \times 10^{-3}$ *M* were measured (*99*). A solvent isotope effect was also observed and k_{cat} was increased by the presence of the general acid ND_4^+. This suggests that water is the actual proton donor and that the proton transfer is the rate-limiting step in these conditions.

8. The rate of O_2^- dismutation is affected by the ionic strength of the medium (*105*, *118*, *327*). For instance, between pH 7 and 8 the activity of bovine Cu_2Zn_2SOD diminishes by about 70% on passing from ionic strength $I = 0.02$ *M* to $I = 0.25$ *M* (*118*). These results have been confirmed for the human enzyme. Interestingly, the ionic changes at pH 8.0 have a small effect on the neutral and acidic human SOD mutants of the Arg-143 residue, which possess the lesser activity (*95*). Above pH 12.0 the effect of solute activity vanishes. This observation implies the presence of electrostatic control of the access of superoxide to the active site (*vide infra*).

9. A wealth of information has been gathered from both theoretical and experimental studies about the role of the active site cavity residues in the electrostatic guidance of superoxide toward the copper center (*45*, *122*). The essential role played by the conserved Arg-143 residue (Arg-141 in the bovine SOD sequence) in catalysis has been demonstrated (*95*, *270*). The positively charged guanidinium group of this residue is located at about 6 Å from the copper, providing the final docking site for the superoxide anion. Substitution of Arg-143 by site-directed mutagenesis with negatively charged (Asp, Glu), neutral (Ile, Ala), or even positively charged (Lys) residues always results in loss of activity (*95*, *104*), paralleling the results of chemical modification studies (*153*, *154*, *328*). However, it must be stressed that, in any case, mutated Cu_2Zn_2SODs do have activities that are still high in absolute value, indicating that the role of Arg-143 is relevant, but not essential for catalysis. A much smaller effect is observed when the mutations affect the residues located at the rim of the cavity. Reductions of activity between 80 and 40% have been reported, depending on the ionic strength and on the type of enzyme when the residues Lys-120 and Glu-130 (Asp-130 in *Xenopus laevis* SOD) have been subjected to single or double substitutions by neutral amino acids (*175*, *329*) (see Section IV).

10. Each monomer seems to function independently, as shown by coupling native subunits with other native or chemically modified subunits (*330*). However, the separated monomers are much less active. The human SOD monomer obtained by site-directed mutagenesis of two dimer interface residues (Phe-50 and Gly-51) shows de-

creased activity (5–10% of the wild-type enzyme) (*60*). The X-ray crystal structures of Cu_2Zn_2SOD show small but significative differences occurring in the active sites in different subunits of the same SOD molecule in both copper oxidation states, which, however, may be averaged in solution (see Section II).

11. Electrochemical studies have shown a linear dependence of Cu_2Zn_2SOD reduction potential on pH between pH 5.0 and about 8.5. The slope of 0.059 V/pH indicates the uptake of one proton by the enzyme on copper reduction (*223*, *227*) (see Section VII).

12. NMR measurements on reduced bovine and human $Cu^I_2Zn_2SOD$ have shown the appearance of a new proton signal in the histidine NH region on copper reduction (*233*). A new hyperfine-shifted exchangeable proton has been observed in $Cu^I_2Co_2SOD$ on copper reduction (*331*). Measurements of proton NOEs and the assignment of their chemical shifts have allowed the determination of interproton distances, which are consistent with the protonation of His-63 (*82*). Together with the EXAFS studies (*203*), NMR has provided the most direct evidence of the detachment and protonation of the bridging histidine on copper reduction (*233*, *331*).

13. A shift to higher frequencies of the absorption maximum in the visible spectrum of the Cu_2Co_2SOD is observed on copper reduction. This blue shift is analogous to that shown by the cobalt-substituted SOD with an empty Cu site. This observation has been interpreted as proof of the protonation of the bridging histidine on copper reduction (*284*).

14. Almost normal activity has been determined for the zinc-depleted enzyme (Cu_2E_2SOD; E = empty) (*332*), indicating that the presence of the histidine bridge is not essential for catalysis.

C. Mechanism of Action of Cu_2Zn_2SOD

Different mechanistic hypotheses that have been proposed for Cu_2Zn_2SOD are consistent with the main experimental evidence obtained for the enzyme so far. However, no hypothesis is able to satisfactorily explain all of the reported observations.

Early proposals (*52*, *171*, *333*) were based on the redox titration experiments and were centered on the alternate protonation and deprotonation of the bridging histidine, concomitant with the reduction and reoxidation of copper by two superoxide molecules consecutively accessing the active site (Fig. 53). This mechanism has been updated in the light of the crystal structure determination of bovine Cu_2Zn_2-SOD (*41*, *44*), as illustrated in Fig. 54.

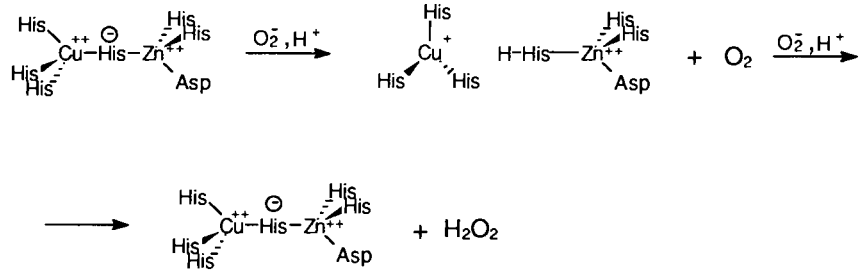

FIG. 53. Presumed scheme of the superoxide dismutation reaction by Cu_2Zn_2SOD prior to elucidation of the 2SOD crystal structure. Arg-141 is not involved in the mechanism.

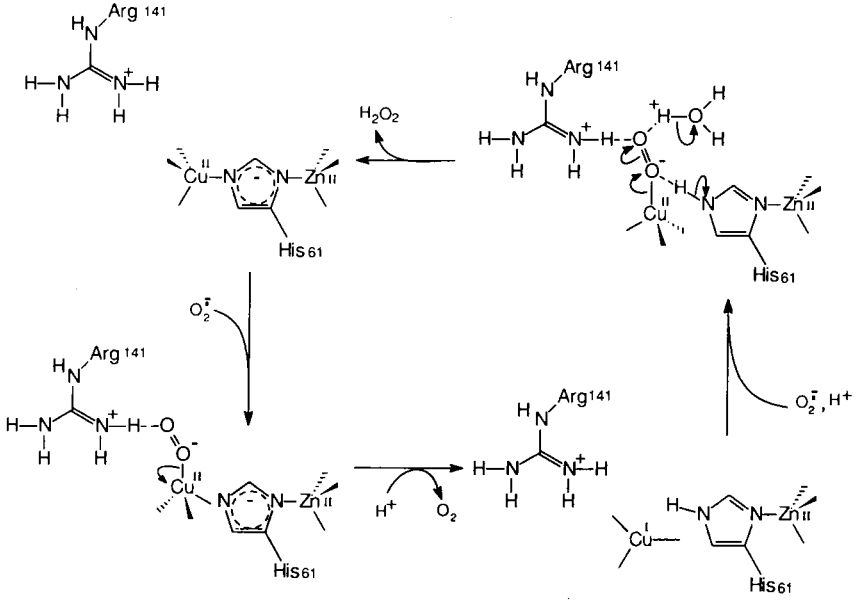

FIG. 54. Scheme of the reaction mechanism of Cu_2Zn_2SOD proposed by Tainer *et al.* (*44*) following the bovine enzyme numbering. The first substrate molecule replaces the axial water molecule and binds to Cu(II), being stabilized by the H bond with Arg-141. In the second step O_2^- reduces copper to Cu(I), with breaking of the His-61 bridge, and leaves as O_2. The Nε2 of His-61 is protonated. The zinc coordination becomes more tetrahedral. In the third step a second O_2^- molecule binds to Cu(I), positioning one of its O atoms at H-bond distance from the HNε2 of His-61 and the other at H-bond distance from the guanidinium group of Arg-141. Electron transfer from Cu(I) and proton transfer from His-61 form Cu-hydroperoxide, which leaves as hydrogen peroxide after receiving a second proton from a water molecule present in the active site.

This proposal highlights the role of Arg-143 in assisting substrate docking. Such behavior is suggested by the finding in the Cu_2Zn_2SOD crystal structure of a "ghost" superoxide molecule constituted by the copper-bound water molecule and by a second water molecule hydrogen bonded to the guanidinium group of Arg-143. The ghost substrate is oriented in such a way as to form a Cu—O—O angle of 120°, as expected for the bound O_2^- anion (*44*). Another feature of this mechanism is that zinc does not play a mere structural role but, helping to keep the copper site distorted, causes an increase of the reduction potential of Cu(II), thus favoring the reduction step. Furthermore, by coordination to the protonated His-63, it helps to position the proton in the proper orientation for H bonding and possible subsequent transfer to peroxide.

The work of Fee and Bull (*99*) points out that the speed of imidazolate bridge breaking and reforming is too low to allow such a process to occur between two successive O_2^- arrivals to the SOD active site. The postulated large rearrangement of the copper coordination during the catalytic cycle is not compatible with the extremely high reaction rates observed.

If we consider the energetics of the process, by taking into account the experimentally measured redox potentials of the Cu^{2+}/Cu^+ and O_2/O_2^- couples (see Section VII), it is possible to estimate that the energy associated with the electron transferred from O_2^- to Cu^{2+} is at most about 54 kJ mol^{-1}.

This is the value of a medium-strength hydrogen bond, and it seems unlikely that this amount of energy introduced into the system by the one-electron reduction causes the breaking and forming of the Cu–N and N–H bonds. However, for a system composed of many particles, such as an enzyme molecule, energy fluctuations of that size are possible and different conformational states may become available. It cannot be excluded that the introduction into the system of a moderate amount of energy like that associated with the above electron transfer can cause a transition toward a state wherein the His-63 bridge is broken and protonated.

The recently determined X-ray crystal structure of the yeast Cu_2Zn_2SOD, in which His-63 is no longer bound to copper (see Section II), shows that the side chain of this residue has moved away from copper toward the opening of the cavity (*334*), in agreement with NMR and MD analysis (*82*, *233*, *331*). If we take this structure as a model for the $Cu_2^IZn_2SOD$ with the bridge broken we can assume that His-63 has its Nε2 nitrogen protonated. In such a case the proton is positioned between the copper and the cavity opening and reduces the

already small solvent-exposed surface of the catalytic copper. It seems likely then that, instead of binding to copper, the O_2^- molecule may hit the histidine N–H moiety and form HO_2. Eventually the electron jumps from copper, originating the HO_2^- product, and the histidine bridge is reformed. The driving force is provided by the reduction of O_2^- to H_2O_2, which compensates the energy spent to reoxidize copper to Cu(II), and by the restoration of the original structure.

A different mechanism, in which the bridge between copper and zinc is not broken and the protons needed by the reaction are provided by the bulk solvent, has been proposed from theoretical calculations (*246*, *335*, *336*). In this mechanism a superoxide molecule forms a complex with Cu(II) thanks to the stabilizing effect of Arg-143. This stable intermediate can oxidize a second superoxide molecule by an outer-sphere electron transfer originating an $E–Cu^I–O_2^-$ complex (E = enzyme), which is subject to proton transfer from the solvent followed by electron transfer from copper, giving rise to $E–Cu^{II}–O_2H^-$. The hydroperoxide anion readily dissociates from the latter complex, leaving the metal in the oxidized state (*246*, *335*).

Alternatively the reduction step may be bypassed, directly obtaining the hydroperoxide complex (*336*). The two mechanisms are summarized in Fig. 55.

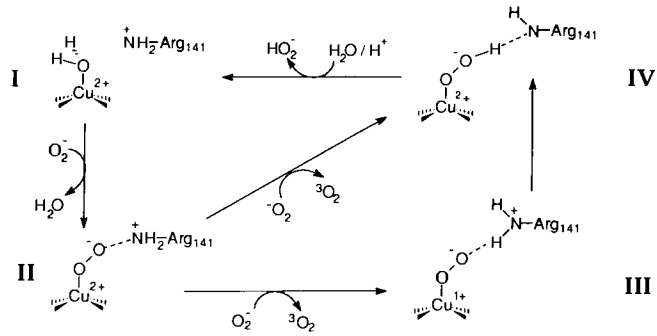

FIG. 55. Reaction scheme of superoxide dismutation following the bovine enzyme numbering. The first O_2^- molecule binds to Cu(II) and is stabilized by the H bond to Arg-141. A second superoxide molecule then approaches the active site and, by an outer-sphere electron transfer via the Cu-bound first O_2^- molecule, reduces the copper to Cu(I) (*44*) (step III). Alternatively, O_2^- directly reduces superoxide to peroxide (*336*) (step IV), leaving as dioxygen. Note that the Cu(I)–superoxide and Cu(II)–peroxide complexes are resonant forms of the same molecular arrangement. The newly formed peroxide is protonated by Arg-141 and leaves as HO_2^-. Arg-141 receives a proton from the solvent, restoring the active enzyme (I). These reaction proposals do not require the breaking and reforming of the Cu–His-61 bridge.

The possibility that the above mechanisms are operative has been supported by crystallographic evidence of the stability of the His-63 bridge in the reduced enzyme and in its complexes with anions (see Section II).

Most of the conflicting experimental evidence can be reconciled if we admit that the two mechanisms may both be operative but under different conditions. In low-substrate concentration conditions, such as those occurring *in vivo*, the traditional mechanism, whereby the proton donor is the protonated His-63 detached from zinc, may be accepted because of the slower turnover rates. On the contrary, under saturating conditions characterized by extremely high turnover rates, the second, outer-sphere, mechanism appears to be more competitive (*82*).

Interestingly, the kinetic results of an earlier study about the catalytic properties of Cu–histidine complexes toward superoxide disproportionation have been interpreted by two alternative mechanisms similar to those described above (*337*). The $[CuHis_2H]^{3+}$ complex was found to be the catalytically active species, with a $k_{cat} = 3.4 \times 10^8\ M^{-1}$ sec^{-1} independent of pH in the range 2–7.

Additional work has shown that a yeast Cu_2Zn_2SOD mutant, in which the bridging histidine has been replaced by a noncoordinating alanine, displays a pH-dependent activity and spectroscopy (*149*). Further studies on the zinc-depleted enzyme show that Cu_2E_2SOD (E = empty) has a pH-dependent dismutase activity toward superoxide (*334*). Such pH-dependent properties have been attributed to the possibility that the mutant and the apo forms have a hydroxyl group strongly bound to copper in place of the usual water molecule (see Section II). In fact, both the His-63AlaSOD mutant and Cu_2E_2SOD show a pK_a of 9.1, typical of copper-bound water in small molecule complexes and proteins. This behavior contrasts with that of Cu_2Zn_2-SOD, which has an abnormally high pK_a (>10.0). These findings are easily explained by considering that the presence of the imidazolate bridge between the metals forces the water and the resulting hydroxyl group to be only loosely bound to copper. Such interpretation is supported by X-ray crystallography and NMR data on the anion complexes of Cu_2Zn_2SOD (*88*, *90*, *269*). The strong ligands cyanide and azide are found closely bound to Cu(II), causing the Cu–His-48 bond to lengthen by about 0.5 Å (see Section II). On the contrary, in the analogous azide complex of reduced $Cu_2^IZn_2SOD$ with the intact bridge, the anion is found at about 3.0 Å from the Cu(I) ion (see Section II).

From the above findings, coupled with the demonstration that in Cu_2E_2SOD the second step of the catalytic process (the reoxidation of

copper by a second O_2^- molecule) is responsible for the observed pH dependence, Valentine *et al.* propose that such pH dependence of the catalytic rate is caused by the slow product release from the reoxidized copper (*334*). When the bridging histidine is absent, the newly formed peroxide/hydrogen peroxide will occupy the available equatorial position in the Cu(II) coordination sphere, resulting in a stronger bond and hence in a worse leaving group. The intact imidazolate bridge plays, in this proposal, an active role by preventing the peroxide to form a too stable bond with copper, thereby acting as a good leaving group.

D. Comparison with MnSOD and FeSOD Mechanisms

Mononuclear SODs contain manganese or iron in their active sites. MnSOD is found in prokaryotes and in mitochondria of higher organisms, whereas FeSOD is present in plants and prokaryotes. The X-ray crystal structures of the oxidized and reduced native enzymes and of the respective azide-inhibited forms have been reported (*338*, *339*). The metal ions are in both cases five-coordinate by three histidines, an aspartate, and a solvent/hydroxide molecule in a trigonal bipyramidal geometry. The active sites of both FeSOD and MnSOD appear to be quite similar and the oxidation states of the metals during catalysis are in both cases +2 and +3. The crystal structures of the "cambialistic" SOD from *Propionibacterium shermanii*, equally active with both iron or manganese in the active site, have been reported (*340*), showing again the same active site structure. These similarities are reflected in the proposed unified mechanism shown in Fig. 56.

The superoxide substrate is supposed to bind the oxidized metal, increasing its coordination number to six. On releasing the product O_2, the bound hydroxyl is protonated, forming a coordinated water molecule. A second superoxide molecule then approaches the catalytic center and binds to the reduced metal. The superoxide is reduced by the metal and protonated by the water, forming the second product, hydroperoxide, which finally leaves the active site, restoring the original catalytic center.

It can be seen that the above mechanism shares similarities with the Cu_2Zn_2SOD mechanism. However, the catalytic rates of FeSODs and MnSODs are two orders of magnitude smaller than that of Cu_2Zn_2SOD and dramatically pH dependent. The main differences are that the superoxide molecule increases, on binding, the metal coordination number to six and that the role of the Cu_2Zn_2SOD histidine

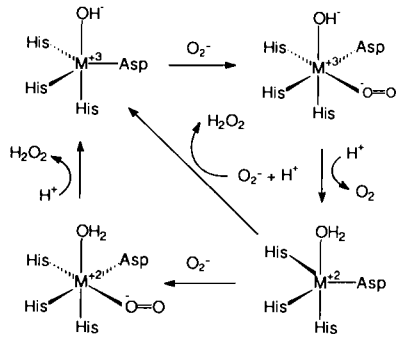

FIG. 56. Reaction scheme proposed for the superoxide dismutation by FeSODs and MnSODs. The first O_2^- molecule binds to the oxidized metal, increasing its coordination number to six. The reduction step follows, in which the metal coordination goes back to five on leaving the dioxygen molecule. A second O_2^- molecule then binds to the reduced metal, oxidizes it back to M(III), becomes protonated, and leaves as hydrogen peroxide.

bridge is here played by the water/hydroxide molecule. The binding mode of the substrate has been proposed on the basis of the structures of the azide-bound forms. A point to be clarified is that the hydroperoxide product does not appear to be a good leaving group due to its affinity toward the trivalent metal ion, thus leading to enzyme inhibition. Furthermore, in the case of FeSOD, it has been shown that exogenous ligands do not bind to the reduced enzyme. This brings support to an outer-sphere mechanism for O_2^- reduction.

X. Concluding Remarks

The very large amount of data currently available on the Cu_2Zn_2 SOD enzyme has enabled a deep understanding of its function and to the rationalization of most aspects of its chemistry and biochemistry. Different techniques have allowed the enzyme to be probed in all its aspects, from the finest details of the active site electronic structure to the overall description of its molecular assembly. The theoretical work has further completed and linked most aspects of this information. However, some parts of the picture are still fuzzy. There are aspects that in our opinion need further study:

1. The details of the electron and proton transfer and the role of the histidinato bridge during catalysis require elucidation to provide yet deeper insights.

2. The role of the quaternary structure in maintaining an active conformation of the enzyme and its dependence from the primary structure should be further analyzed in light of the information coming from the studies on active and inactive monomeric Cu_2Zn_2SODs.
3. The role of electrostatics in the guidance of superoxide to the active site has still to be completely rationalized.

With respect to the above last two points, X-ray and NMR methods should provide the structural information necessary to understand the function of single amino acids and may also provide the basis to correlate the differences in primary structure with the activity and function of the enzyme.

Once again, as always occurs in science, we have here an example of how the process of gaining basic knowledge on a system never ends. As we proceed to obtain a deeper understanding, more new questions arise and unexpected and intriguing aspects appear.

ACKNOWLEDGMENTS

We thank C. Luchinat and J. S. Valentine for carefully reading the manuscript. We are grateful to L. Banci, M. Borsari, K. Djinovic, B. Meier, and P. L. Orioli for valuable suggestions and helpful discussions. We are also grateful to M. Benvenuti for editorial work.

NOTE ADDED IN PROOF: The first crystallographic determination of a Cu_2Zn_2SOD from a prokaryotic organism has just appeared in the literature. This refers to the structure of Cu_2Zn_2SOD from the symbiont bacterium *Photobacterium leiognathi.* The structure has been determined at 1.9 Å resolution and refined to $R = 0.193$ (*75b*). This prokaryotic SOD presents several interesting original features. Actually, with eukaryotic SODs it shares the eight-stranded Greek-key β-barrel fold and a similar active site with the copper and zinc ions coordinated by the same type of residues in the same geometry. Furthermore, *P. leiognathi* Cu_2Zn_2SOD, like eukaryotic Cu_2Zn_2SODs, displays a homodimeric structure in which monomers are related by a noncrystallographic twofold axis. However, the similarities stop there, as the homodimer is formed by the interaction of two monomers through β-strands diametrically opposite those forming the monomer–monomer interface in the eukaryotic enzymes. The dimer interface is larger than that of the bovine SOD molecule and it involves mainly side chain contacts. The authors suggest that independent evolution has achieved a completely different mutual arrangement of the SOD monomers to obtain the same result. A further dramatic difference is found in the structure and in the residues forming the active site channel. Bovine SOD residues Glu-130, Glu-131, and Lys-134, which are responsible for the long-range guidance of the substrate, are missing in *P. leiognathi* SOD, which requires adopting a completely different strategy for attraction of superoxide into the active site.

This is realized by the insertion in the disulfide loop of a 8-residue loop containing the residues Lys-57, Asp-58, and Lys-60, which are indicated as the major candidates for providing the long-range guidance for the substrate, since they originate a positive electrostatic potential and are located in such a way as to be separated by the same distance in the dimer as the corresponding bovine SOD residues.

The results of *P. leiognathi* SOD structural determination and the consequent analysis strongly support the existence of a primordial SOD precursor that has evolved divergently to form the two distinct classes of prokaryotic and eukaryotic Cu_2Zn_2SODs in contrast with the previous proposal of gene transfer from the Leiognathid fish as the origin for *P. leiognathi* (*75c*).

References

1. Mann, T.; Keilin, D. *Proc. R. Soc. London* **1938,** *126,* 303.
2. McCord, J. M.; Fridovich, I. *J. Biol. Chem.* **1969,** *244,* 6049.
3. Davies, K. J. *Biochem. Soc. Symp.* **1995,** *61,* 1.
4. Halliwell, B. *Nutr. Rev.* **1994,** *52,* 253.
5. Richter, C.; Gogvadze, V.; Laffranchi, R.; Schlapbach, R.; Schweizer, M.; Suter, M.; Walter, P.; Yaffee, M. *Biochim. Biophys. Acta* **1995,** *1271,* 67.
6. Balentine, J. D. In "Pathology of Oxygen Toxicity"; Academic Press: New York, 1982; p. 359.
7. Meier, B.; Radeke, H. H.; Selle, S.; Younes, M.; Sies, H.; Resch, K.; Habermehl, G. G. *Biochem. J.* **1989,** *263,* 539.
8. McCord, J. M. *New Engl. J. Med.* **1985,** *312,* 159.
9. Foyer, C. H.; Hall, D. O. In "Chemical and Biochemical Aspects of Superoxide and Superoxide Dismutase"; Bannister, J. V., and Hill, H. A. O., Eds.; Elsevier/North-Holland: New York, Amsterdam, Oxford, 1980; pp. 380–389.
10. Elstner, E. F. In "Chemical and Biochemical Aspects of Superoxide and Superoxide Dismutase"; Bannister, J. V., and Hill, H. A. Q., Eds.; Elsevier/North-Holland: New York, Amsterdam, Oxford, 1980; pp. 390–401.
11. Allen, J. F. In "Superoxide and Superoxide Dismutases"; Michelson, A. M., McCord, J. M., and Fridovich, I., Eds.; Academic Press: New York, 1977; pp. 417–436.
12. Halliwell, B. *Prog. Biophys. Mol. Biol.* **1978,** *33,* 1.
13. Bilinski, T.; Kravwiec, Z.; Liczmanski, A.; Litwinska, J. *Biochem. Biophys. Res. Commun.* **1985,** *130,* 533.
14. Carlioz, A.; Touati, D. *EMBO J.* **1986,** *5,* 623.
15. Peng, T. X.; Moya, A.; Ayala, F. J. *Proc. Natl. Acad. Sci. U.S.A.* **1986,** *83,* 684.
16. Philips, J. P. S.; Campbell, D.; Michaud, M.; Charbonneau, M.; Hilliker, A. J. *Proc. Natl. Acad. Sci. U.S.A.* **1989,** *86,* 2761.
17. Bracco, F.; Scarpa, M.; Rigo, A.; Battistin, L. *Proc. Soc. Exp. Biol. Med.* **1991,** *196,* 36.
18. Deng, H.-X.; Hentati, A.; Tainer, J. A.; Lqbal, Z.; Cyabyab, A.; Hang, W.-Y.; Getzoff, E. D.; Hu, P.; Herzfeldt, B.; Roos, R. P.; Warner, C.; Deng, G.; Soriano, E.; Smyth, C.; Parge, H. E.; Ahmed, A.; Roses, A. D.; Hallewell, R. A.; Pericak-Vance, M. A.; Siddique, T. *Science* **1993,** *261,* 1047.
19. McCord, J. M.; Gurney, M. E. *Science* **1994,** *266,* 1586.
20. Wiedau-Pazos, M.; Goto, J. J.; Rabizadeh, S.; Gralla, E. B.; Roe, J. A.; Lee, M. K.; Valentine, J. S.; Bredesen, D. E. *Science* **1996,** *271,* 515.

21. Clark, I. A.; Chaudiri, G.; Cowden, W. B. *UCLA Symp. Mol. Cell. Biol., New Ser.* **1988,** *82,* 53.
22. Ferrante, A.; Mades, M.; Bates, E. J. D.; Goh, D. H. B.; Beard, L. J. *Immunology* **1988,** *63,* 507.
23. Klempner, M. S.; Dinarello, W. R.; Henderson, W. R.; Gallin, J. I. *J. Clin. Invest.* **1979,** *64,* 996.
24. Tsujimoto, M.; Yokota, S.; Vilcek, J.; Weissmann, G. *Biochem. Biophys. Res. Commun.* **1986,** *137,* 1094.
25. (a) Meier, B.; Redeke, H. H.; Selle, S.; Younes, M.; Sies, H.; Resch, H.; Hebermehl, G. G. *Biochem. J.* **1989,** *263,* 539; Stallings, W. C.; Pattridge, K. A.; Strong, R. K.; Ludwig, M. L.; Yamakura, F.; Isobe, T.; Steinman, H. M. In "Patterson and Patterson"; Gluşker, J. P., Patterson, B. K., and Rossi, M., Eds.; Pergamon Press: Oxford, 1987; pp. 505–513. (b) Youn, H.-D.; Youn, H.; Lee, J.-W.; Yim, Y.-I.; Lee, J. K.; Hah, Y. C.; Kang, S.-O. *Arch. Bioch. Biophys.* **1996,** *334,* 341.
26. Tyler, D. *Biochem. J.* **1975,** *147,* 493.
27. Battistoni, A.; Rotilio, G. *FEBS Lett.* **1995,** *374,* 199.
28. Getzoff, E. D.; Tainer, J. A.; Stempien, M. M.; Bell, G. I.; Hallewell, R. A. *Proteins: Struct. Funct. Genet.* **1989,** *5,* 322.
29. Pace, C. N. *Methods Enzymol.* **1986,** *131,* 266.
30. Biliaderis, C. G.; Weselake, R. J.; Petkau, A.; Friesen, A. D. *Biochem. J.* **1987,** *248,* 981.
31. Roe, J.; Butler, A.; Sholler, D.; Valentine, J.; Marky, L.; Breslauer, K. *Biochemistry* **1988,** *27,* 950.
32. Mei, G.; Rosato, N.; Silva, N.; Rusch, R.; Gratton, E.; Savini, I.; Finazzi-Agrò, A. *Biochemistry* **1992,** *31,* 7224.
33. Inouye, K.; Osaki, A.; Tonomura, B. *J. Biochem.* **1994,** *115,* 507.
34. Marmocchi, F.; Venardi, G.; Bossa, F.; Rigo, A.; Rotilio, G. *FEBS Lett.* **1978,** *94,* 109.
35. Bannister, J. V.; Anastasi, A.; Bannister, W. H. *Biochem. Biophys. Res. Commun.* **1978,** *81,* 469.
36. Kanematsu, S.; Asada, K. *Plant Cell Physiol.* **1989,** *30,* 381.
37. Richardson, D. C.; Bier, C. J.; Richardson, J. S. *J. Biol. Chem.* **1972,** *247,* 6368.
38. Thomas, K. A.; Rubin, B. H.; Bier, C. J.; Richardson, J. S.; Richardson, D. C. *J. Biol. Chem.* **1974,** *249,* 5677.
39. Richardson, D. C.; Thomas, K. A.; Richardson, J. S. *Biochem. Biophys. Res. Commun.* **1975,** *63,* 986.
40. Richardson, J. S.; Thomas, K. A.; Rubin, B. H.; Richardson, D. C. *Proc. Natl. Acad. Sci. U.S.A.* **1975,** *72,* 1349.
41. (a) Tainer, J. A.; Getzoff, E. D.; Beem, K. M.; Richardson, J. S.; Richardson, D. C. *J. Mol. Biol.* **1982,** *160,* 181; (b) Lewis, P. N.; Momany, F. A.; Sheraga, H. A. *Biochim. Biophys. Acta* **1973,** *303,* 211.
42. Hendrickson, A.; Konnert, J. A. "Biomolecular Structure, Function, Conformation and Evolution"; Pergamon Press: Oxford, 1980; pp. 43–57.
43. Hendrickson, W. A.; Konnert, J. H. In "Computing in Crystallography"; Diamond, R., Ramaseshan, S., and Venkatesan, K., Eds.; Indian Academy of Sciences: Bangalore, 1980; pp. 1–23.
44. Tainer, J. A.; Getzoff, E. D.; Richardson, J. S.; Richardson, D. C. *Nature* **1983,** *306,* 284.
45. Getzoff, E. D.; Tainer, J. A.; Weiner, P. K.; Kollman, P. A.; Richardson, J. S.; Richardson, D. C. *Nature* **1983,** *306,* 287.

46. Desideri, A.; Falconi, M.; Polticelli, F.; Bolognesi, M.; Djinovic, K.; Rotilio, G. *J. Mol. Biol.* **1992,** *223,* 337.
47. Bernstein, F. C.; Koetzle, T. F.; Williams, G. J. B.; Meyer, Jr., E. F. Rodgers, J. R.; Kennard, O.; Shimanouchi, T.; Tasumi, M. *J. Mol. Biol.* **1977,** *112,* 535.
48. Rypniewski, W. R.; Mangani, S.; Bruni, B.; Orioli, P. L.; Casati, M.; Wilson, K. S. *J. Mol. Biol.* **1995,** *251,* 282.
49. Djinovic, C. K.; Battistoni, A.; Carrì, M.; Polticelli, F.; Desideri, A.; Rotilio, G.; Coda, A.; Wilson, K.; Bolognesi, M. *Acta Crystallogr.* **1996,** *D52,* 176.
50. Meyer, E. F. *Protein Sci.* **1992,** *1,* 1543.
51. Levitt, M.; Park, B. H. *Structure* **1993,** *1,* 223.
52. Klug, D.; Rabani, J.; Fridovich, I. *J. Biol. Chem.* **1972,** *247,* 4839.
53. Sundberg, R. J.; Martin, B. R. *Chem. Rev.* **1074,** *74,* 471.
54. Forma, H. J.; Fridovich, I. *J. Biol. Chem.* **1973,** *248,* 2645.
55. Lipscomb, W. N. In "Methods for Determining Metal Ion Environments in Proteins: Structure and Function of Metalloproteins"; Darnall, D., and Wilkins, R., Eds.; Elsevier North-Holland: New York; 1980; pp. 265–302.
56. Ogihara, N. L.; Parge, H. E.; Hart, J. P.; Weiss, M. S.; Goto, J. J.; Crane, B. R.; Tsang, J.; Slater, K.; Roe, J. A.; Valentine, J. *Biochemistry* **1996,** *35,* 2316.
57. Lepock, J. R.; Arnold, L. D.; Torrie, B. H.; Andrews, B.; Kruuv, J. *Arch. Biochem. Biophys.* **1985,** *241,* 243.
58. Forman, H.; Fridovich, I. *J. Biol. Chem.* **1973,** *248,* 2645.
59. Malinowski, D.; Fridovich, I. *Biochemistry* **1979,** *18,* 5055.
60. Bertini, I.; Piccioli, M.; Viezzoli, M. S.; Chiu, C. Y.; Mullenbach, G. T. *Eur. J. Biophys.* **1994,** *23,* 167.
61. Hallewell, R. A.; Masiarz, F. R.; Najarian, R. C.; Puma, J. P.; Quiroga, M. R.; Randolph, A.; Sanchez-Pescador, R.; Scandella, C.; Smith, B.; Steimer, K. S.; Mullenbach, G. T. *Nucleic Acids Res.* **1985,** *13,* 2017.
62. Hallewell, R. A.; Mills, R.; Tekamp-Olson, P.; Blacher, R.; Rosenberg, S.; Otting, F.; Masiarz, F. R.; Scandella, C. *Biotechnology* **1987,** *5,* 363.
63. Parge, H. E.; Hallewell, R. A.; Tainer, J. *Proc. Natl. Acad. Sci. U.S.A.* **1992,** *89,* 6109.
64. Getzoff, E. D.; Cabelli, D. E.; Fisher, C. L.; Parge, H. E.; Viezzoli, M. S.; Banci, L.; Hallewell, R. A. *Nature* **1992,** *358,* 347.
65. Schininà, M. E.; Barra, D.; Bossa, F.; Calabrese, L.; Montesaro, L.; Carrì, M. T.; Mariottini, P.; Amaldi, F.; Rotilio, G. *Arch Biochem. Biophys.* **1989,** *272,* 507.
66. Capo, C. R.; Polticelli, F.; Calabrese, L.; Schininà, M. E.; Carrì, M. T.; Rotilio, G. *Biochem. Biophys. Res. Commun.* **1990,** *173,* 1186.
67. Battistoni, A.; Carrì, M. T.; Mazzetti, P.; Rotilio, G. *Biochem. Biophys. Res. Commun.* **1992,** *186,* 1339.
68. Desideri, A.; Falconi, M.; Polticelli, F.; Bolognesi, M.; Djinovic, K.; Rotilio, G. *J. Mol. Biol.* **1992,** *223,* 337.
69. Hamilton, W. C. *Acta Crystallogr.* **1965,** *18,* 502.
70. Asada, K.; Urano, M.; Takahashi, M. *Eur. J. Biochem.* **1973,** *36,* 257.
71. Kitagawa, Y.; Tsunasawa, S.; Tanaka, N.; Katsube, Y.; Sakiyama, F.; Asada, K. *J. Biochem.* **1986,** *99,* 1289.
72. Kitagawa, Y.; Tanaka, N.; Hata, Y.; Kusonoki, M.; Lee, G.; Katsube, Y.; Asada, K.; Alibara, S.; Morita, Y. *J. Biochem.* **1991,** *109,* 447.
73. Frigerio, F.; Falconi, M.; Gatti, G.; Bolognesi, M.; Desideri, A.; Marmocchi, F.; Rotilio, G. *Biochem. Biophys. Res. Commun.* **1989,** *160*(2), 677.

74. Djinovic, K.; Gatti, G.; Coda, A.; Antolini, L.; Pelosi, G.; Desideri, A.; Falconti, M.; Marmocchi, F.; Rotilio, G.; Bolognesi, M. *Acta Crystallogr.* **1991,** B47, 918.
75. (a) Djinovic, K.; Gatti, G.; Coda, A.; Antolini, L.; Pelosi, G.; Desideri, A.; Falconi, M.; Marmocchi, F.; Rotilio, G.; Bolognesi, M. *J. Mol. Biol.* **1992,** *225,* 791. (b) Bourne, Y.; Redford, S. M.; Steinman, H. M.; Lepock, J. R.; Tainer, J. A.; Getzoff, E. D. *Proc. Natl. Acad. Sci. U.S.A.* **1996,** *93,* 12774. (c) Martin, J. P.; Fridovich, I. *J. Biol. Chem.* **1981,** *256,* 6080.
76. Djinovic, K.; Coda, A.; Antilini, L.; Pelosi, G.; Desideri, A.; Falconi, M.; Rotilio, G.; Bolognesi, M. *J. Mol. Biol.* **1992,** *226,* 227.
77. Beckman, J.; Beckman, T.; Chen, J.; Marshall, P.; Freeman, B. *Proc. Natl. Acad. Sci. U.S.A.* **1990,** *87,* 1621.
78. Ischiropoŭlos, H.; Zhu, L.; Chen, J.; Tsai, M.; Martin, J. C.; Smith, C. D.; Beckman, J. S. *Arch. Biochem. Biophys.* **1992,** *298,* 431.
79. Smith, C. D.; Carson, M.; van der Woerd, M.; Chen, J.; Ischiropoulos, H.; Beckman, J. S. *Arch. Biochem. Biophys.* **1992,** *299,* 350.
80. McRee, D. E.; Redford, S. M.; Getzoff, E. D.; Lepock, J. R.; Hallewell, R. A.; Tainer, J. A. *J. Biol. Chem.* **1990,** *265,* 14234.
81. Roberts, V. A.; Fisher, C. L.; Redford, S. M.; McRee, D. E.; Parge, H. E.; Getzoff, E. D.; Tainer, J. A. *Free Radical Res. Commun.* **1990,** *12–13,* 269.
82. Banci, L.; Bertini, I.; Bruni, B.; Carloni, P.; Luchinat, C.; Mangani, S.; Orioli, P. L.; Piccioli, M.; Rypniewski, W.; Wilson, K. *Biochem. Biophys. Res. Commun.* **1994,** *202,* 1088.
83. (a) Orpen, G.; Brammer, L.; Allen, F. H.; Kennard, O.; Watson, D. G. *J. Chem. Soc., Dalton Trans.* **1989,** S1; (b) unpublished results from our laboratory.
84. Stragsm G.; Kraut, J. *J. Mol. Biol.* **1968,** *35,* 503.
85. Bondi, A. *J. Phys. Chem.* **1964,** *68,* 441.
86. Lee, D.-H.; Nei, N.; Huntly, N. N.; Tyeklier, Z.; Kerlin, K. D.; Kaderli, S.; Jung, B.; Zuberbühler, A. D. *J. Am. Chem. Soc.* **1995,** *117,* 12498.
87. Djinovic Carugo, K.; Battistoni, A.; Carri, M. T.; Polticelli, F.; Desideri, A.; Rotilio, G.; Coda, A.; Bolognesi, M. *FEBS Lett.* **1994,** *349,* 93.
88. Banci, L.; Bertini, I.; Buchinat, C.; Scozzafava, A. *J. Biol. Chem.* **1989,** *264,* 9742.
89. Banci, L.; Bencini, A.; Bertini, I.; Luchinat, C.; Piccioli, M. *Inorg. Chem.* **1990,** *29,* 4867.
90. Djinovic, K.; Polticelli, F.; Desideri, A.; Rotilio, G.; Wilson, K.; Bolognesi, M. *J. Mol. Biol.* **1994,** *240,* 179.
91. Rotilio, G.; Bray, R. C.; Fielden, E. M. *Biochim. Biophys Acta* **1972,** *268,* 605.
92. Cabelli, D. E.; Bielski, B. H. *J. Phys. Chem.* **1983,** *87,* 1809.
93. Bielski, B. H. J.; Cabelli, D. E.; Arudi, R. L.; Ross, A. B. *J. Phys. Chem. Ref. Data* **1985,** *14,* 1041.
94. Salmon, G. A.; Sykes, A. G. *Methods Enzymol.* **1993,** *227,* 522.
95. Fisher, C. L.; Cabelli, D. E.; Tainer, J. A.; Hallewell, R. A.; Getzoff, E. D. *Proteins: Struct. Funct. Genet.* **1994,** *19,* 24.
96. Banci, L.; Bertini, I.; Cabelli, D. E.; Hallewell, R. A.; Tung, J. W.; Viezzoli, M. S. *Eur. J. Biochem.* **1991,** *196,* 123.
97. Klug-Roth, D.; Fridovich, I.; Rabani, J. *J. Am. Chem. Soc.* **1973,** *95,* 2786.
98. Bray, R. C.; Clocke, S. A.; Fielden, E. M.; Roberts, P. B.; Rotilio, G.; Calabrese, L. *Biochem. J.* **1974,** *139,* 43.
99. Fee, J. A.; Bull, C. *J. Biol. Chem.* **1986,** *261,* 13000.
100. Rigo, A.; Viglino, P.; Rotilio, G. *Anal. Biochem.* **1975,** *68,* 1.

101. Argese, E.; Orsega, E.; De Carli, B.; Scarpa, M.; Rigo, A. *Bioelectrochem. Bioenerg.* **1984,** *13,* 385.
102. Banci, L.; Bertini, I.; Viezzoli, M. S.; Argese, E.; Orsega, E.; Chin, C. Y.; Mullenbach, G. T. *JBIC,* **1997,** *2,* 295.
103. Briggs, R. G.; Fee, J. A. *Biochim. Biophys. Acta* **1978,** *537,* 86.
104. Beyer, Jr., W. F.; Fridovich, I.; Mullenbach, G. T.; Hallewell, R. A. *J. Biol. Chem.* **1987,** *262,* 11182.
105. Cudd, A.; Fridovich, I. *J. Biol. Chem.* **1982,** *257,* 11443.
106. Mota De Freitas, D.; Luchinat, C.; Banci, L.; Bertini, I.; Valentine, J. S. *Inorg. Chem.* **1987,** *26,* 2788.
107. Mota De Freitas, D.; Valentine, J. S. *Biochemistry* **1984,** *23,* 2079.
108. Paoletti, F.; Aldinucci, D.; Mocali, A.; Caparrini, A. *Anal. Biochem.* **1986,** *154,* 536.
109. Paoletti, F.; Mocali, A. *Methods Enzymol.* **1990,** *186,* 209.
110. Paoletti, F.; Mocali, A.; Aldinucci, D. *Chem. Biol. Interactions* **1990,** *76,* 3.
111. Beauchamp, C.; Fridovich, I. *Anal. Biochem.* **1971,** *44,* 276.
112. Bertini, I.; Banci, L.; Luchinat, C.; Bielski, B. H. J.; Cabelli, D.; Mullenbach, G. T.; Hallewell, R. A. *J. Am. Chem. Soc.* **1989,** *111,* 714.
113. Argese, E.; Rigo, A.; Viglino, P.; Orsega, E.; Marmocchi, F.; Cocco, D.; Rotilio, G. *Biochim. Biphys. Acta* **1984,** *787, 205.*
114. Terenzi, M.; Rigo, A.; Franconi, C.; Mondovi, B.; Calabrese, L.; Rotilio, G. *Biochim. Biophys. Acta* **1974,** *351,* 230.
115. Banci, L.; Bertini, I.; Cabelli, D.; Hallewell, R. A.; Luchinat, C.; Viezzoli, M. S. *Inorg. Chem.* **1990,** *29,* 2398.
116. O'Neill, P.; Davies, S.; Fielden, E. M.; Calabrese, L.; Capo, C.; Marmocchi, F.; Natoli, G.; Rotilio, G. *Biochem. J.* **1988,** *251,* 41.
117. Polticelli, F.; O'Neill, P.; Costanzo, S.; Lania, A.; Rotilio, G.; Desideri, A. *Arch. Biochem. Biophys.* **1995,** *321,* 123.
118. Argese, E.; Viglino, P.; Rotilio, G.; Scarpa, M.; Rigo, A. *Biochemistry* **1987,** *26,* 3224.
119. Banci, L.; Bertini, I.; Luchinat, C.; Viezzoli, M. S. *Inorg. Chem.* **1993,** *32,* 1403.
120. Banci, L.; Bertini, I.; Turano, P. *Eur. Biophys. J.* **1991,** *19,* 141.
121. Rigo, A.; Viglino, P., Rotilio, G.; Tomat, R. *FEBS Lett.* **1995,** *50,* 86.
122. Klapper, I.; Hagstrom, R.; Fine, R.; Sharp, K.; Honig, B. *Proteins: Struct. Funct. Genet.* **1986,** *1,* 47.
123. Sharp, K.; Fine, R.; Honig, B. *Science* **1987,** *236,* 1460.
124. Banci, L.; Bertini, I.; Chiu, C. Y.; Mullenbach, G. T.; Viezzoli, M. S. *Eur. J. Biochem.* **1995,** *234,* 855.
125. Sines, J. J.; Allison, S. A.; McCammon, J. A. *Biochemistry* **1990,** *29,* 9403.
126. Sines, J. J.; McCammon, J. A.; Allison, S. A. *J. Comp. Chem.* **1992,** *13,* 66.
127. Falconi, M.; Rotilio, G.; Desideri, A. *Proteins: Struct. Funct. Genet.* **1991,** *10,* 149.
128. Polticelli, F.; Falconi, M.; O'Neill, P.; Petruzelli, R.; Galtieri, A.; Lania, A.; Calabrese, L.; Rotilio, G.; Desideri, A. *Arch. Biochem. Biophys.* **1994,** *312,* 22.
129. Carloni, P.; Blochl, P. E.; Parrinello, M. *J. Phys. Chem.* **1995,** *99,* 1338.
130. Luty, B. A.; El Amrani, S.; McCammon, J. A. *J. Am. Chem. Soc.* **1993,** *115,* 11874.
131. Koppenol, W. H. In "Oxygen and Oxoradicals in Chemistry and Biology"; Rodgers, M. A. J., and Powers, E. L., Eds.; Academic Press: New York, 1981; pp. 671–674.
132. Shen, J.; Wong, C. F.; Subrasmaniam, S.; Albright, T. A.; McCammon, J. A. *J. Comp. Chem.* **1990,** *11,* 346.
133. Allison, S. A.; McCammon, J. A. *J. Chem. Phys.* **1985,** *89,* 1072.
134. Bacquet, R. J.; McCammon, J. A.; Allison, S. A. *J. Phys. Chem.* **1988;** *92,* 7134.

135. Shen, J.; McCammon, J. A. *Chem. Phys.* **1991,** *158,* 191.
136. Shen, J.; Subramanian, S.; Wong, C. F.; McCammon, J. A. *Biopolymers* **1989,** *28, 2085.*
137. Shen, J.; McCammon, J. A. *J. Comp. Chem.* **1986,** *7,* 346.
138. Davis, M. E.; McCammon, J. A. *Chem. Rev.* **1990,** *90,* 509.
139. Banci, L.; Carloni, P.; La Penna, G.; Orioli, P. L. *J. Am. Chem. Soc.* **1992,** *114,* 6994.
140. Banci, L.; Carloni, P.; Orioli, P. L. *Proteins: Struct. Funct. Genet.* **1994,** *18,* 216.
141. Banci, L.; Cabelli, D. E.; Getzoff, E. D.; Hallewell, R. A.; Viezzoli, M. S. *J. Inorg. Biochem.* **1993,** *50,* 89.
142. Takahara, M.; Sagai, H.; Inouye, S.; Inouye, M. *Biotechnology* **1988,** *6,* 195.
143. Hallewell, R. A.; Laria, I.; Tabrizi, A.; Carlin, G.; Getzoff, E. D.; Tainer, J. A.; Cousens, L. S.; Mullenbach, G. T. *J. Biol. Chem.* **1989,** *264,* 5260.
144. Steinman, H. *J. Biol. Chem.* **1987,** *262,* 1882.
145. Buechel, D. E.; Gronenborn, B.; Mueller-Hill, B. *Nature* **1980,** *283,* 541.
146. Tibell, L.; Hjalmarsson, K.; Edlund, T.; Skogman, G.; Engstrom, A.; Aasa, R.; Markland, S. In "Oxy-Radicals in Molecular Biology and Pathology"; Cerutti, P. A., Fridovich, I., and McCord, J. M., Eds.; Liss: New York, 1988; pp. 233–245.
147. Tibell, L.; Hjalmarsson, K.; Edlund, T.; Skogman, G.; Engstrom, A.; Marklund, S. L. *Proc. Natl. Acad. Sci. U.S.A.* **1987,** *84,* 6634.
148. Studier, F. W.; Rosenberg, A. H.; Dunn, J. J.; Dubendorff, J. W. *Methods Enzymol.* **1990,** *185,* 66.
149. Graden, J. A.; Ellerby, L. M.; Roe, J. A.; Valentine, J. S. *J. Am. Chem. Soc.* **1994,** *116,* 9743.
150. Lu, Y.; Gralla, E. B.; Roe, J. A.; Valentine, J. S. *J. Am. Chem. Soc.* **1992,** *114,* 3560.
151. Battistoni, A.; Carri, M. T.; Mazzetti, A. P.; Rotilio, G. *Biochem. Biophys. Res. Commun.* **1992,** *186,* 1339.
152. Chen, Y.-L.; Park, S.; Thornburg, R. W.; Tabatabai, L. B.; Kintanar, A. *Biochemistry* **1995,** *34,* 12265.
153. Malinowski, D. P.; Fridovich, I. *Biochemistry* **1979,** *18,* 5909.
154. Borders, Jr., C. L.; Johansen, J. T. *Biochem. Biophys. Res. Commun.* **1980,** *96,* 1071.
155. Bermingham-McDonough, O.; Mota De Freitas, D.; Kunamoto, A.; Saunders, J. E.; Blech, D. M.; Borders, C. L.; Valentine, J. S. *Biochem. Biophys. Res. Commun.* **1982,** *108,* 1376.
156. Borders, C. L.; Fridovich, I. *Arch. Biochem. Biophys.* **1985,** *241,* 472.
157. Marmocchi, F.; Mavelli, I.; Rigo, A.; Stevanato, R.; Bossa, F.; Rotilio, G. *Biochemistry* **1982,** *21,* 2853.
158. Cocco, D.; Rossi, L.; Barra, D.; Bossa, F.; Rotilio, G. *FEBS Lett.* **1982,** *150, 303.*
159. Mota De Freitas, D.; Ming, L. J.; Ramasamy, R.; Valentine, J. S. *Inorg. Chem.* **1990,** *29,* 3512.
160. Boccu', E.; Velo, G. P.; Veronese, F. M. *Pharmacol. Res. Comm.* **1982,** *14,* 113.
161. Conforti, A.; Franco, L.; Milanino, R.; Velo, G. P.; Boccu', E.; Largajolli, R.; Schiavon, O.; Veronese, F. M. *Pharmacol. Res. Comm.* **1987,** *19,* 287.
162. Veronese, F. M.; Caliceti, P.; Pastorino, A.; Schiavon, O.; Sartore, L.; Banci, L.; Monsu Scolaro, L. *J. Control. Rel.* **1989,** *10,* 145.
163. Banci, L.; Bertini, I.; Caliceti, P.; Monsu' Scolaro, L.; Schiavon, O.; Veronese, F. M. *J. Inorg. Biochem.* **1990,** *39,* 149.
164. Rotilio, G.; Morpurgo, L.; Giovagnoli, L.; Calabrese, L.; Mondovi, B. *Biochemistry* **1972,** *11,* 2187.

165. Fielden, E. M.; Roberts, P. B.; Bray, R. C.; Rotilio, G. *Biochem. Soc. Trans.* **1973,** *1,* 52.
166. Fuchs, H. J. R.; Borders, Jr., C. L. *Biochem. Biophys. Res. Commun.* **1983,** *116,* 1107.
167. Rotilio, G.; Morpurgo, L.; Calabrese, L.; Mondovi, B. *Biochim. Biophys. Acta* **1973,** *302, 229.*
168. Bertini, I.; Luchinat, C.; Viezzoli, M. S.; Wang, Y. *Arch. Biochem. Biophys.* **1989,** *269,* 586.
169. Uchida, K.; Kawakishi, S. *J. Biol. Chem.* **1994,** *269,* 2405.
170. Bannister, J. V.; Bannister, W. H.; Wood, W. *Eur. J. Biochem.* **1971,** *18,* 178.
171. Fielden, E. M.; Roberts, P. B.; Bray, R. C.; Lowe, D. J.; Mautner, G. N.; Rotilio, G.; Calabrese, L. *Biochem. J.* **1974,** *139,* 49.
172. Banci, L.; Bertini, I.; Bauer, D.; Hallewell, R. A.; Viezzoli, M. S. *Biochemistry* **1993,** *32,* 4384.
173. Valentine, J. S.; Pantoliano, M. W.; McDonnell, P. J.; Burger, A. R.; Lippard, S. J. *Proc. Natl. Acad. Sci. U.S.A.* **1979,** *76,* 4245.
174. Scozzofava, A.; Viezzoli, M. S. *Mol. Chem. Neuropath.* **1993,** *19,* 193.
175. Polticelli, F.; Bottaro, G.; Battistoni, A.; Carri, M. T.; Djinovic, K.; Bolognesi, M.; O'Neill, P.; Rotilio, G.; Desideri, A. *Biochemistry* **1995,** *34,* 6043.
176. Lu, Y.; LaCroix, L. B.; Lowery, M. D.; Solomon, E. I.; Bender, C. J.; Peisach, J.; Roe, J. A.; Gralla, E. B.; Valentine, J. S. *J. Am. Chem. Soc.* **1993,** *115,* 5907.
177. Lu, Y.; Roe, J. A.; Gralla, E. B.; Valentine, J. S. In "Bioinorganic Chemistry of Copper"; Karlin, K. D., Ed.; Chapman & Hall: New York, 1993; p. 64.
178. Lu, Y.; Roe, J. A.; Bender, C. J.; Peisach, J.; Banci, L.; Bertini, I.; Gralla, E. B.; Valentine, J. S. *Inorg. Chem.* **1996,** *35,* 1692.
179. Banci, L.; Bertini, I.; Borsari, M.; Viezzoli, M. S.; Hallewell, R. A. *Eur. J. Biochem.* **1995,** *232,* 220.
180. Pantoliano, M. W.; McDonnel, P. J.; Valentine, J. S. *J. Am. Chem. Soc.* ***1979,*** *101,* 6454.
181. Fee, J. A.; Phillips, W. D. *Biochim. Biophys. Acta* **1975,** *412,* 26.
182. Dunbar, J. C.; Johansen, J. T.; Uchida, T. *Carlsberg Res. Commun.* **1982,** *47,* 163.
183. Beem, K. M.; Rich, P.; Rajagopalan, K. V. *J. Biol. Chem.* **1974,** *249,* 4229.
184. Pantoliano, M. W.; Valentine, J. S.; Mammone, R. J.; Scholler, D. M. *J. Am. Chem. Soc.* **1982,** *104,* 1717.
185. Ming, L. J.; Valentine, J. S. *J. Am. Chem. Soc.* **1990,** *112,* 6374.
186. Cotton, F. A.; Wilkinson, G. "Advanced Inorganic Chemistry"; Wiley: New York, 1990.
187. Banci, L.; Bertini, I.; Luchinat, C.; Monnanni, R.; Scozzafava, A. *Inorg. Chem.* **1987,** *26,* 153.
188. Roe, J. A.; Peoples, R.; Scholler, D. M.; Valentine, J. S. *J. Am. Chem. Soc.* **1990,** *112,* 1538.
189. Fee, J. A. *J. Biol. Chem.* **1973,** *248,* 4229.
190. Hirose, J.; Iwatsuka, K.; Kidani, Y. *Biochem. Biophys. Res. Commun.* **1981,** *98,* 58.
191. Ming, L. J.; Valentine, J. S. *J. Am. Chem. Soc.* **1990,** *112,* 4256.
192. Viezzoli, M. S.; Wang, Y. *Inorg. Chim. Acta* **1988,** *153,* 189.
193. Dunbar, J. C.; Holmquist, B.; Johansen, J. T. *Biochemistry* **1984,** *23,* 4324.
194. Dunbar, J. C.; Holmquist, B.; Johansen, J. T. *Biochemistry* **1984,** *23,* 4330.
195. Ming, L. J.; Banci, L.; Luchinat, C.; Bertini, I.; Valentine, J. S. *Inorg. Chem.* **1988,** *27,* 728.
196. Bailey, D. B.; Ellis, P. D.; Fee, J. A. *Biochemistry* **1980,** *19,* 591.

197. Kofod, P.; Bauer, R.; Danielsen, E.; Larsen, E.; Bjerrum, M. J. *Eur. J. Biochem.* **1991,** *198,* 607.
198. Bauer, R.; Demeter, I.; Hasemann, V.; Johansen, J. T. *Biochem. Biophys. Res. Commun.* **1980,** *94,* 1296.
199. Bjerrum, M. J.; Kofod, P.; Bauer, R.; Danielsen, E. In "Proc. 5th Conf. Superoxide and Superoxide Dismutase"; Czapski, G., Ed.; Jerusalem, 1989.
200. Hirose, J.; Iwatzuka, K.; Kidani, Y. *Biochem. Biophys. Res. Commun.* **1981,** *98,* 58.
201. Hirose, J.; Yamada, M.; Hayakawa, C.; Nagao, H.; Noji, M.; Kidani, Y. *Biochem. Int.* **1984,** *8,* 401.
202. Forman, H. J.; Fridovich, I. *J. Biol. Chem.* **1973,** *248,* 2645.
203. Blackburn, N. J.; Hasnain, S. S.; Binsted, N.; Diakun, G. P.; Garner, C. D.; Knowles, P. F. *Biochem. J.* **1984,** *219,* 985.
204. Banci, L.; Bencini, A.; Bertini, I.; Luchinat, C.; Viezzoli, M. S. *Gazz. Chim. Ital.* **1990,** *120,* 179.
205. Gaber, B. P.; Brown III, R. D.; Koenig, S. H.; Fee, J. A. *Biochim. Biophys. Acta* **1972,** *271,* 1.
206. Boden, N.; Holmes, M. C.; Knowles, P. F. *Biochem. J.* **1979,** *177,* 303.
207. Bertini, I.; Banci, L.; Brown III, R. D.; Koenig, S. H.; Luchinat, C. *Inorg. Chem.* **1988,** *27,* 951.
208. Banci, L.; Bertini, I.; Hallewell, R. A.; Luchinat, C.; Viezzoli, M. S. *Eur. J. Biochem.* **1989,** *184,* 125.
209. Solomon, I. *Phys. Rev.* **1955,** *99,* 559.
210. Bertini, I.; Luchinat, C.; Mancini, M.; Spina, G. In "Magneto-Structural Correlations in Exchange-Coupled Systems"; Gatteschi, D., Kahn, O., and Willett, R. D., Eds.; Reidel Publishing Company: Dordrecht, 1985; pp. 421–461.
211. Bertini, I.; Lanini, G.; Luchinat, C.; Mancini, M.; Spina, G. *J. Magn. Reson.* **1985,** *63,* 56.
212. Bertini, I.; Briganti, F.; Luchinat, C.; Mancini, M.; Spina, G. *J. Magn. Reson.* **1985,** *63,* 41.
213. Koenig, S. H.; Brown III, R. D. In "Metal Ions in Biological Systems, Vol. 21"; Sigel, H., Ed.; Marcel Dekker: New York, 1987; p. 239.
214. Bertini, I.; Galas, O.; Luchinat, C.; Parigi, G. *J. Magn. Reson.* **1995,** *113,* 151.
215. Bertini, I.; Luchinat, C.; Banci, L.; Viezzoli, M. S. *Biol. Met.* **1990,** *3,* 146.
216. Bertini, I.; Scozzafava, A. In "Metal Ions in Biological Systems"; Sigel, H., Ed.; Marcel Dekker: New York and Basel, 1981; pp. 31–74.
217. Bertini, I.; Luchinat, C.; Messori, L. *Biochem. Biophys. Res. Commun.* **1981,** *101,* 577.
218. Fee, J. A.; Gaber, B. P. *J. Biol. Chem.* **1972,** *247,* 60.
219. Banci, L.; Bertini, I.; Luchinat, C.; Monnanni, R.; Scozzafava, A. *Inorg. Chem.* **1988,** *27,* 107.
220. Bertini, I.; Luchinat, C.; Monnanni, R.; Scozzafava, A.; Borghi, E. *Inorg. Chim. Acta* **1984,** *91,* 109.
221. St. Clair, C. S.; Gray, H. B.; Valentine, J. S. *Inorg. Chem.* **1992,** *31,* 925.
222. Lawrence, G. D.; Sawyer, D. T. *Biochemistry* **1979,** *18,* 3045.
223. Fee, J. A.; DiCorleto, P. E. *Biochemistry* **1973,** *12,* 4893.
224. Verhagen, M. F. J. M.; Meussen, E. T. M.; Hagen, W. R. *Biochim. Biophys. Acta* **1995,** *1244,* 99.
225. Armstrong, F. A. *Struct. Bonding* **1990,** *72,* 137.
226. Berg, H. In "Comprehensive Treatise of Electrochemistry"; Srinivasan, S., Chiz-

madzhev, Y. A., Bockris, J. O'M., Conway, B. E., and Yeager, E., Eds.; Plenum: New York, 1985; p. 190.
227. Azab, H. A.; Banci, L.; Borsari, M.; Luchinat, C.; Sola, M.; Viezzoli, M. S. *Inorg. Chem.* **1992,** *31,* 4649.
228. Zuman, P. In "The Elucidation of Organic Electrode Processes"; Academic Press: New York, 1969; p. 176.
229. Ozaki, S.; Hirose, J.; Kidani, Y. *Inorg. Chem.* **1988,** *27,* 3746.
230. Bertini, I.; Hiromi, K.; Hirose, J.; Sola, M.; Viezzoli, M. S. *Inorg. Chem.* **1993,** *32,* 1106.
231. Bertini, I.; Banci, L.; Luchinat, C.; Piccioli, M. *Coord. Chem. Rev.* **1990,** *100,* 67.
232. Mangani, S.; Orioli, P. L.; Carloni, P. *Inorg. Chim. Acta* **1994,** *216,* 121.
233. Bertini, I.; Luchinat, C.; Monnanni, R. *J. Am. Chem. Soc.* **1985,** *107,* 2178.
234. Solomon, E. I.; Hare, J. W.; Dooley, D. M.; Dawson, J. H.; Stephens, P. J.; Gray, H. B. *J. Am. Chem. Soc.* **1980,** *102,* 168.
235. Dawson, J. H.; Dooley, D. M.; Clark, R.; Stephens, P. J.; Gray, H. B. *J. Am. Chem. Soc.* **1979,** *101,* 5046.
236. Dooley, D. M.; Rawlings, J.; Dawson, J. H.; Stephens, P. J.; Andreasson, L.-E.; Malmstrom, B. G.; Gray, H. B. *J. Am. Chem. Soc.* **1979,** *101,* 5038.
237. Rosenberg, R. C.; Root, C. A.; Bernstein, P. K.; Gray, H. B. *J. Am. Chem. Soc.* **1975,** *97,* 2092.
238. Solomon, E. I.; Hare, J. W.; Gray, H. B. *Proc. Natl. Acad. Sci. U.S.A.* **1976,** *97,* 2092.
239. Pantoliano, M. W.; Valentine, J. S.; Nafie, L. A. *J. Am. Chem. Soc.* **1982,** *104,* 6310.
240. Fawcett, T. G.; Bernarducci, E. E.; Krogh-Jespersen, K.; Schugar, H. J. *J. Am. Chem. Soc.* **1980,** *102,* 1686.
241. Bernarducci, E.; Schwindinger, W. F.; Hughey, J. L.; Krogh-Jespersen, K.; Schugar, H. J. *J. Am. Chem. Soc.* **1981,** *103,* 1686.
242. Rotilio, G.; Calabrese, L.; Bossa, F.; Barra, D.; Finazzi Agro', A.; Mondovì, B. *Biochemistry* **1972,** *11,* 2182.
243. Beem, K. M.; Rich, W. E.; Rajagopalan, K. V. *J. Biol. Chem.* **1974,** *249,* 7298.
244. Beem, K. M.; Richardson, D. C.; Rajagopalan, K. V. *Biochemistry* **1977,** *16,* 1930.
245. Liebermann, R. A.; Sands, R. H.; Fee, J. A. *J. Biol. Chem.* **1982,** *257,* 336.
246. Osman, R.; Basch, H. *J. Am. Chem. Soc.* **1984,** *106,* 5710.
247. Fee, J. A.; Peisach, J.; Mims, W. B. *J. Biol. Chem.* **1981,** *256,* 1910.
248. Huettermann, J.; Kappl, R.; Banci, L.; Bertini, I. *Biochim. Biophys. Acta* **1988,** *956,* 173.
249. Reinhard, H.; Kappl, R.; Huttermann, J.; Viezzoli, M. S. *J. Phys. Chem.* **1994,** *98,* 8806.
250. Dykanov, S.; Felli, I. C.; Viezzoli, M. S.; Spoyalov, A.; Huttermann, J. *FEBS Lett.* **1994,** *345,* 55.
251. Lippard, S. J.; Burger, A. R.; Ugurbil, K.; Pantoliano, M. W.; Valentine, J. S. *Biochemistry* **1977,** *16,* 1136.
252. Fee, J. A.; Briggs, R. G. *Biochim. Biophys. Acta* **1975,** *400,* 439.
253. Fee, J. A. *Biochim. Biophys. Acta* **1973,** *295,* 107.
254. Bencini, A.; Gatteschi, D. In "Transition Metal Chemistry"; Melson, G. A., and Figgis, B. N., Eds.; Marcel Dekker: New York and Basel, 1982; pp. 1–178.
255. Bencini, A.; Gatteschi, D. "Electron Paramagnetic Resonance of Exchange-Coupled Systems"; Springer-Verlag: Berlin and New York, 1990.
256. Strothkamp, K. G.; Lippard, S. J. *J. Am. Chem. Soc.* **1982,** *104,* 852.
257. Morgenstern-Badarau, I.; Cocco, D.; Desideri, A.; Rotilio, G.; Jordanov, J.; Dupre', N. *J. Am. Chem. Soc.* **1986,** *108,* 300.

258. Ming, L. J.; Valentine, J. S. *J. Am. Chem. Soc.* **1987,** *109,* 4426.
259. Calabrese, L.; Cocco, D.; Desideri, A. *FEBS Lett.* **1979,** *106,* 142.
260. Banci, L.; Bertini, I.; Luchinat, C.; Monnanni, R.; Scozzafava, A.; Salvato, B. *Gazz. Chim. Ital.* **1986,** *116,* 51.
261. Desideri, A.; Paci, M.; Capo, C.; Calabrese, L.; Rotilio, G. *J. Inorg. Biochem.* **1988,** *33,* 277.
262. Bertini, I.; Lanini, G.; Luchinat, C.; Messori, L.; Monnanni, R.; Scozzafava, A. *J. Am. Chem. Soc.* **1985,** *107,* 4391.
263. Rigo, A.; Viglino, P.; Rotilio, G. *Biochem. Biophys. Res. Commun.* **1975,** *63,* 1013.
264. Rigo, A.; Stevanato, R.; Viglino, P.; Rotilio, G. *Biochem. Biophys. Res. Commun.* **1977,** *79,* 776.
265. Strothkamp, K. G.; Lippard, S. J. *Biochemistry* **1981,** *20,* 7488.
266. Bertini, I.; Luchinat, C.; Scozzafava, A. *J. Am. Chem. Soc.* **1980,** *102,* 7349.
267. Bertini, I.; Borghi, E.; Luchinat, C.; Scozzafava, A. *J. Am. Chem. Soc.* **1981,** *103,* 7779.
268. Han, J.; Blackburn, N. J.; Loehr, T. M. *Inorg. Chem.* **1992,** *31,* 3223.
269. Djinovic, K.; Battistoni, A.; Carri, M. T.; Polticelli, F.; Desideri, A.; Rotilio, G.; Coda, A.; Bolognesi, M. *FEBS Lett.* **1994,** *349,* 93.
270. Banci, L.; Bertini, I.; Luchinat, C.; Hallewell, R. A. *J. Am. Chem. Soc.* **1988,** *110,* 3629.
271. Bertini, I.; Luchinat, C.; Macinai, R.; Piccioli, M.; Scozzafava, A.; Viezzoli, M. S. *J. Magn. Reson. Ser. B* **1994,** *B104,* 95.
272. Morpurgo, L.; Giovagnoli, C.; Rotilio, G. *Biochim. Biophys. Acta* **1973,** *322,* 204.
273. Dooley, D. M.; McGuirl, M. A. *Inorg. Chem.* **1986,** *25,* 1261.
274. Viglino, P.; Rigo, A.; Stevanato, R.; Ranieri, G. A.; Rotilio, G.; Calabrese, L. *J. Magn. Reson.* **1979,** *34,* 265.
275. Banci, L.; Bertini, I.; Luchinat, C.; Scozzafava, A.; Turano, P. *Inorg. Chem.* **1989,** *28,* 2377.
276. Van Camp, H. L.; Sands, R. H.; Fee, J. A. *Biochim. Biophys. Acta* **1982,** *704,* 75.
277. Sette, M.; Paci, M.; Desideri, A.; Rotilio, G. *Biochemistry* **1992,** *31,* 12410.
278. Searcy, D. G.; Whitehead, J. P.; Maroney, M. J. *Arch. Biochem. Biophys.* **1995,** *318,* 251.
279. Wittenkeller, L.; Abraha, A.; Ramasamy, R.; Mota De Freitas, D.; Theisen, L. A.; Crans, D. C. *J. Am. Chem. Soc.* **1991,** *113,* 7872.
280. Cass, A. E. G.; Hill, H. A. O.; Smith, B. E.; Bannister, J. V.; Bannister, W. H. *Biochemistry* **1977,** *16,* 3061.
281. Cass, A. E. G.; Hill, H. A. O.; Smith, B. E.; Bannister, J. V.; Bannister, W. H. *Biochem. J.* **1977,** *165,* 587.
282. Cass, A. E. G.; Hill, H. A. O.; Hasemann, V.; Johansen, J. T. *Carlsberg Res. Commun.* **1978,** *43,* 439.
283. Banci, L.; Bertini, I.; Luchinat, C.; Viezzoli, M. S. *Inorg. Chem.* **1990,** *29,* 1438.
284. McAdam, M. E.; Fielden, E. M.; Lavelle, F.; Calabrese, L.; Cocco, D.; Rotilio, G. *Biochem. J.* **1977,** *167,* 271.
285. Moss, T. H.; Fee, J. A. *Biochem. Biophys. Res. Commun.* **1975,** *66,* 799.
286. Bertini, I.; Luchinat, C.; Piccioli, M.; Vicens Oliver, M.; Viezzoli, M. S. *Eur. Biophys. J.* **1991,** *20,* 269.
287. Merli, A.; Rossi, G.; Djinovic, K.; Bolognesi, M.; Desideri, A.; Rotilio, G. *Biochem. Biophys. Res. Commun.* **1995,** *210,* 1040.
288. Ming, L. J.; Banci, L.; Luchinat, C.; Bertini, I.; Valentine, J. S. *Inorg. Chem.* **1988,** *27,* 4458.

289. Gurbiel, R. J.; Peoples, R.; Doan, P. E.; Cliine, J. F.; McCracken, J.; Peisach, J.; Hoffman, B. M.; Valentine, J. S. *Inorg. Chem.* **1993,** *32,* 1813.
290. Bertini, I.; Luchinat, C. In "Bioinorganic Chemistry"; Bertini, I., Gray, H. B., Lippard, S. J., and Valentine, J. S., Eds.; University Science Books: Mill Valley, 1994; pp. 37–106.
291. Bailey, D. B.; Ellis, P. D.; Fee, J. A. *Biochemistry* **1980,** *19,* 591.
292. Armitage, I. M.; Uiterkamp, A. J. M. S.; Chlebowski, J. F.; Coleman, J. E. *J. Magn. Reson.* **1978,** *29,* 375.
293. Summers, M. F.; van Rijn, J.; Reedijk, J.; Marzilli, L. G. *J. Am. Chem. Soc.* **1986,** *108,* 4254.
294. Bauer, R.; Demeter, I.; Hasemann, V.; Johansen, J. T. *Biochem. Biophys. Res. Commun.* **1980,** *94,* 1296.
295. Bertini, I.; Luchinat, C. "NMR of Paramagnetic Molecules in Biological Systems"; Benjamin/Cummings: Menlo Park, CA, 1986.
296. Banci, L.; Bertini, I.; Luchinat, C.; Scozzafava, A. *J. Am. Chem. Soc.* **1987,** *109,* 2328.
297. Banci, L.; Bertini, I.; Luchinat, C.; Piccioli, M.; Scozzafava, A.; Turano, P. *Inorg. Chem.* **1989,** *28,* 4650.
298. Banci, L.; Bertini, I.; Luchinat, C.; Piccioli, M.; Scozzafava, A. *Gazz. Chim. Ital.* **1993,** *123,* 95.
299. Bertini, I.; Piccioli, M.; Scozzafava, A.; Viezzoli, M. S. *Magn. Reson. Chem.* **1993,** *31,* S17.
300. Paci, M.; Desideri, A.; Sette, M.; Falconi, M.; Rotilio, G. *FEBS Lett.* **1990,** *261,* 231.
301. Sette, M.; Paci, M.; Desideri, A.; Rotilio, G. *Eur. J. Biochem.* **1993,** *213,* 391.
302. Bertini, I.; Luchinat, C.; Ming, L. J.; Piccioli, M.; Sola, M.; Valentine, J. S. *Inorg. Chem.* **1992,** *31,* 4433.
303. Burger, A. R.; Lippard, S. J.; Pantoliano, M. W.; Valentine, J. S. *Biochemistry* **1980,** *19,* 4139.
304. Hill, H. A. O.; Lee, W. K.; Bannister, J. V.; Bannister, W. H. *Biochem. J.* **1980,** *185,* 245.
305. Fee, J. A.; Ward, R. L. *Biochem. Biophys. Res. Commun.* **1976,** *71,* 427.
306. Valentine, J. S.; Pantoliano, M. W. In "Copper Proteins"; Spiro, T. G., Ed.; Wiley: New York, 1981; pp. 291.
307. Fridovich, I. *Adv. Enzymol. Relat. Areas Mol. Biol.* **1986,** *58,* 61.
308. Sawyer, D.; Valentine, J. *Acc. Chem. Res.* **1981,** *14,* 393.
309. Sawyer, D.; Valentine, J. *Acc. Chem. Res.* **1982,** *15,* 200.
310. Sawyer, D. *Phys. Chem.* **1989,** *93,* 7977.
311. Sawyer, D. In "Oxygen Chemistry"; Oxford University Press: New York, Oxford, 1991; pp. 160–187.
312. Koppenol, W.; Butler, J. *FEBS Lett.* **1977,** *83,* 1.
313. Koppenol, W. *Nature* **1976,** *262,* 420.
314. Rigo, A.; Stevanato, R.; Finazzi-Agrò, A.; Rotilio, G. *FEBS Lett.* **1977,** *80,* 130.
315. Behar, D.; Czapski,G.; Rabani, J.; Dorfman, L.; Schwarz, H. *J. Phys. Chem.* **1970,** *74,* 3209.
316. Czapski, G.; Goldstein, S.; Mmeyerstein, D. *Free Radical Res. Commun.* **1987,** *4,* 241.
317. Fridovich, I. *Annu. Rev. Biochem.* **1995,** *64,* 97.
318. Brieland, K. J.; Fantone, J. C. *Arch. Biochem. Biophys.* **1991,** *284,* 78.
319. Rabani, J.; Nielsen, S. *J. Phys. Chem.* **1969,** *73,* 3736.
320. Bielski, B.; Cabelli, D. *J. Radiat. Biol.* **1991,** *59,* 291.

321. Klug, D.; Fridovich, I.; Rabani, J. *J. Am. Chem. Soc.* **1973,** *95,* 2786.
322. Calabrese, L.; Rotilio, G.; Mondovì, B. *Biochim. Biophys. Acta* **1972,** *263,* 827.
323. Hodgson, E.; Fridovich, I. *Biochem. Biophys. Res. Commun.* **1973,** *54,* 270.
324. Hodgson, E. K.; Fridovich, I. *Biochemistry* **1975,** *14,* 5294.
325. Bull, C.; Fee, J. A. *J. Am. Chem. Soc.* **1985,** *107,* 3295.
326. Marcus, R. *J. Chem. Phys.* **1965,** *43,* 2654.
327. Cudd, A.; Fridovich, I. *FEBS Lett.* **1982,** *144,* 181.
328. Borders, C. L. J.; Saunders, J. E.; Blech, D. M.; Fridovich, I. *Biochem. J.* **1985,** *230,* 771.
329. Polticelli, F.; Battistoni, A.; Bottaro, G.; Carri, M. T.; O'Neill, P.; Desideri, A.; Rotilio, G. *FEBS Lett.* **1994,** *352,* 76.
330. Malinowski, D.; Fridovich, I. *Biochemistry* **1979,** *18,* 237.
331. Bertini, I.; Capozzi, F.; Luchinat, C.; Piccioli, M.; Viezzoli, M. S. *Eur. J. Biochem.* **1991,** *197,* 691.
332. Pantoliano, M. W.; Valentine, J. S.; Burger, A. R.; Lippard, S. J. *J. Inorg. Biochem.* **1982,** *17,* 325.
333. Fridovich, I.; Hodgson, E. K. *Biochemistry* **1975,** *14,* 5299.
334. Ellerby, M. L.; Cabelli, D. E.; Graden, J. A.; Valentine, J. S. *J. Am. Chem. Soc* **1996,** *118,* 6556.
335. Osman, R. In "Superoxide and Superoxide Dismutase in Chemistry, Biology and Medicine"; Rotilio, G., Ed.; Elsevier: New York, 1996; pp. 141–144.
336. Rosi, M.; Sgamellotti, A.; Tarantelli, F.; Bertini, I.; Luchinat, C. *Inorg. Chem.* **1986,** *25,* 1005.
337. Weinstein, J.; Bielski, B. *J. Am. Chem. Soc.* **1980,** *102,* 4916.
338. Stallings, W. C.; Powers, T. B.; Pattridge, K. A.; Fee, J. A.; Ludwig, M. L. *Proc. Natl. Acad. Sci. U.S.A.* **1983,** *80,* 3884.
339. Lah, M. S.; Dixon, M.; Pattridge, K. A.; Stallings, W. C.; Fee, J. A.; Ludwig, M. L. *Biochemistry* **1995,** *34,* 1646.
340. Schmidt, M.; Meier, B.; Parak, F. *JBIC* **1996,** *1,* 532.
341. Collaborative Computational Project, *Acta Crystallogr.* **1994,** *D50,* 760.
342. Banci, L.; Bertini, I.; Cabelli, D. E.; Hallewell, R. A.; Luchinat, C.; Viezzoli, M. S. *Free Radical Res. Commun.* **1991,** *12–13,* 239.
343. Calabrese, L.; Polticelli, F.; Galtieri, A.; Barra, D.; Schinina', E.; Bossa, F. *FEBS Lett.* **1989,** *250,* 49.
344. Marklund, S. *J. Biol. Chem.* **1976,** *251,* 7504.
345. Heikkila, R. E. In "CRC Handbook of Methods for Oxygen Radical Research"; Greenwald, R. A., Ed.; CRC Press: Boca Raton, Florida, 1985; pp. 233–235.
346. Bertini, I.; Banci, L.; Luchinat, C.; Hallewell, R. A. In "Annals of the New York Academy of Sciences; Blanch, H. W., and Klibanov, A. M., Eds.; New York Academy of Science: New York, 1988; pp. 37–52.
347. Bordo, D.; Djinovic, K.; Bolognesi, M. *J. Mol. Biol.* **1994,** *238,* 366.
348. Connolly, M. *J. Appl. Crystallogr.* **1983,** *16,* 548.
349. Connolly, M. *Science* **1983,** *221,* 709.
350. Rotilio, G.; Gray, J. C.; Fielden, E. M. *Biochim. Biophys. Acta* **1972,** *268,* 147.
351. Cass, A. E. G.; Hill, H. A. O.; Bannister, J. V.; Bannister, W. H. *Biochem. J.* **1979,** *177,* 477.
352. Vega, A. J.; Fiat, D. *Mol. Phys.* **1976,** *31,* 347.
353. Calabrese, L.; Cocco, D.; Desideri, A. *FEBS Lett.* **1979,** *106,* 142.
354. Rosi, M.; Sgamellotti, A.; Tarantelli, F.; Bertini, I.; Luchinat, C. *Inorg. Chim. Acta* **1985,** *107,* L21.